YURII YEHOROV

EXPLORING SOLUTIONS TO MITIGATE UNIDIRECTIONAL GRAIN GROWTH AND TO SET OPERATIONAL ENVELOP FOR WIRE + ARC ADDITIVE MANUFACTURING OF ALUMINIUM ALLOYS

FEDERAL UNIVERSITY OF UBERLÂNDIA
MECHANICAL ENGINEERING FACULTY
2018

YURII YEHOROV

EXPLORING SOLUTIONS TO MITIGATE UNIDIRECTIONAL GRAIN GROWTH AND TO SET OPERATIONAL ENVELOP FOR WIRE + ARC ADDITIVE MANUFACTURING OF ALUMINIUM ALLOYS

Thesis presented to the Graduate Program in Mechanical Engineering of the Federal University of Uberlândia, as part of the requirements to obtain the title of Master **IN MECHANICAL ENGINEERING** in the specialty **MATERIALS AND MANUFACTURING PROCESSES**

Line of research: Manufacturing Processes (Machining and Welding).

Supervisor: Prof. PhD. Américo Scotti

UBERLÂNDIA - MG

2018

YURII YEHOROV

EXPLORING SOLUTIONS TO MITIGATE UNIDIRECTIONAL GRAIN GROWTH AND TO SET OPERATIONAL ENVELOP FOR WIRE + ARC ADDITIVE MANUFACTURING OF ALUMINIUM ALLOYS

Thesis **APPROVED** by Post-graduation Program in Mechanical Engineering of Federal University of Uberlândia.

Line of research: Manufacturing Processes (Machining and Welding)

Assessment Committee:

_____
Prof. Dr. Américo Scotti - FEMEC - UFU

_____
Prof. Dr. Louriel Oliveira Vilarinho - FEMEC - UFU

_____
Profa. Dra. Yevgenia Chvertko - Igor Sikorsky KPI

_____
Prof. Dr. Sérgio Luiz Henke - UFPR

Uberlândia, 7th of August 2018

Dados Internacionais de Catalogação na Publicação (CIP)
Sistema de Bibliotecas da UFU, MG, Brasil.

Y43e
2018

Yehorov, Yurii, 1994-
Exploring solutions to mitigate unidirectional grain growth and to set operational envelop for wire + ARC additive manufacturing of aluminium alloys [recurso eletrônico] / Yurii Yehorov. - 2018.

Orientador: Américo Scotti.
Dissertação (mestrado) - Universidade Federal de Uberlândia, Programa de Pós-Graduação em Engenharia Mecânica.
Modo de acesso: Internet.
Disponível em: http://dx.doi.org/10.14393/ufu.di.2018.574
Inclui bibliografia.
Inclui ilustrações.

1. Engenharia mecânica. 2. Alumínio. 3. Processos de fabricação. 4. Engenharia industrial. I. Scotti, Américo, 1995-, (Orient.) II. Universidade Federal de Uberlândia. Programa de Pós-Graduação em Engenharia Mecânica. III. Título.

CDU: 621

Gloria Aparecida - CRB-6/2047

UNIVERSIDADE FEDERAL DE UBERLÂNDIA
Coordenação do Programa de Pós-Graduação em Engenharia Mecânica
Av. João Naves de Ávila, nº 2121, Bloco 1M, Sala 212 - Bairro Santa Mônica, Uberlândia-MG, CEP 38400-902
Telefone: (34) 3239-4282 - www.posgrad.mecanica.ufu.br - secposmec@mecanica.ufu.br

TERMO

ALUNO: Yurii Yehorov **MATRÍCULA:** 11622EMC021
ÁREA DE CONCENTRAÇÃO: Materiais e Processos de Fabricação **LINHA DE PESQUISA:** Processos de Fabricação (Usinagem e Soldagem)
PÓS-GRADUAÇÃO EM ENGENHARIA MECÂNICA: NÍVEL MESTRADO
TÍTULO DA DISSERTAÇÃO: Exploring Solutions to Mitigate Unidirectional Grain Growth and to Set Operational Envelop for Wire + Arc Additive Manufacturing of Aluminium Alloys
ORIENTADOR: Prof. Américo Scotti

A Dissertação foi **APROVADA** em reunião pública, realizada na Sala de Reuniões do LTAD do Bloco 5F, Campus Santa Mônica, em 11 de julho de 2018, às 08:00 horas, com a seguinte Banca Examinadora, que assina digitalmente, com exceção da Profª. Yevgenia Chvertko que por ser estrangeira e não possuir número de CPF não teve seu cadastro no SEI efetivado, razão pela qual não assina digitalmente este documento:

Prof. Americo Scotti (orientador) - UFU
Prof. Louriel Oliveira Vilarinho - UFU
Prof. Prof. Sérgio Luiz Henke - UFPR
Profª. Yevgenia Chvertko - KPI

Uberlândia, 07 de agosto de 2018

Documento assinado eletronicamente por **Américo Scotti**, **Professor(a) do Magistério Superior**, em 07/08/2018, às 11:53, conforme horário oficial de Brasília, com fundamento no art. 6º, § 1º, do Decreto nº 8.539, de 8 de outubro de 2015.

Documento assinado eletronicamente por **Louriel Oliveira Vilarinho**, **Professor(a) do Magistério Superior**, em 07/08/2018, às 12:54, conforme horário oficial de Brasília, com fundamento no art. 6º, § 1º, do Decreto nº 8.539, de 8 de outubro de 2015.

Documento assinado eletronicamente por **Sérgio Luiz Henke**, **Usuário Externo**, em 07/08/2018, às 17:28, conforme horário oficial de Brasília, com fundamento no art. 6º, § 1º, do Decreto nº 8.539, de 8 de outubro de 2015.

A autenticidade deste documento pode ser conferida no site https://www.sei.ufu.br/sei/controlador_externo.php?acao=documento_conferir&id_orgao_acesso_externo=0, informando o código verificador **0625025** e o código CRC **DB1F8E4C**.

Referência: 07/08/2018 - Processo nº 23117.050786/2018-31 SEI nº 0625025

Criado por cristiane, versão 2 por cristiane em 07/08/2018 07:01:56.

I want to dedicate this work to my little nephew Eva,
She's just awesome!

"The past and the present are our means, the future alone our aim"
B. Pascal

GRATITUDES

To evolution.

To my advisor, Américo Scotti, for guidance, teaching and patience.

To Prof. Ruham Pablo Reis, Prof. Valtair Antônio Ferraresi, Prof. Louriel Oliveira Vilarinho, Prof. Arthur Alves Fiocchi, Profa. Yevheniia Chvertko, Prof. Sergii Fomichov, Prof. Igor Skachkov, Prof. Volodimir Kochubey, Prof. Andrii Pirumov, Prof. Pavlo Sidorenko and Prof. Roman Ryzhov for the teaching in the areas of welding and manufacturing.

To the Graduate Program in Mechanical Engineering of the Federal University of Uberlândia and Welding Faculty of National Technical University of Ukraine "Igor Sikorsky Kyiv Polytechnic Institute" for the opportunity.

To CAPES, CNPq and FAPEMIG for the essential financial support (CAPES for the Master scholarship April / 2017 - August / 2018).

To the Welding Laboratory (LAPROSOLDA), Laboratory of Teaching and Research in Machining (LEPU), Laboratory of Conventional Machining (LUC) and Laboratory of Tribology and Materials (LTM) for technical and laboratory support.

And to all who in one way or another contributed to my professional, academic and personal training.

YEHOROV, Y. **Exploring Solutions to Mitigate Unidirectional Grain Growth and to Set Operational Envelop for Wire + Arc Additive Manufacturing of Aluminium Alloys.** 2018. 92 p. Master Thesis, Federal University of Uberlândia, Uberlândia, Minas Gerais, Brasil.

Abstract

Wire Arc Additive Manufacturing (WAAM) is a novel process with high industrial application. However, there are still some limitations, such as anisotropy of mechanical properties, which delays a wide implementation of WAAM. Moreover, as long as WAAM is a new technology, its operational envelope is not utterly known. The first objective of this work was to assess solutions to mitigate unidirectional grain growth in WAAM of aluminium, that leads to anisotropy of the mechanical properties of the printed part. In the scope of this objective, two methodological approaches were employed. The first approach used the switchback welding technique in comparison with a reference (the conventional unidirectional deposition) and also a traditional method for reduce unidirectional growth (bidirectional deposition). The second one used nanoparticles inoculation in the deposited metal. Both approaches showed ability to mitigate epitaxial growth of big columnar grains and to refine microstructure, however switchback technique show to be easier to implement. The second objective of this work was to find an operational envelope of the process, i.e., a range of travel speeds for a given deposition rate and for a given ratio deposition rate/travel speed. This study showed there are a range of pool volume during the deposition that must be respected to reach sound printed walls.

Keywords: WAAM, aluminium, switchback, inoculation

YEHOROV, Y. **Explorando Soluções para Mitigar o Crescimento Unidirecional de Grãos e para Estabelecer Envelopes Operacionais para Wire + Arc Additive Manufacturing de Ligas de Alumínio.** 2018. 92 p. Tese de Mestrado, Universidade Federal de Uberlândia, Uberlândia, Minas Gerais, Brazil.

Resumo

Wire Arc Additive Manufacturing (WAAM) é um novo processo com alta potencial de aplicação industrial. No entanto, ainda existem algumas limitações, como a anisotropia das propriedades mecânicas, que atrasa uma ampla implementação do WAAM. Além disso, enquanto WAAM é uma nova tecnologia, seu envelope operacional não é totalmente conhecido. O primeiro objetivo deste trabalho foi avaliar soluções para mitigar o crescimento unidirecional de grãos em alumínio por WAAM, o que leva à anisotropia das propriedades mecânicas da parte impressa. No âmbito deste objetivo, duas abordagens metodológicas foram empregadas. A primeira abordagem utilizou a técnica de soldagem de reversão em comparação com uma referência (a deposição unidirecional convencional) e um método tradicional para reduzir o crescimento unidirecional (deposição bidirecional). Uma segunda utilizou inoculação no metal depositado por nanopartículas. Ambas as abordagens mostraram capacidade de mitigar o crescimento epitaxial de grandes grãos colunares e refinar a microestrutura, no entanto, a técnica de reversão mostrou ser mais fácil de implementar. O segundo objetivo deste trabalho foi encontrar um envelope operacional do processo, ou seja, uma faixa de velocidades de deslocamento para uma determinada taxa de deposição e para uma determinada relação de taxa de deposição / velocidade de deslocamento. Este estudo mostrou que há uma faixa de volume do banho em fusão durante a deposição que deve ser respeitada para alcançar paredes impressas com boa qualidade.

Palavras chave: WAAM, alumínio, switchback, inoculação

ЄГОРОВ, Ю. **Вивчення рішень для подолання однонаправленого зростання зерна та для визначення операційних меж для Wire Arc Additive Manufacturing алюмінієвих сплавів.** 2018. 92 ст. Магістерська Дисертація. Федеральний Університет Уберландії, Бразилія.

Анотація (abstracts in ukrainian)

Wire Arc Additive Manufacturing (WAAM) це новий процес із високим потенціалом застосування. Проте існують деякі обмеження, такі як анізотропія механічних властивостей, що затримує широке впровадження WAAM. Більше того, поки WAAM - це нова технологія, її операційні межі майже не відомі. Перша мета цієї роботи полягала в оцінці рішень, спрямованих на пом'якшення односпрямованого зростання зерна під час WAAM алюмінію, що призводить до анізотропії механічних властивостей друкованої деталі. В рамках цієї мети були використані два методологічних підходи. Перший підхід - використання технологію зварювання switchback в порівнянні з еталонним (звичайним однонаправленим наплавленням) та традиційним методом зменшення односпрямого росту (двонаправлене наплавлення). У другому методі використана інокуляція металу наночастинками. Обидва підходи продемонстрували здатність до подолання епітаксійного зросту великих стовбчастих зерен та до поліпшення мікроструктури, однак техніку switchback легше впровадити. Друга мета цієї роботи полягала в тому, щоб знайти операційні межі процесу, тобто діапазон швидкості руху для заданої швидкості осадження та для заданого відношення швидкість осадження до швидкості руху. Це дослідження показало, що під час осадження існує цілий діапазон об'ємів басейнів, які необхідно дотримуватися, щоб досягти гарних друкованих стін.

Ключові слова: WAAM, алюміній, switchback, інокуляція

LIST OF THE ABBREVIATIONS AND SYMBOLS

AM	Additive Manufacturing
D_g	Average grain diameter
BCM	Beaded cylinder morphology of humping
BTF	Buy-to-fly ratio
CTWD	Contact Tip Work Distance
ρ_c	Density of the body submerged in water
t	Deposition time
DCEN	Direct current electrode negative
DED	Direct energy deposition
DMLS	Direct Metal Laser Sintering
EBM	Electron Beam Melting
GMAW	Gas Metal Arc Welding
GTAW	Gas Tungsten Arc Welding
GRM	Gouging region morphology of humping
G	Grain size number
HAZ	Heat Affected Zone
LM	Laser melting
LMD	Laser metal deposition
LS	Laser sintering
L_L	Lenght of the layer
N_0	Nucleation density
ΔT_n	Nucleation undercooling
SMAW	Shielded Metal Arc Welding
SAW	Submerged Arc Welding
F	Switchback backward stroke distance
S_b	Switchback backward stroke speed
TS_{eq}	Switchback equivalent speed
S	Switchback forvard stroke distance
S_f	Switchback forvard stroke speed
f	Switchback oscillation frequency
L_{sb}	Swithchback torch pass
G	Temperature gradient
TS	Travel speed
ΔT_c	Undercooling of columnar growth
E	Upthrusting force
V_f	Volume of displaced water
V_p	Volume of pores
V_c	Volume of the body submerged in water
ρ_f	Water density
Wc	Weight force
WAAM	Wire + Arc Additive Manufacture
WFS	Wire Feed speed

CONTENTS

CHAPTER I

INTRODUCTION

Since Charles Hall and Paul Héroult have invented the industrial method of electrolytic manufacturing of aluminium (Bickert, 2013), this metal has become one of the most common materials for engineering. Aluminium alloys are one of the most used material, with wide application in different areas of engineering, such as electrical conductors, shipbuilding, aviation, architecture, art, etc. For example, MOURITZ (2012) quantifies aluminium alloys contents in different commercially available aircrafts ranging from 61 % in the aircraft Airbus A380 (Fig 1.1 (c)) and more than 80 % in the Boeing 737 (Fig 1.1 (a)).

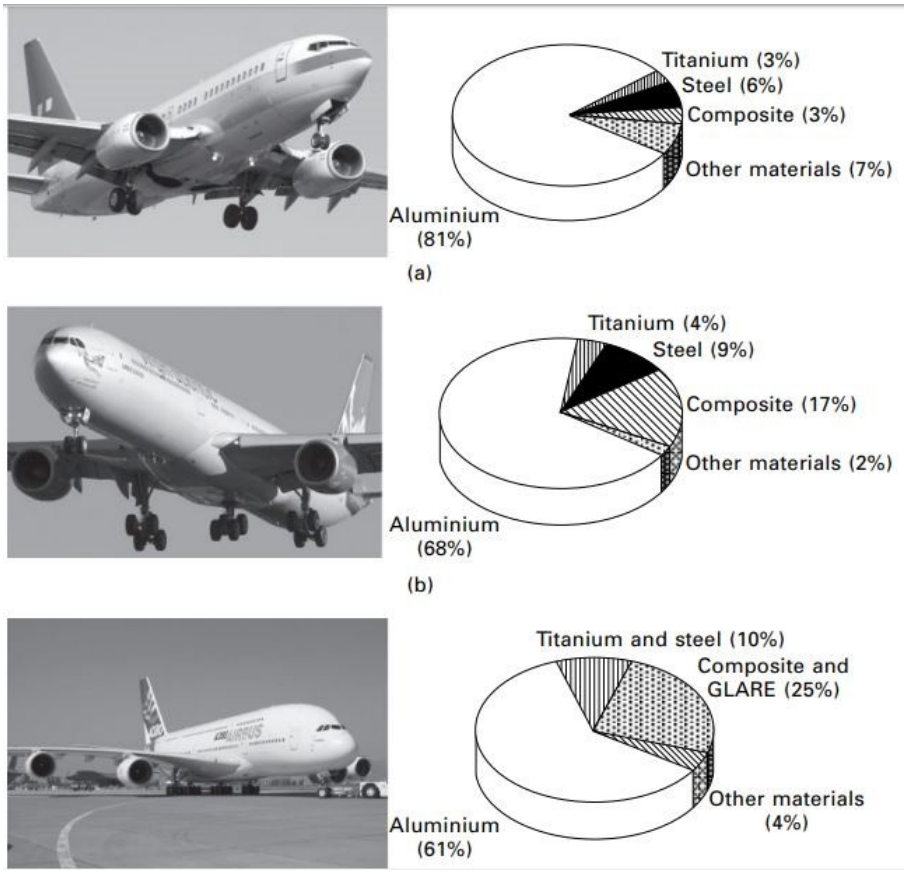

Figure 1.1 - Weight percentages of the materials of Airbus A320. After MOURITZ (2012)

The high interest to aluminium alloys is due to properties such as

- Light weight;
- High corrosion resistance;
- High electrical and thermal conductivity;
- Ductility;
- Machinability and weldability;
- Recyclability.

Due to the industrial importance of the aluminium alloys, there is a fast developing of the manufacturing technologies associated to this metal. Usually, production of the parts is carried with subtractive machining techniques, such as milling or turning. These methods have some significant disadvantages. The first is that geometry of the produced parts depends on the geometrical characteristics of the cutting tools, which limits the variety of design solutions that could be applied to solve specific engineering problems. The second disadvantage is that subtractive manufacturing techniques are expensive for customized parts. Welding would be another popular manufacturing means for aluminium alloy parts. Welding, in turn, has low dimensional precision and undergo metallurgical modification of the parts, in addition to distortions. To overcome these limitations, new manufacturing methods have been developed, as, for example, the new technic denominated Additive Manufacturing (AM).

According to ISO/ASTM 52900 (2015), Additive Manufacturing is a process of making parts and assemblies from 3D model data, usually layer upon layer, as opposed to subtractive manufacturing methodologies. There are a lot of AM technics based on different processes, yet Laser AM processes are the most used in industry and most studied ones. There are many types of Laser based AM processes, such as Laser sintering (LS), Laser melting (LM) and Laser metal deposition (LMD), according to GU (2015). Most of them are using metal powder as a filler material. Metal powder as a filler material for AM has significant advantages, such as high dimensional precision, high stability of the process, etc. However, it has disadvantages as well. SAMES et al. (2016) point out that very significant limitations of the powder based AM technologies are low deposition rates and high cost. To overcome limitations of the powder based AM technologies one can suppose selecting the wire and arc additive manufacturing process (WAAM).

Wire + Arc Additive Manufacture (WAAM) is an additive manufacturing technology that uses wire feedstock and electric arc as a heat source to produce parts. WAAM fits well the production of medium and large parts with high structural integrity in a variety of materials. WAAM has also the potential to produce high value structural parts faster than conventional manufacturing processes, with extremely reduced material waste and, what is most important, at

lower cost. Manufacturing potential of the WAAM can be visualized in Fig. 1.2, which demonstrates parts that have already been produced by the research group of Cranfield University, in UK.

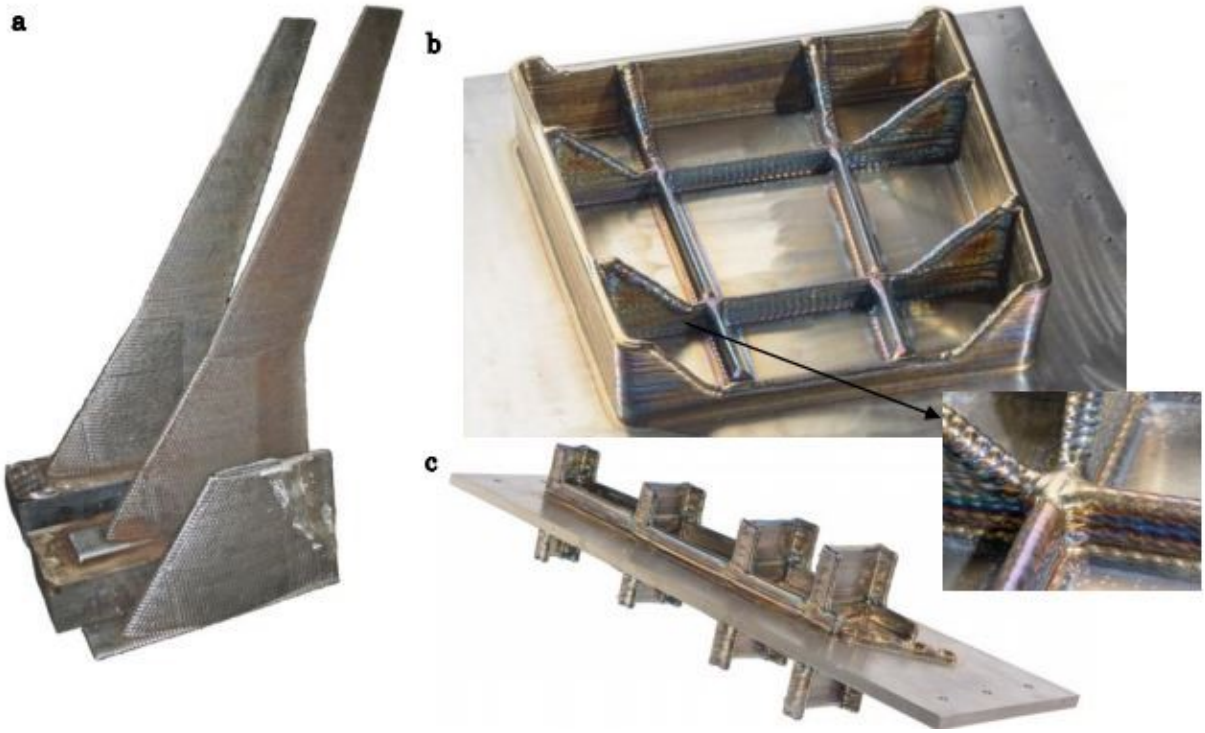

Figure 1.2 – Parts produced by WAAM. (a) Steel wing manufactured for a wind tunnel model; (b) titanium landing gear rib for Bombardier; and (c) thin-walled titanium component for Fokker. After COLEGROVE et al. (2016)

Detailed comparison of the costs of conventional manufacturing process and WAAM was made by MARTINA and WILLIAMS (2015). According to their report, replacement of traditional machining from a solid block by WAAM can reduce the costs up to 69% for titanium and up to 55% for steel. The cost reduction is a result of the significant decreasing of the buy-to-apply ratio (BTA). BTA if a parameter proposed as an analog to BTF ratio (by-to-fly) that is widely used in aviation industry, which shows how much of the material that were bought and will be present in the produced part after manufacturing. WAAM allow to decrease the BTF because it delivers near net shapes that needs only surface finishing to the desired dimensions.

BEKKER et al. (2016) provided the comparison of the cost of the WAAM as well to other popular metal AM processes, such as Electron Beam Melting (EBM) and Direct Metal Laser Sintering (DMLS). This comparison is illustrated in Fig. 1.3 and suggest a lower cost for WAAM.

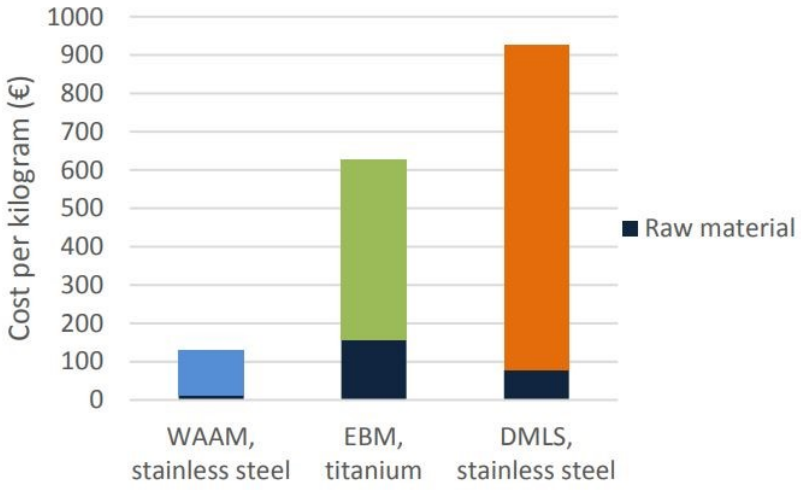

Figure 1.3 – Cost estimation per kg of metal by WAAM, EBM and DMLS. After BEKKER et al. (2016)

Considering importance of Aluminium alloys as an engineering material and all advantages of AM and in special WAAM comparing to the conventional production methods, wide implementation of WAAM of aluminium seems to be extremely perspective. However, there are some limitations that need to be overcome. DING et al. (2015) points some general limitations of the process as residual stress, relatively poor precision of the dimensions and poor surface finish of the produced parts. This list can be complemented with information from the work of WILLIAMS et al. (2015), who mentioned that some materials like titanium or aluminium are likely to present porosity and anisotropy of the mechanical properties. The overcoming of each of these limitations is a big scientifical problem that should be solved carefully and step by step. It would be perfect to provide solutions for all limitations in one work, but it does not seem to be feasible due to the complicity of the problems.

Anisotropy of the mechanical properties makes stress calculations of the constructions more difficult, increasing the possibility of mistakes, and, consequentially, can cause even human casualties. By solving this problem, WAAM would turn more attractive for heavy industry. Therefore, the general objective of presented work was to find ways of avoiding anisotropy of the mechanical properties in WAAM of aluminium alloys.

DEBROY et al. (2018) mentioned that epitaxial growth and competitive growth of the columnar dendrites occur during solidification of AM and columnar grains are generally coarse. This texture justifies the anisotropic mechanical properties. Thus, to avoid anisotropy of the mechanical properties, the mitigation of this epitaxial grain growth make sense. In line with this reasoning, two different (and likely innovative) approaches are considered, namely, with the use of a special welding technique called switchback and with a technique that has been for many years applied in casting for another purpose (grain refinement), i.e., inoculation. As far as these

approaches are concerned, none of them has been reported in current literature. For that reason, the general objective of the work is split into two specific objectives, which are the assessment of the usage of switchback technique and of inoculation during layer depositions in WAAM of aluminium alloys.

Another relevant point related to the possibility of broadening the application of WAAM, also not mentioned in current literature, are related to the opportunity of increasing even further production capacity without losing quality of the printed part. Therefore, a third specific objective of this work was to understand the role played by the layer melted volume over the geometric quality of the deposit carried out with WAAM of aluminium alloys. This can be done by assessing the travel speed limits for a same deposition rate or by assessing of the operational envelope for different production rates i.e. different deposition rates keeping the same ratio deposition rate/travel speed that could provide sufficient quality of the WAAM printed part and assess the usability of those limits in terms of economical portfolio of the process.

CHAPTER II

MITIGATION OF THE COLUMNAR EPITAXIALLY GRAIN GROWTH IN WAAM BY APPLYING DIFFERENT WELDING TECHNIQUES

2.1. Background (Bibliographic review)

2.1.1. 3D printing: Additive Manufacturing

Basically, 3D printing is the process of production when material is deposited layer by layer until desired shape is achieved. 3D printing can be used to produce full shapes or near net shapes of different materials, such as composites, polymers, metals, etc. The agglomeration of 3D printing processes that are intended to print metal parts is called Additive Manufacturing.

In the last ten years, aerospace industry has shown interest in this technology due to the increasing of use of titanium and aluminium alloys. There are several AM technologies with different application purposes, each one presenting accordingly their advantages and disadvantages. There exists a great number of articles covering overviews of the existing AM technologies (for instance, Vayre *et al., 2012,* Vaezi et al., 2013, Stavropoulos and Foteinopoulos, 2018), but most of them miss sight of the AM technology named Wire + Arc Additive Manufacturing (WAAM). Despite most studied and used AM technologies are laser based, some researchers, like DING et al. (2011), from research group of Cranfield University in UK, or HOYE (2015), from the research group of Wollongong University of Australia insist, that it is better to use WAAM for production of parts of medium and large size due to the high deposition rate of the arc welding processes and high efficiency of material use. Thus, solving the problems that are refrain of widely implement WAAM is an important engineering challenge.

According to the International Organization of Standardization (ISO, 2015), all existing AM technologies are classified into seven groups, as presented in Fig. 2.1 with the corresponding material applications. Only four out of these seven groups are meant to production of metals parts. And only one group uses direct energy deposition of metals (DED). Inside of that group, different processes are classified according to the feedstock and heat sources (Fig. 2.2). WAAM process would fit into this group, considering its wire feeding and electrical arc-based heat source.

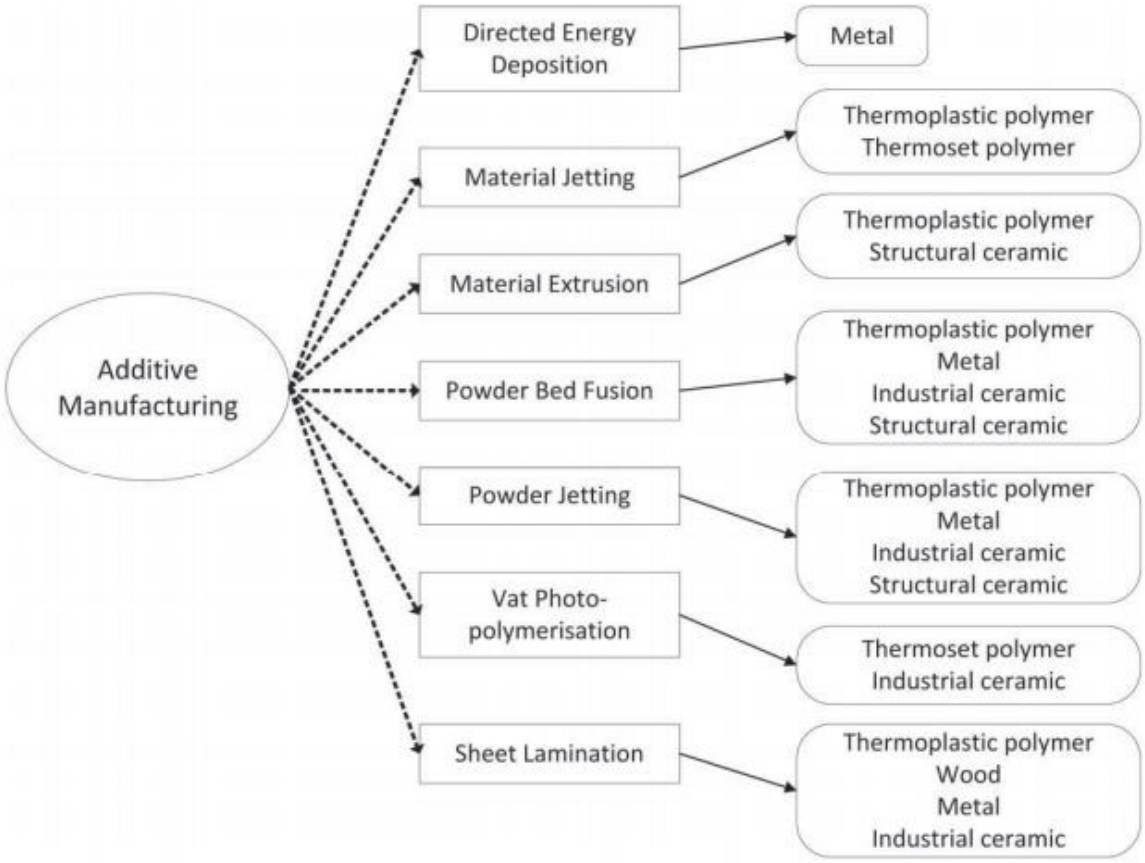

Fig. 2.1 - AM processes classification as organized by DEREKAR (2018)

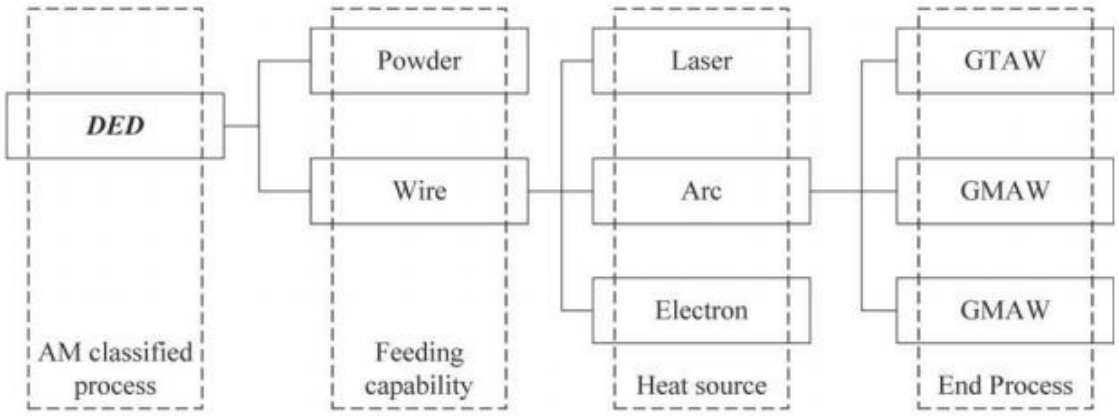

Fig. 2.2 – Subclassification of the direct energy deposition (DED), as organized by DEREKAR (2018)

WAAM can be defined as a series of processes qualified to produce near net shape parts, by sequential layer depositions by an arc welding process. The concept of arc welding additive manufacturing as a means of building up components was firstly announced in the 1990s in Europe, fact reported by RIBEIRO, NORRISH (1996) and SPENCER et al. (1998). One of the first publications about such a method of production was a patent provided by BARKER (1920), called Method of Making Decorative Articles. Barker suggested the use of MMA welding process

to build up decorative pieces (Fig. 2.3). In 1971, an equipment for making circular cross-sectional pressure vessels solely by progressive deposition of the weld metal was firstly patented by UJIIE (1971). In 1983, KUSSMAUL et al. (1983). produced a piece using SMAW process. Thus, the idea of reaching near net shape parts using welding is not new, yet this approach has been widely used only in the last two decades.

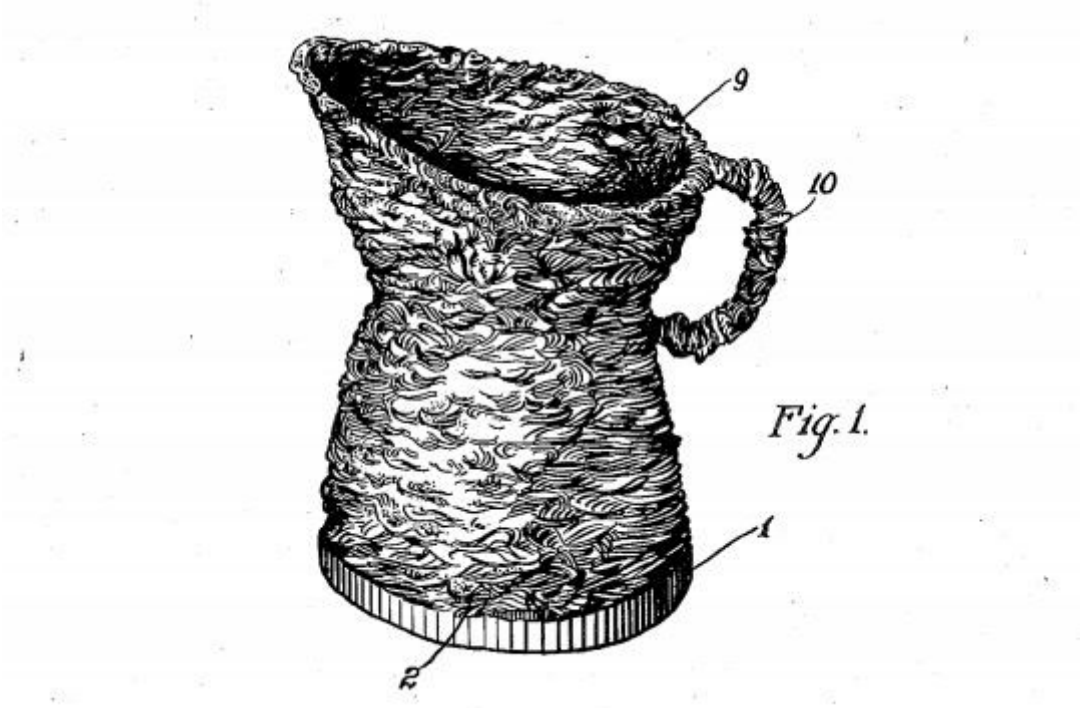

Fig. 2.3 – Schematic of the first WAAM process idealized by Barker, in 1920

Developing of the computer sciences changed the industry of the called 3D printing and presence of the new program complexes made possible to print parts with more complex geometry. One of the first demonstrations of how computer science can affect the 3D printing industry was showed in 1992 (Dickens et al., 1992). These researchers succeeded to print complex geometry forms (Fig. 2.4) using online point-to-point programming with a robotic GMAW process. Soon after that, it was developed the system that allowed slicing of the computer-aided 3D model (Ribeiro, 1996). Nowadays, WAAM is a fast-developing technology and every year appears more and more publications that offers solutions of different problems that hold up the widely WAAM implementation in industry. DEREKAR (2018) summarize through a diagram the WAAM history (Fig. 2.5).

WAAM has a number of characteristics that makes it interesting for heavy industry. Difference in cost of raw materials in form of wire and powder can be up to 50 times in favor of wire. For example, production of the titanium parts using WAAM can be up to 70% cheaper than conventional methods (Martina and Williams, 2015). Another great advantage of WAAM is that, as pointed by DONOGHUE et al. (2016), deposition rates up to 10 kg/h can be reached, against

600 g/h during powder based processes (Gu, 2015), figures that encourage production of big shapes.

Fig. 2.4 – Welded Thermostat Housing, provided by Dickens in 1992

However, WAAM was not as wide used as other AM processes, because of a few reasons, such as:

- High heat input, that could cause high residual stresses as well as part distortion;
- Poor accuracy and insufficient surface smoothness of the fabricated part, that could not be acceptable for many applications, in accordance with DING et al. (2015);
- Automated CAD software for WAAM was not created yet;
- Lack of good control system that allowed to monitor and control parameters during AM.
-

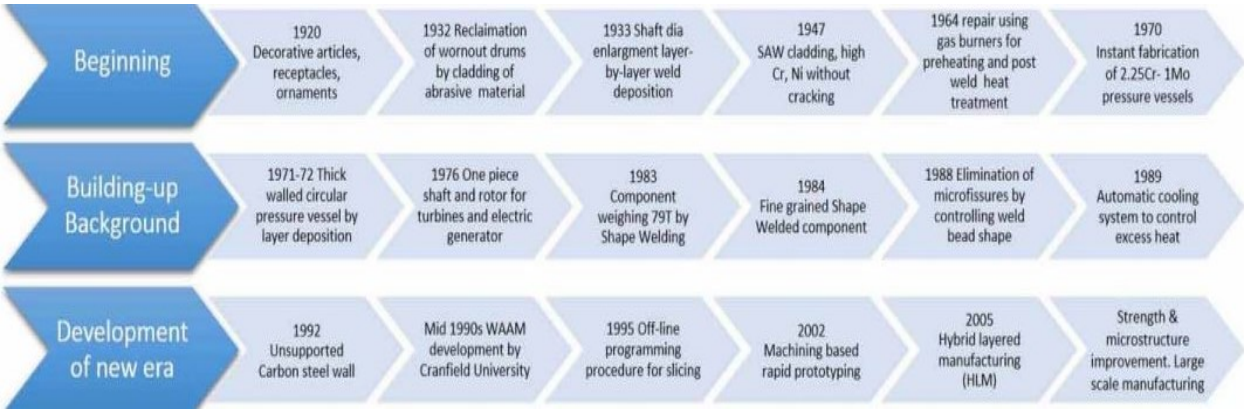

Fig. 2.5 – Chronological development of WAAM, from DEREKAR (2018)

2.1.2. Processes used in AM and their characteristics

The contemporary WAAM system consists of a power source, an automatic wire-feed system, a computer numerically controlled worktable or a robotic system, and some accessories (e.g. shielding gas, preheating or cooling system). A typical robotic WAAM system is shown in Fig. 2.6. In this context, a significant aspect of the WAAM system choice is the welding process. There are three main welding processes used for WAAM:

- GTAW;
- GMAW;
- Plasma.

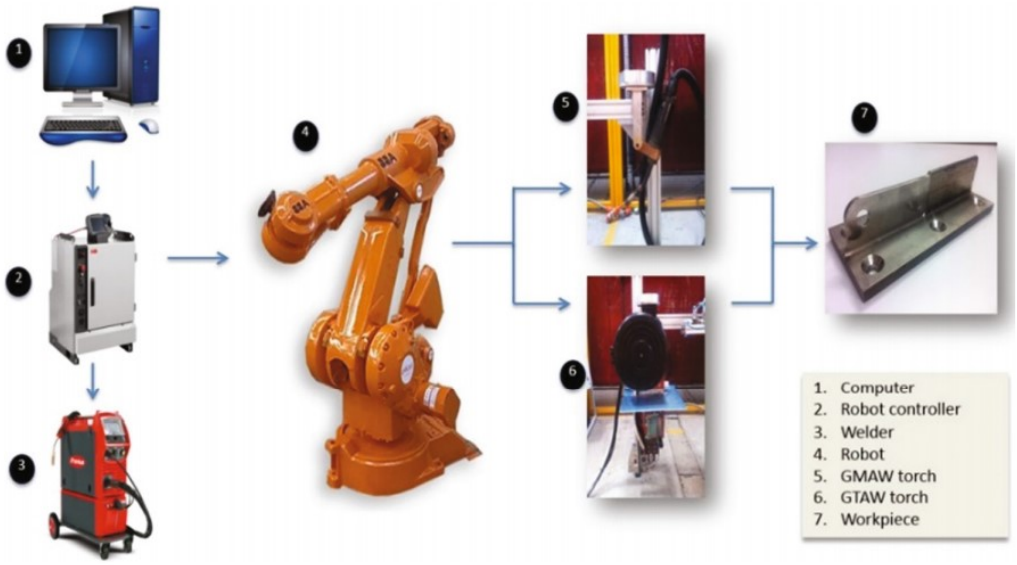

Fig. 2.6 – Schematic diagram of the developed experimental WAAM system (Pan et al. 2018)

Pan et al. (2018) featured the main characteristics of the three mains processes used in WAAM, as presented in Table 2.1. Extending Pan et al.'s description, in summary GTAW based systems use non-consumable tungsten electrode to carry the arc as a heat source and separately fed wire that is melted by the arc and deposited on the substrate. During the deposition, wire feed orientation influences material transfer and the quality of the layer formation. Some researchers considered to use twin-wire GTAW process to produce intermetallic materials (schematic of twin wire GTAW AM is shown on Fig. 2.7). For example, MA, CUIURI, HOYE et al. (2015) have studied the mechanical properties and microstructure of the titanium aluminides using twin wire GTAW AM process. Meanwhile, SHEN, PAN, CUIURI et al. (2016) dedicated their study to the fabrication of Fe-FeAl functionally graded material also using twin wire GTAW AM process.

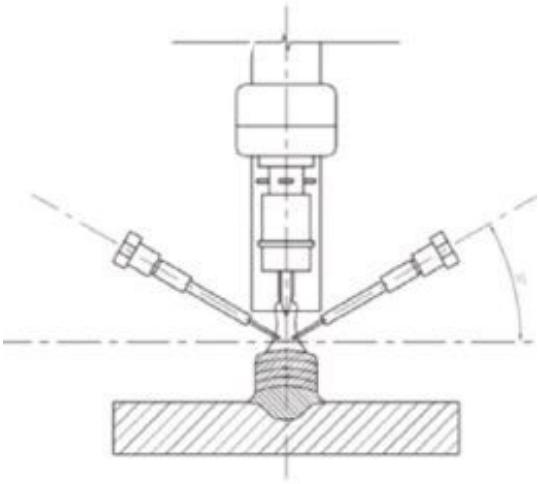

Fig. 2.7 – Schematic of the twin wired GTAW process (Ma et al. 2015)

GMAW process uses consumable wire melted by the arc and deposited on the substrate. There are different metal transfer modes with GMAW based WAAM, but usually it is used Short-circuit transfer due to lower heat input, as mentioned by ALMEIDA et al. (2010). Amongst the most popular GMAW processes, the waveform controlled CMT is the most applied one to WAAM. Finally, Plasma based process uses plasma flow as a heat source and the wire is separately fed just like GTAW process. Due to the high density of the energy, plasma-based process allows to decrease distortion of the weld and achieve smaller welds with higher welding speed, what was investigated by MANION and HEIZMAN (1999).

Table 2.1 – WAAM heat sources features after Pan et al. (2018)

Arc welding process	Features
Cold Metal Transfer (CMT)	High quality, zero spatter, low heating input process with reciprocating consumable wire electrode, heat source – electric arc
TIG	High quality, separate wire process, with no consumable electrode, heat source – electric arc
Plasma	High stability, separate wire process, with no consumable hidden electrode, heat source- plasma flow

From the geometric point of view, dimensional precision and wall waviness are the main concerns of AM. Dimensional precision would be defined as the difference between the target dimensions (nominal design wall width and high) and the useful thickness and height of the erect wall. The closer-fitting the dimensional precision, the less material to be subtracted after layers deposition (low buy-to-apply index). However, a wide wall waviness after layers deposition also means a great amount of material to be subtracted, even though the target dimension could have been reached.

Although not published yet, there are 3 commandments developed by the welding group Laprosolda to reach minimization of waviness deviation, as follows:

1st Commandment:

The arc pressure should be minimized to avoid pool lateral sag (downward lateral running).

This can be reached, for a given material and wall thickness, by using short arc, lower current-travel speed ratio, lower interlayer temperature and gas composition that favors cathodic emission concentrated in the arc center line

2st Commandment:

The pool should present a proper volume for a given deposition rate and current (a too small pool volume means low heat transferred to the prior layer, and a too large pool is prone to run downward).

There is always an adequate range of pool volumes (for a given material, wall thickness, and arc energy). This range can be determined by increasing progressively the travel speed for a given wire freed speed previously defined.

3rd Commandment:

The material underneath each layer under deposition should be as cool as possible, so that the heat transfer through the erect wall becomes easier.

The faster is the heat transfer from the pool of the layers under deposition, smaller and less fluid becomes the pool, preventing pool collapse to the sides.

2.1.3. GMAW processes

The schematic of the GMAW process is shown on Fig. 2.8. According to O'BRIEN (1991), the concept of GMAW process was known since the 20's years of last century, but it became commercially applicable only in 1948.

Complementary GMAW operational principles were described by MESSLER (2004). According to this author, GMAW process uses a continuous wire electrode and an externally supplied inert shielding gas. The consumable electrode provides the filler material to the weld. The shielding gas plays two roles in GMAW. Firstly, it protects the arc and welding zone from interaction with atmosphere and, second, it provides desired arc characteristics through ionization. There are a wide range of gases (e.g., argon, helium, carbon dioxide, and hydrogen, occasionally with a small amount of oxygen added) that can be used, depending on the properties of the metal being welded, the design of the joint, and the desired arc characteristics.

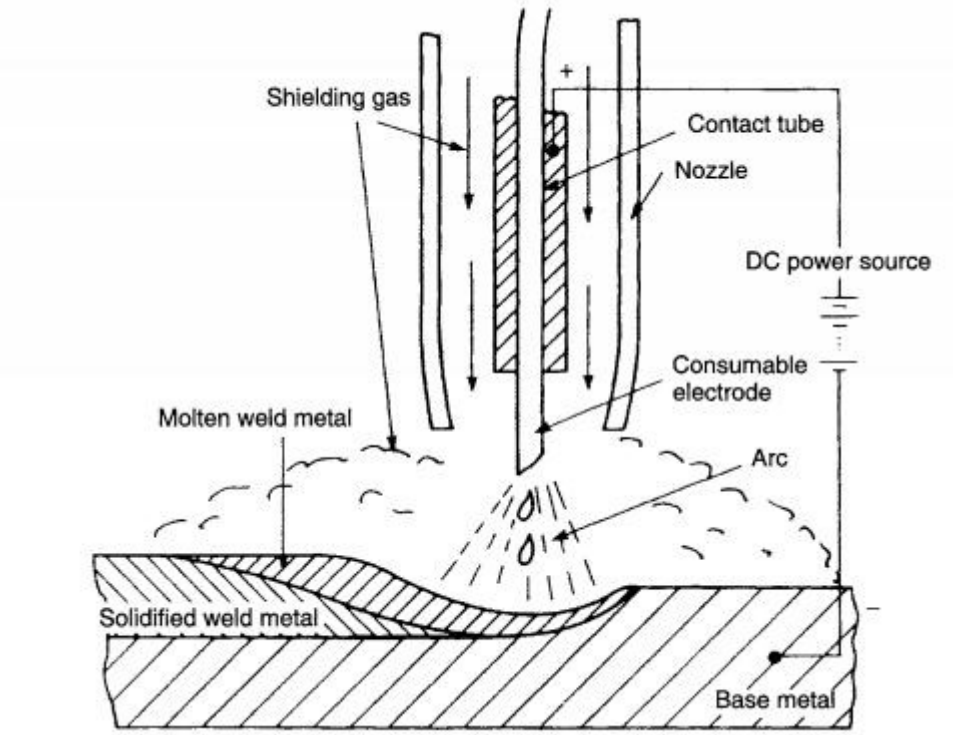

Fig. 2.8 – Schematic diagram of the GMAW process, by MESSLER (1993)

O'BRIEN (1991) identifies the advantages of GMAW process compared to other arc welding processes as:

- GMAW can weld in all positions, unlike submerged metal arc welding (SAW);
- Because of the continuous electrode feed, the metal deposition rates in GMAW are significantly higher than shielded metal arc welding (SMAW);
- Due to higher metal filler deposition rates, welding speeds in GMAW can be higher than those obtained with SMAW;
- Because of the wire feed is continuous with GMAW, longer welds can be done without stops and starts;
- GMAW has no restriction on the length of the electrode as in SMAW;
- With spray transfer in GMAW, deeper penetration of the weld is possible compared to SMAW;
- Due to the absence of slag, there is less problem with cleaning.

  He also points out some limitations of this process:
- The welding equipment is more complex and hence costlier and less portable compared to SMAW;
- Protection against air drafts is required;
- Higher levels of radiated heat and arc intensity are produced.

Metal transfer mode has a significant impact on the quality of the weld, heat input and arc stability during GMAW process. Usually metal transfer modes are classified as:

- Globular;
- Spray;
- Streaming Spray;
- Short-circuit.

During the globular transfer mode, melted filler material crosses the arc in form of globules formed due to the action of the arc forces. Globular transfer is also called open-arc welding, which can take place when using a non-pulsed current source. Sequence of the formation and transfer of the globular drop is shown on Fig. 2.9. The main characteristic of globular transfer mode is that a drop size is bigger than the diameter of the electrode wire and a few drops per second takes place. Current is relatively low compared to the current levels associated with spray transfer but larger than the current levels associated with short-circuit transfer. The forces affecting different transfer modes and particularly globular transfer mode were well described by WANG et al. (2014). In the opinion of the thesis author, this mode is likely not good for WAAM, because it provides a lot of spatters and when big globular drop falls into the molten welding pool it affects waves on the surface of the pool that can distort wall formation.

Spray transfer mode is illustrated on Fig. 2.10. Spray transfer appears when the welding current is higher than a given transition current. The transition current is directly proportional to the surface tension of melted metal, but inversely proportional to the diameter of the electrode wire. At higher values of the welding current, the drop size decreases and the electrode tip becomes tapered, and simultaneously there is an increase in the number of drops. With spray transfer mode, welding cannot be used in any welding position, only in the flat position. This is due to the high welding energy and large pool. In the opinion of the thesis author, this transfer mode is better for WAAM than globular due to less spattering and smaller size of the drops, but to reach this transfer mode to use higher current (fact that would lead to an increased heat input), or to use smaller diameter of the wire (what would decrease deposition rate) is necessary.

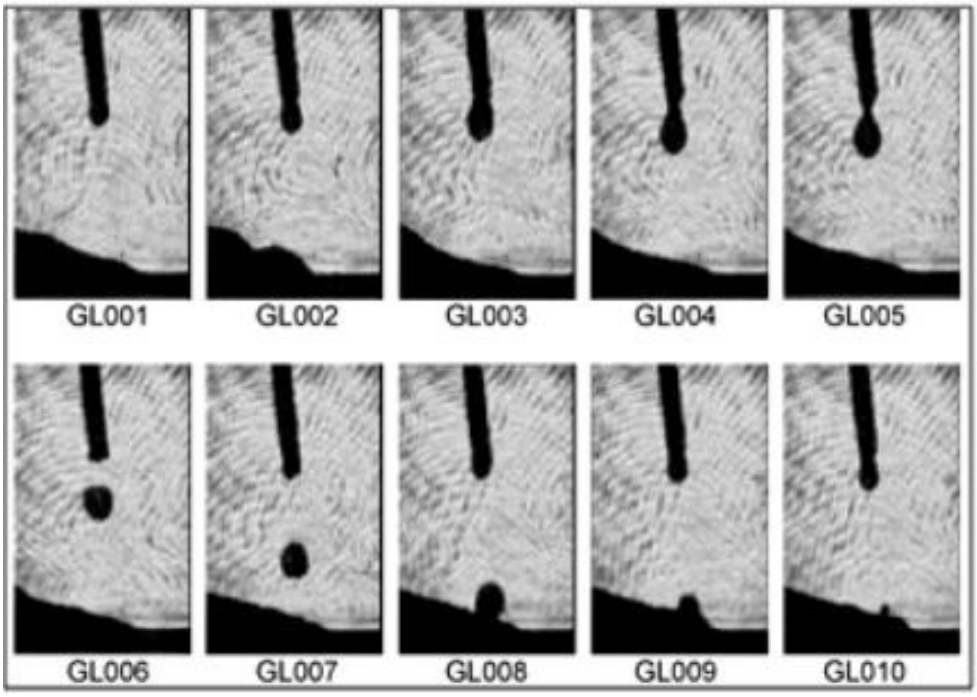

Fig. 2.9 – Schematic of the globular drop formation and transfer (from FERRARESI et al., 2003).

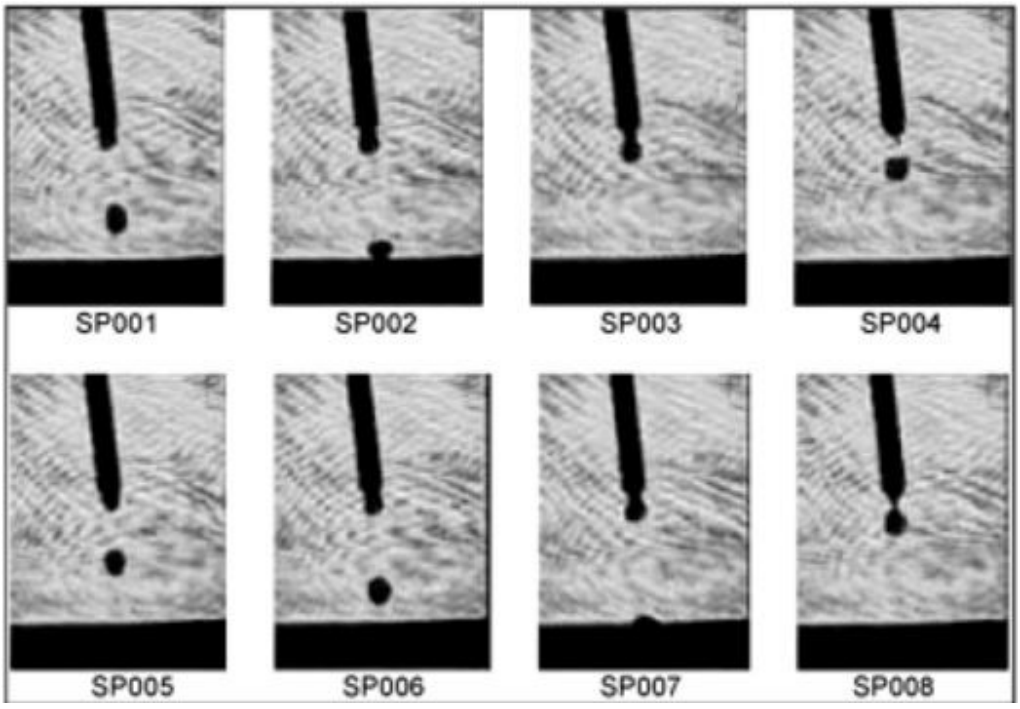

Fig. 2.10 – Schematic of the drop formation and transfer during spray mode. (from FERRARESI et al., 2003)

When current reaches values much higher than transition current, very fine stream of small droplets is formed axially through the arc. That transfer mode is called streaming transfer. This transfer is seen when the electrical resistance of wire is relatively high and the diameter is small and welding current is above 300 A (Norrish, 1992). Due to the very high current this transfer mode cannot be applied in WAAM

Short-circuit transfer occurs with the lowest ranges of welding current. This transfer mode is illustrated on Fig. 2.11. SCOTTI et al. (2012) said that to be classified as a pure short-circuiting mode, there must be a contact (short-circuit) between the droplet under formation and the pool before drop detachment. During the short-circuit periods, the arc extinguishes. A liquid metal bridge is formed and then grows as the droplet is sucked into the molten pool (by surface tension). As the short-circuit current at this stage is not very pronounced, there is insufficient electromagnetic force to constrict (pinch effect) the metal bridge. Then, owing to a reduced electrical resistance in the bridging, the current increases progressively, heating the wire by Joule effect (absence of anodic heating at this moment). The bridge is necked out by the combined effect of the surface tension and the progressive electromagnetic forces (pinch effect), the latter as a consequence of the increased current at the final stage.

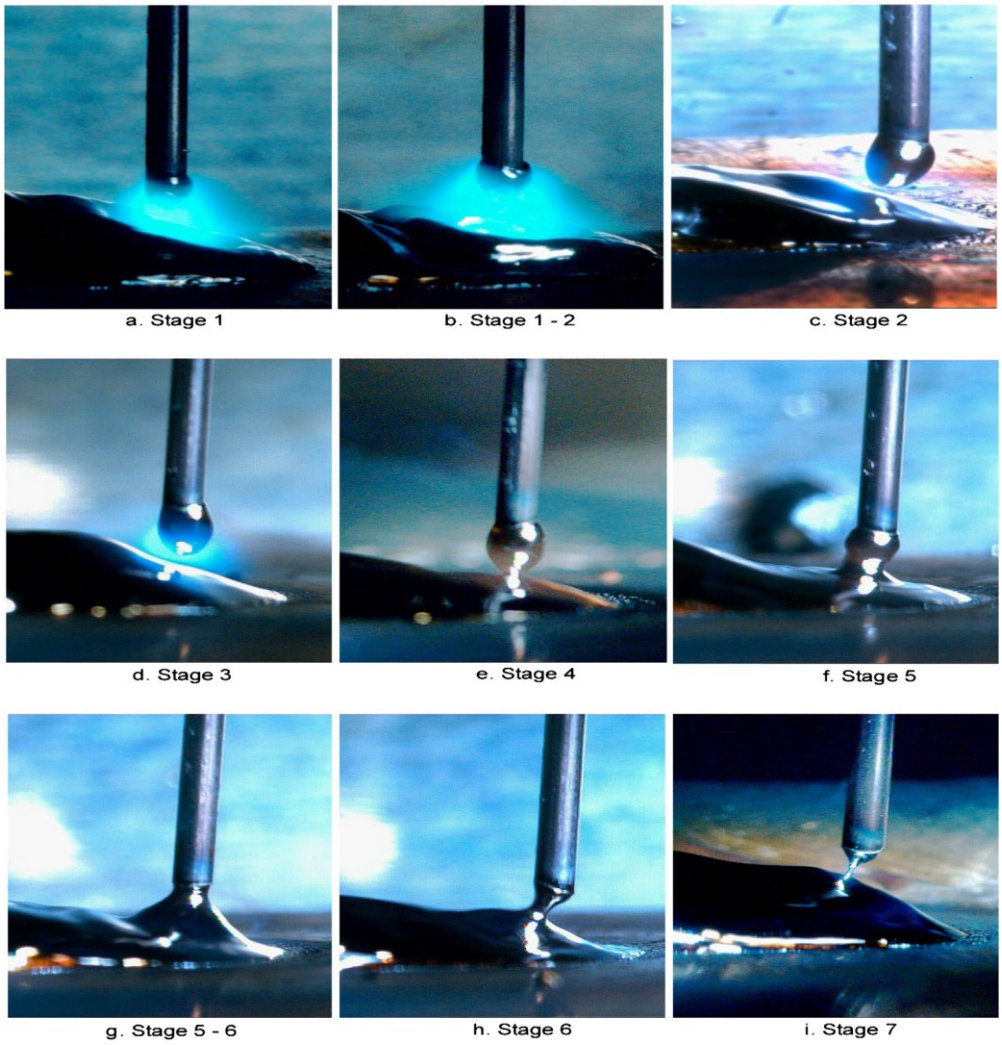

Fig. 2.11 – Schematic of the drop formation and transfer during short-circuit mode (from CUIURI, 2000)

Although there is an equilibrium between the wire melting rate and its feeding speed during the short-circuiting mode, just after the end of the short-circuit, the first parameter becomes higher than the latter one (due to the still increased post short-circuit current), leading to a limited

increase of the arc length. At this point, there is also an accelerated formation of a new droplet at the tip of the electrode wire. As the current subsequently falls, the rate of the wire melting matches the wire feed speed during the following few milliseconds. Afterwards, as the current intensity becomes smaller, the wire feeding rate exceeds the wire melting rate, causing the wire to gradually approach the weld pool. Short-circuiting transfer provide less heat input that makes it more applicable for WAAM.

But the abovementioned transfer modes are “natural”. They occur as a function of the set electrical parameters, i.e., current and voltage (Scotti et al. 2012). They are widely used for regular welding applications, but for special applications such as joining of thin sheet metals, welding in the vertical position or operation requiring low spatter, “natural” metal transfer modes may have some limitations. That limitation can be overcome by automatic adjustment and control provided by special electronic solutions. Metal transfer mode achieved by such a solution as Control Metal Transfer. Considering that different controlled metal transfer processes are based on different principles, it is required to classify this metal transfer. Such a classification was suggested by Scotti et al. (2012) and summarized as below.

- Spray transfer controlled by pulsed current (DC and AC) (the current is automatically adjusted by the machine using an algorithm to form the appropriate pulse and base periods);
- Contact transfer controlled by current (the current is controlled during and/or before the short-circuit stage);
- Contact transfer controlled by current and wire feeding (not only current, but also the feeding of the wire, forward and backwards, is controlled during and/or before the short-circuit stage).

2.1.4. Homoepitaxial columnar grain growth in AM

Grain structure of a metal meets high importance in engineering because it determines the mechanical properties of a component. For instance, fine equiaxed grains can reduce solidification cracking (Garland, 1975) and improve toughness, ductility and strength (Hall, 1951). In contrast, large columnar grains can cause anisotropy of the mechanical properties. This is the reason for having grain structural formation in weldable aluminium alloys been well studied by the number of scientists. For example, GANAHA et al. (1980) studied grain texture of different aluminium alloys welded using GTAW process. In recent years, researches on grain structure of intermetallic alloys based on aluminium are turning more popular. For example, LIN et al. 2003 studied the microstructure after GTA welding of the aluminium-lithium-zirconium alloy using different filler material varying the content of Li and Zi. They observed equiaxed grains zone around the fusion boundary and figured out that the zone width depends proportionally of the content of lithium and zirconium.

According to the theories of alloy solidification, constitutional supercooling mode does not happen in welding, despite the fast cooling rate. The weld metal grain structures near the fusion boundary are dominated by the epitaxial nucleation and growth process (the crystal grows on a partially melted substrate of the same material, yet with enlarged grains due to a high temperature that the subtract is exposed), as illustrated in Fig 2.12. Thus, this grain growth phenomenon is named homoepitaxy. The subsequent growth is influenced by both the preferred crystallographic direction and the dominant local heat flow direction at the growth interface. Consequently, in the bulk weld metal, grains with their easy growth direction parallel to the direction of the maximum temperature gradient will grow easer and crowd out their less favorably oriented neighboring grains. This phenomenon has been referred as directional solidification.

Cellular and columnar grains epitaxially grow from the substrate grain instead of forming new grains because epitaxial growth requires a minimal undercooling to proceed, whereas nucleation of new weld metal grains requires that a significant free energy barrier be overcome. According to WEI et al. (2016(a)), columnar grains grow in a curved pattern rather than along straight lines from the fusion boundary towards the center of the molten pool. At low heat source moving speed, only curved columnar grains are formed, while a transition to equiaxed morphologies will take place at faster heat source movements. YUNJIA et al. (1989) mentioned that epitaxially grown long columnar grain structure is not even broken up by multiple pass welds.

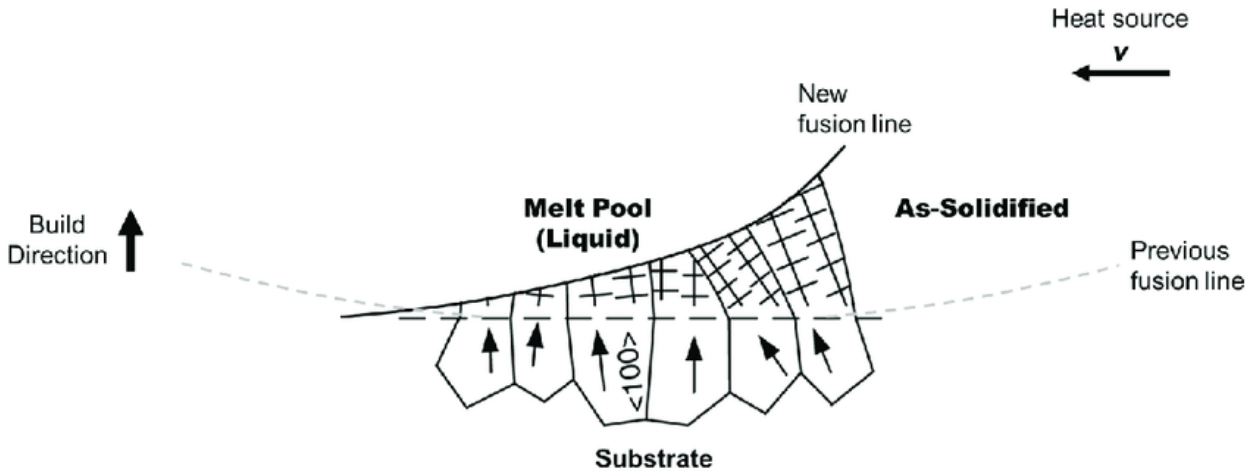

Fig. 2.12 – Schematic illustration of competitive epitaxial grain growth in the melt pool during solidification as the heat source moves away, after YUNJIA et al., 1989 (the arrows in the grains of the substrate indicate the easiest growth direction)

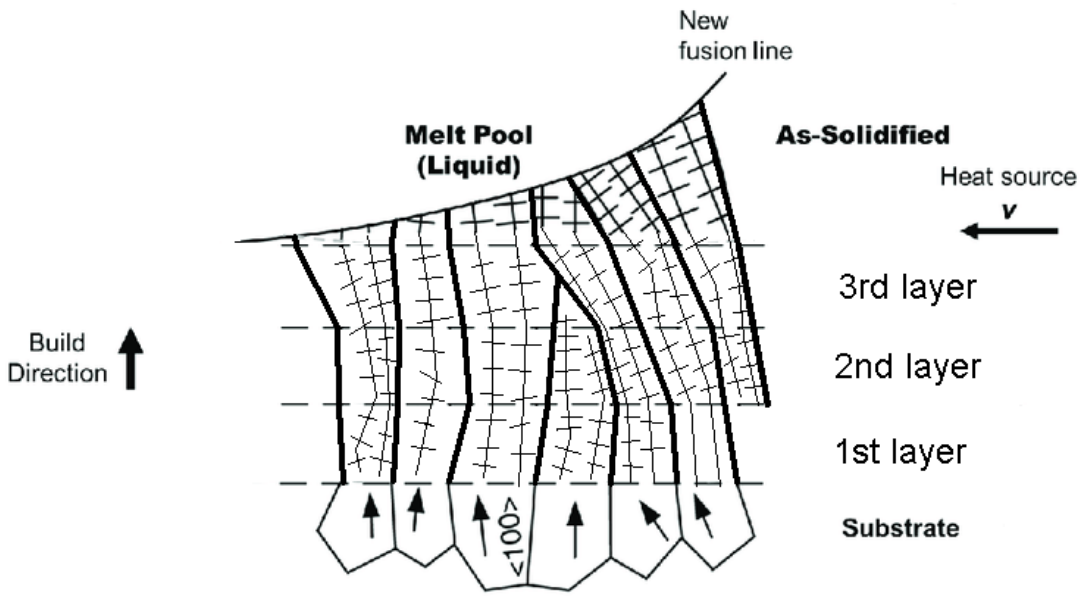

Fig. 2.13 – Schematic illustration of competitive epitaxially columnar grain growth through the layers during WAAM

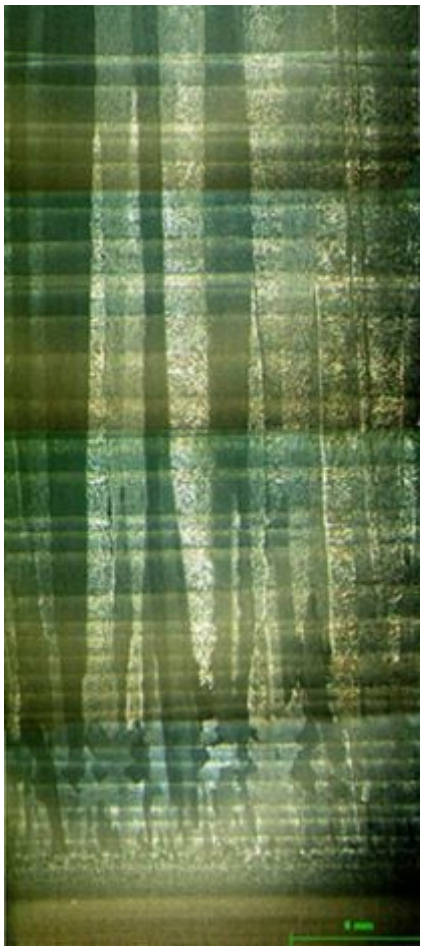

Fig. 2.14 – Through layer columnar grains formed during WAAM production of the Ti-6Al-4V wall, after WANG et al. (2011)

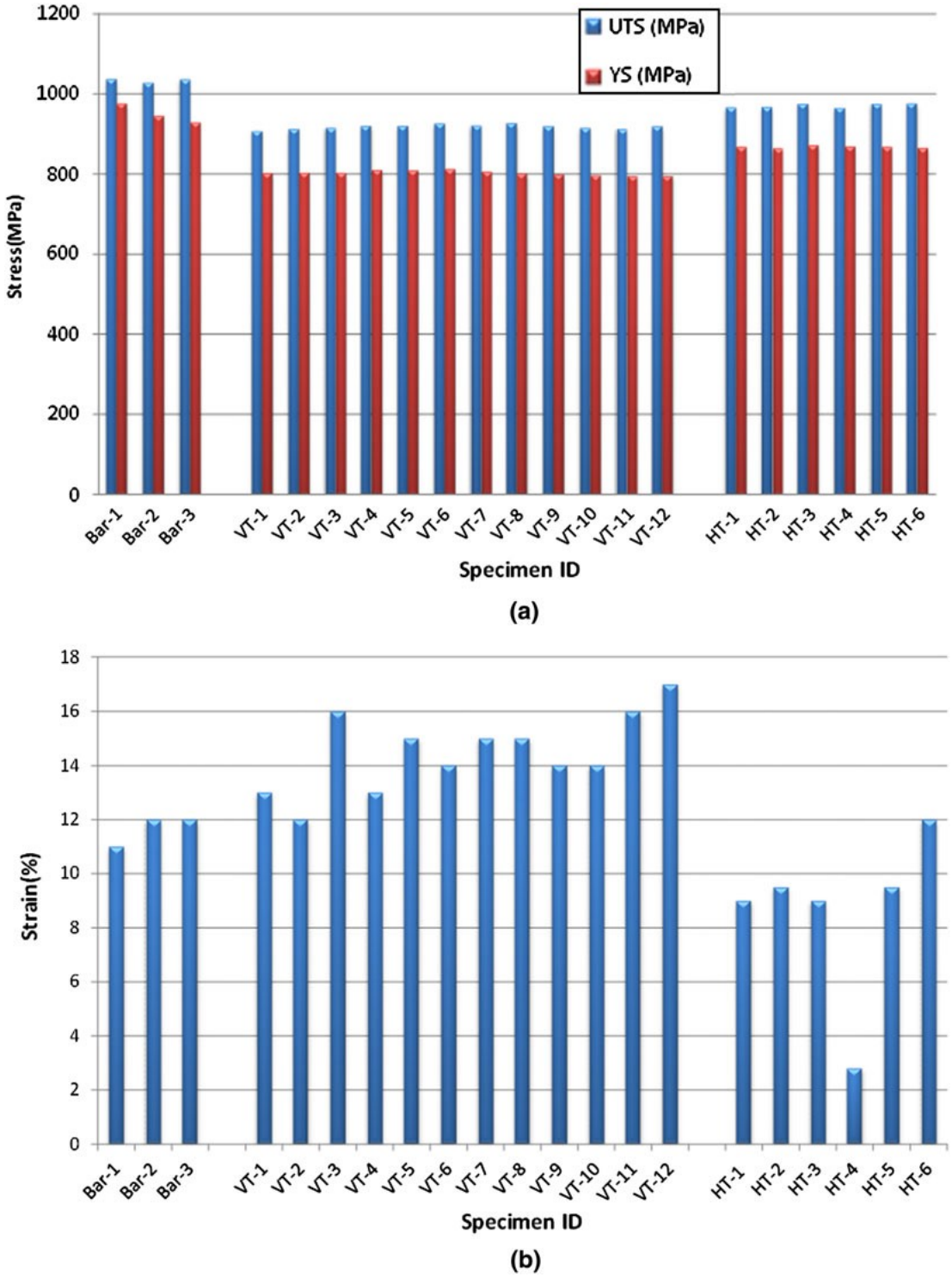

Fig. 2.15 – Tensile test results of Wang et al. (2013): (a) yield and ultimate stress vs specimen; and (b) strain vs specimen (specimens referred as Bar are the reference samples, made of forged Ti-6Al-4V bar; the ones referred as VT are vertical specimens taken from WAAM different parts of the wall in through layer direction; the ones referred as HT are specimens taken from WAAM walls in longitudinal direction)

Nucleation with grain growth following epitaxial and directional columnar solidification (Fig. 2.13) are typical of WAAM, since, as cited by WEI et al. (2016(b)) maximum heat flow direction in

AM is perpendicular to the trailing edge of the molten pool towards the substrate. As a result, long grains are formed, as illustrated in Fig. 2.14. According to YAN et al. (2017), the re-melting of the previous layer during AM generally induces heterogeneous nucleation at the melt pool boundary and epitaxial grain growth with cellular or dendritic solidification front. Therefore, grain size of the substrate or from the previously deposited layer determines the transverse and longitudinal columnar grain dimensions.

WANG et al. 2013 suggest that these columnar grains in WAAM can cause anisotropy of the mechanical properties, as quantified in Fig. 2.15. ZHU et al. (2015) in their review about LMD of Ti alloy, point out that that for some authors the as-deposited samples exhibited higher strength and lower ductility for the longitudinal direction than for the transverse direction, although they found themselves and from other publications diverging results. As property anisotropy is undesirable, layer building strategies on the mechanical properties of printed part have been the main focus of several works.

There are different approaches to avoid or mitigate epitaxial growth of big columnar grains. One of the divulgated methods is to apply high pressure interpass rolling. This approach was firstly used in 1984 by KURKIN and ANUFRIEV (1984) to prevent distortion of thin welded wall. In 2009, ALTENKIRCH et al. (2009) described high pressure interpass rolling as a means of decreasing residual stresses. Only in 2013 that COLEGROVE et al. (2013) firstly used it to improve the microstructure of WAAM printed walls. The principle of this method is to roll under high pressure each layer after its deposition, illustrated in Fig. 2.16.

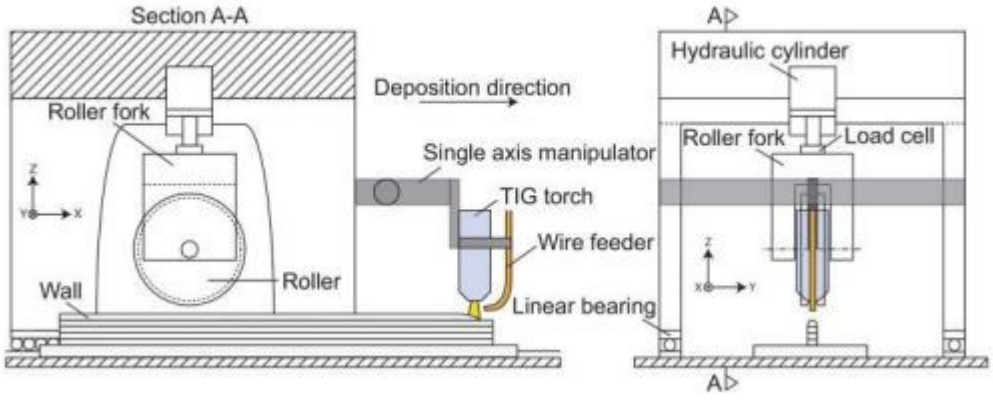

Fig. 2.16 – Schematic diagram of high pressure interpass rolling in WAAM (from WILLIAMS et al., 2015)

When applied to WAAM structures, rolling resulted in a reduction of the grain due to the enhanced recrystallization that occurs with the deposition of the subsequent layer on the plastically deformed layer (Martina et al., 2015). The effect of the high pressure interpass rolling on the wall texture can be seen on Fig. 2.17. As one can see, interpass rolling shows significant impact on grain size. The other advantage of this approach is that it simultaneously reduces residual stress (McAndrew et al. 2018). However, it has some limitations too. It would be very difficult to print a part with complicated geometrical shape due to the constructional features of

the equipment. To provide ability for the roller to repeat complicated trajectory of the torch, a design of a very complicated and expensive motion system would be required.

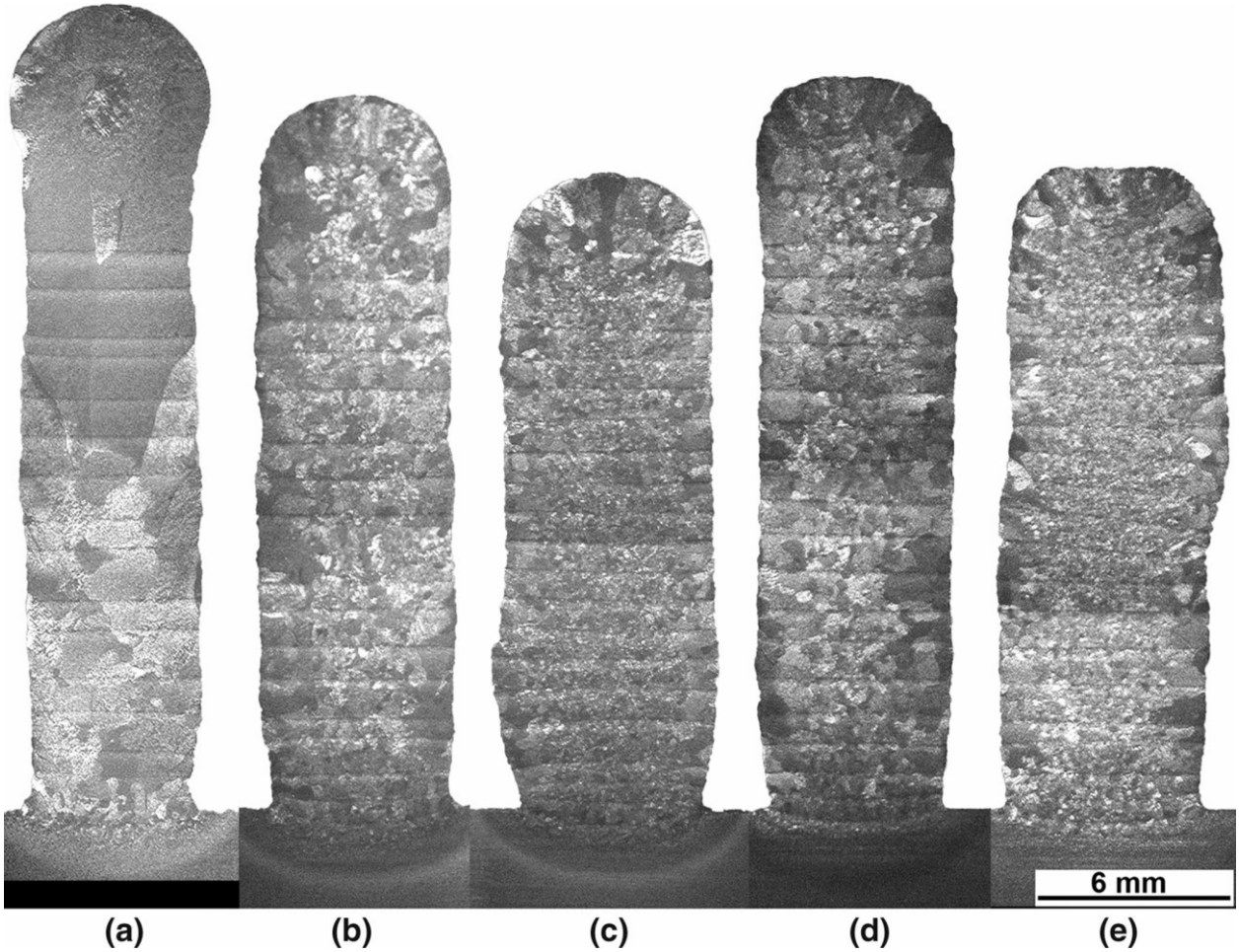

Fig. 2.17 – Optical microscopy of cross sections of Ti-6Al-4V WAA Manufactured walls taken from YZ plane from: (a) control sample; (b) sample rolled at 50 kN with a profiled roller; (c) sample rolled at 75 kN with a profiled roller; (d) sample rolled at 50 kN with a flat roller; and (e) sample rolled at 75 kN with a flat roller (from MARTINA et al., 2014)

Another published method for mitigation of the mechanical property anisotropy is to change of the layer deposition direction at each deposition start (bidirectional depositions). As columnar growths follow the heat flow direction and as each layer when deposited in a bidirectional mode changes accordingly the direction of heat flow, a “zig-zag” solidification pattern is formed in the longitudinal direction (layer by layer) of the printed wall. The effect of using of bidirectional deposition on the texture of a IN718 LMD wall was shown by, for instance, DINDA et al. (2012), as illustrated in Fig. 2.18. This “zig-zag” solidification pattern is supposed to reduce the mechanical property anisotropy, although some setbacks exist also to this approach. One of the limitations would be the fabrication with uninterrupted deposition, such as a circular component. Another one would be an overheating at the ends, if the direction reversion is carry out with a dwell time.

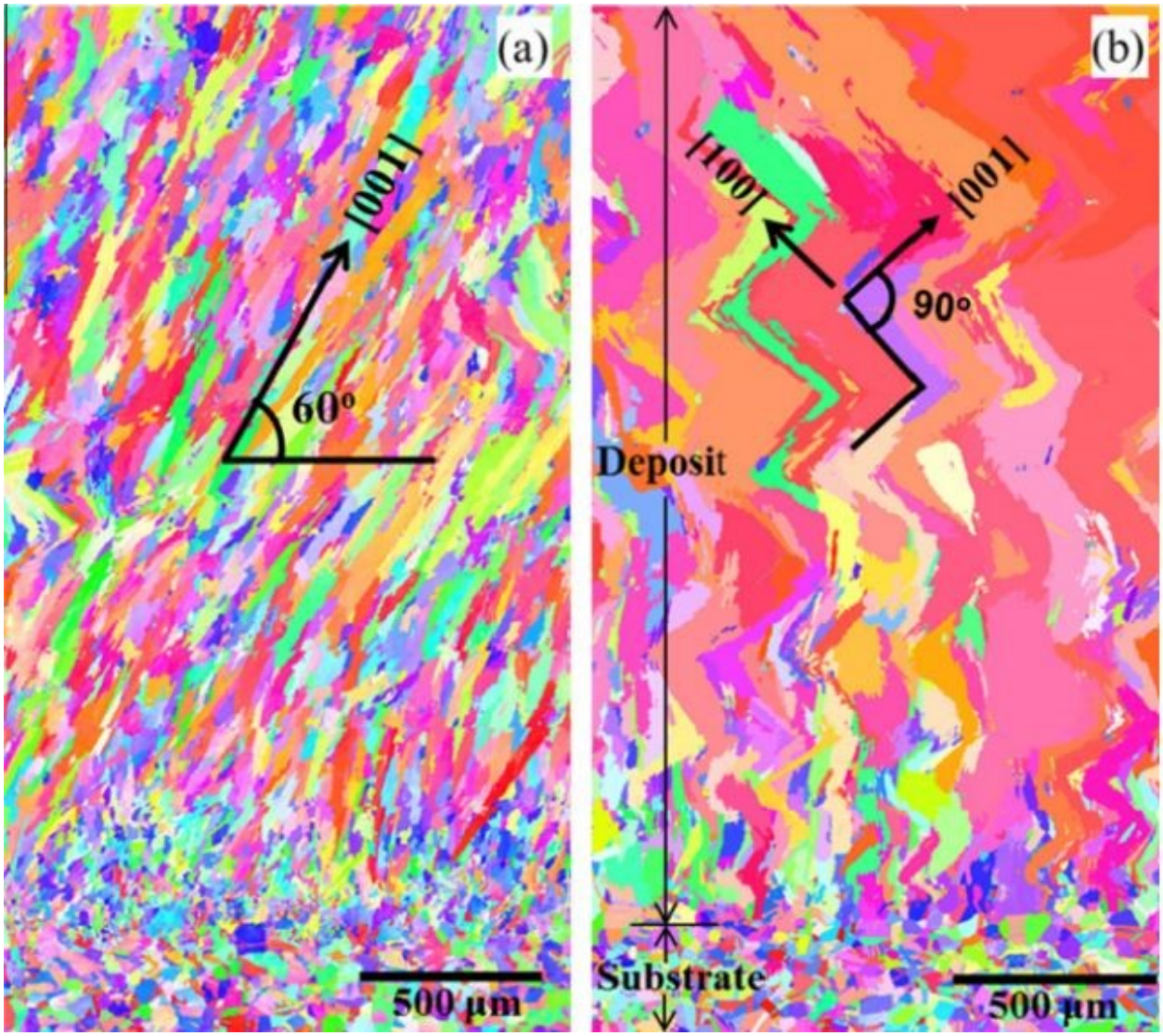

Fig. 2.18 – Solidification patterns of: a) unidirectional printed IN718 wall; b) bidirectional printed IN718 wall (from DINDA et al., 2012)

2.1.5. Switchback Welding Mode

Switchback mode is a welding technique that uses short-amplitude longitudinal oscillation of the welding torch, in contrast to the stringer mode, in which the torch moves continuously forward. This welding technique was described by KANEKO et al. (2009). According to him and illustrated in Fig. 2.19, first, a welding torch is linearly moved forward at a travel speed (S_f). After having the torch moved the forward stroke distance (S), the travelling direction is reversed, and the torch is moved backward at a travel speed (S_b). Usually S_b is the same as S_f, yet not compulsory. After the torch is moved in the backward stroke distance (B), the travelling direction is again reversed and the torch is moved forwards. Usually, the distance B is shorter than the forward stroke distance (F). In this way, a welding torch is periodically moved forwards and backward.

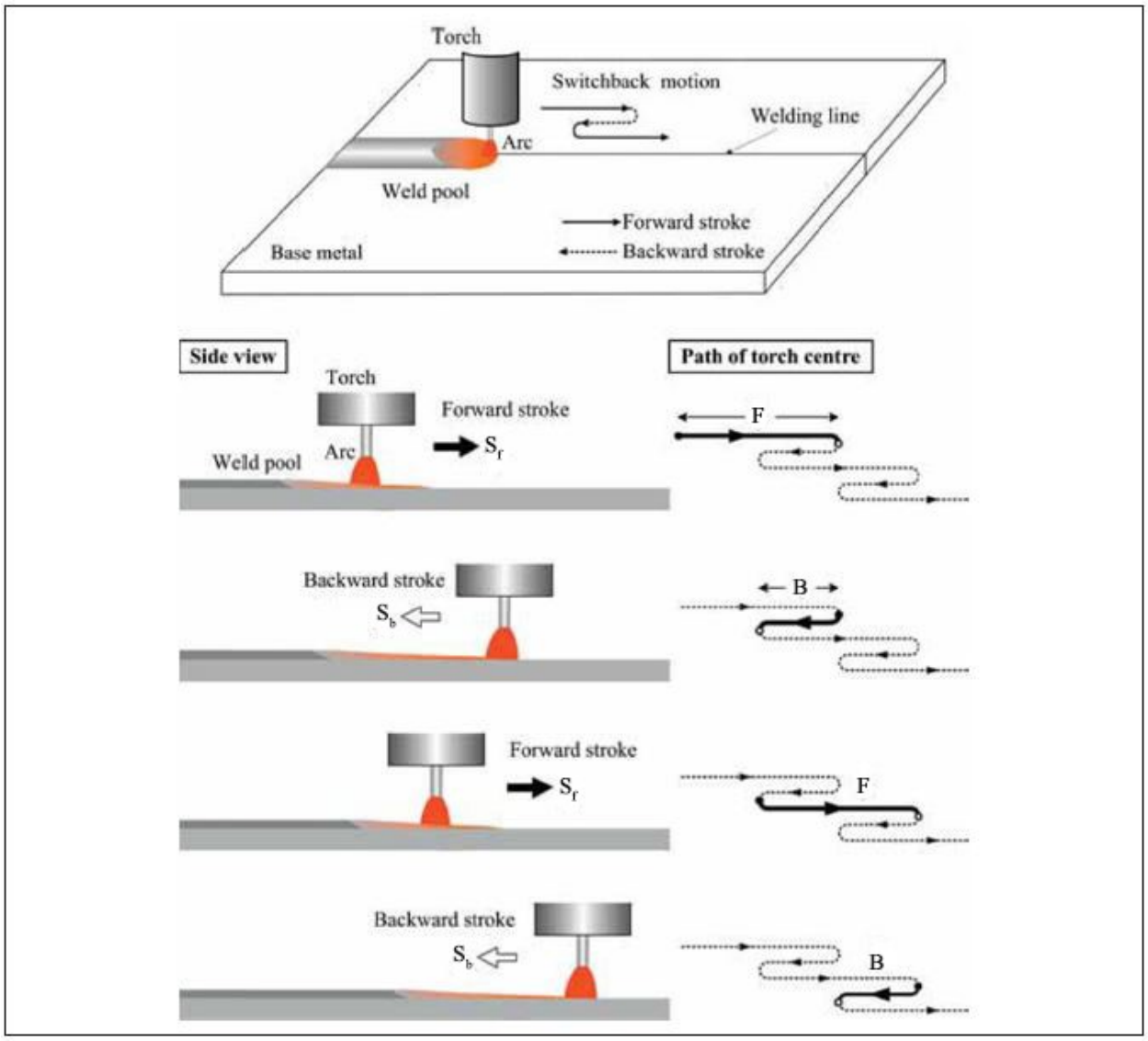

Fig. 2.19 – Switchback schematic (from KANEKO et al. 2009)

This technique was developed as a means of increasing travel speed, avoiding dragon back like bead formation. It has not been widely studied, yet there are already promising results, also in regard to metallurgical improvement. For example, ALMEIDA et al. (2012) noticed that the usage of switchback technique with selected parameters leads to the recrystallization of the bottom part of the weld bead (Fig. 2.20). Thus, in spite of the fact that switchback technique has not found wide application in welding, in the case of confirmation of expected effects from using of this technique in WAAM, it can be a good solution for preventing epitaxial columnar growths in additive manufacturing industry.

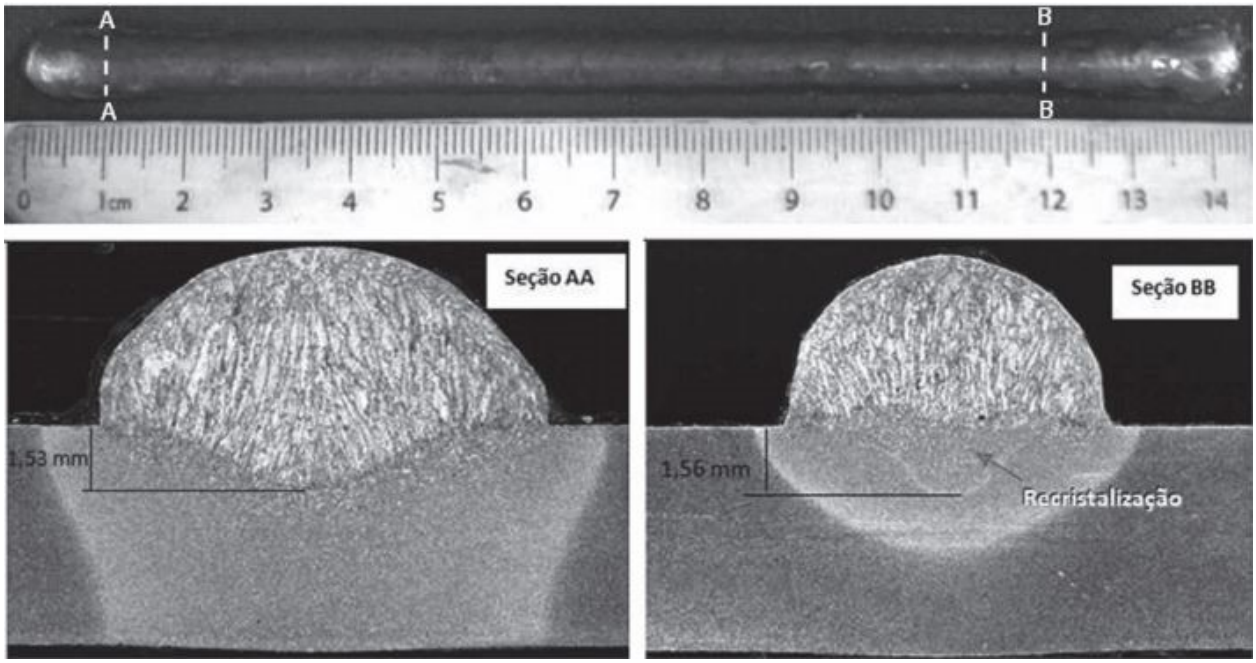

Fig. 2.20 – Cross sections at different positions of switchback welding with 140 mm of forward stroke and 140 mm of backward stroke: section AA is approximately 10 mm from the reversal point, while section B-B is at 120 mm (after ALMEIDA et al., 2012)

2.2. Objective

To assess the potential of the switchback mode technique to mitigate homoepitaxial and continuous columnar grain growth and perform grain refinement in WAAM of aluminium, as a means of avoiding the limitations of the approaches of high pressure interpass rolling and of bidirectional depositions, which are, respectively, to manufacture complicated geometrical shapes and to carry out uninterrupted deposition/overheating at the ends.

2.3. Methodology, equipment, consumables and methods

2.3.1 Methodology

To assess the application of the switchback technique for mitigating continuous columnar grain growth, the proposed methodology was to compare this approach with known benchmarks, such as unidirectional and bidirectional layer depositions, as illustrated in Fig. 2.21. Therefore, three walls using WAAM were planned. Each wall, over a same substrate size, consisted of the same number of the layers and built with the same welding process and set of parameters, such as wire (composition and size), shielding gas, arc current, arc length, travel speed (equivalent travel speed for switchback), wire feed rate, etc. One wall was produced using the same welding direction for each layer (unidirectional deposition). The second wall was printed using opposite

welding direction for each layer (bidirectional deposition). The last wall was made using switchback technique.

GENG et al. (2016) demonstrated that a bead shape stability is easily reached with WAAM when small interlayer temperature is applied (dragon back like layers appeared in the research conditions when interlayer temperatures changed from room temperature to 80 °C, and turned progressively more remarkable when the interlayer temperature reached 120 °C). Therefore, to control the interlayer temperature at each layer/wall is essential to be able to make comparisons amongst AM walls. Consequently, to prevent the big changes of heat flow amongst the layers, the first layer was deposited over the longitudinal edge of test plates of similar aluminium and the start/interlayer temperature before each layer was kept as much the same as possible.

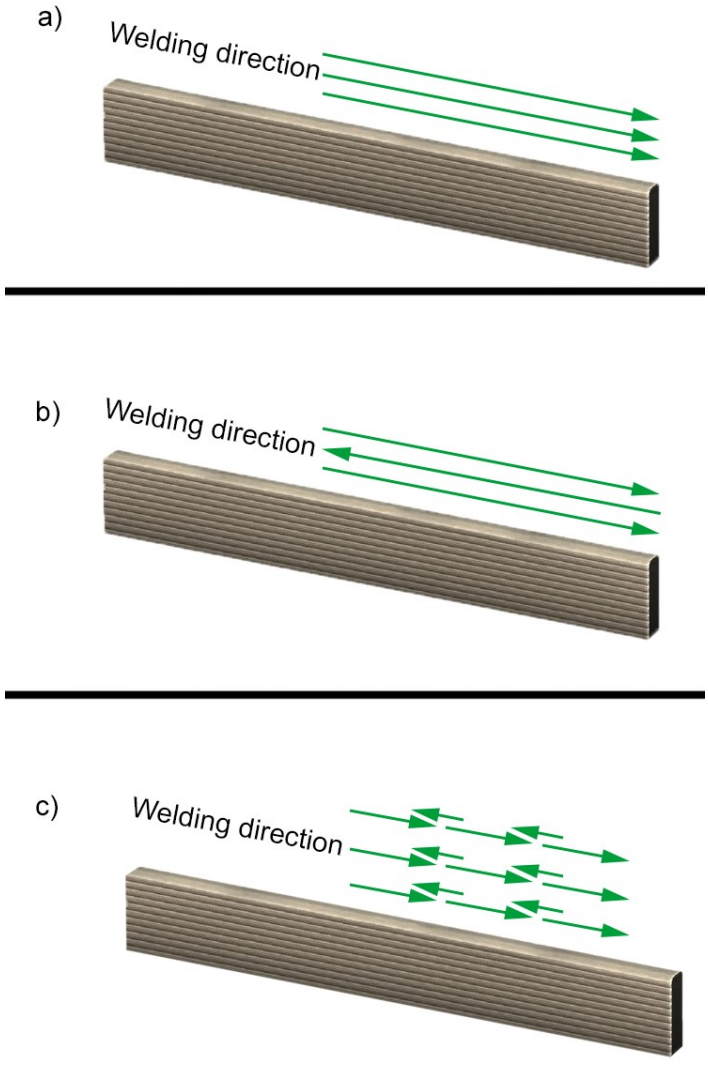

Fig. 2.21 – Schematic of the wall printing procedures: a) Unidirectional deposition (without changing of the deposition direction); b) Bidirectional deposition (deposition with changes of the welding direction); c) switchback deposition

The produced walls were compared to each other in terms of some criterial parameters. These parameters can be divided into two groups:

- Quality parameters;
- Economical parameters.

Quality parameters have direct relation to the subject of the work, i.e., they can affect mechanical properties of the printed part. The chosen quality parameters in this work were microstructure (grain growth pattern and grain sizes) and porosity. Economical parameters are the ones that can increase the economical attractiveness of the WAAM, based on the wall geometry (average height and width and buy-to-apply factor).

2.3.2. Experimental procedure

In the scope of this work, a GMAW Fronius CMT (Fig. 2.24) was chosen as deposition process, due to its low heat input (Almeida et al., 2010) that provides lower layer distortion. In addition, CMT is qualified by the author as the most efficient arc welding process to accomplish the three Laprosolda's commandments, as described in section 2.1.2. A computer numerically controlled (CNC) customized 3-xis worktable was chosen instead of a robotic system because it can be easily programmed by G-Code to weld any geometrical configuration if needed. The welding torch moved only in the z axis, while the support with fixed test plate moved on the horizontal plane. To protect the welding zone, a home designed trailing gas device was used. The experimental rig with mounted support and trailing gas is shown on Fig.2.22.

The printed walls consisted of 15 layers. The first layer was deposited over the longitudinal edge of test plates of a commercially pure aluminium (190 x 50 x 6 mm), nominal composition shown in Table 2.2, fixed in a plate holder as illustrated in Fig.2.23. An advantage of this approach is to reduce thermal buckling of the substrate, considering the higher moment of inertia of this plate positioning. Substrate bucking during the deposition would interfere in the layers formation, impairing the comparisons. The criterion to keep the same interlayer temperature was to cool down the walls after each layer deposition with the aid of compressed air until the different parts of the walls could be grasped with bare hands.

Table 2.2 – Nominal chemical composition of the pure commercial aluminium

	%					
	Al	**Mn**	**Cu**	**Si**	**Zn**	**Fe**
Min	base	-	0.05	-	-	-
max		0.05	0.02	0.95	0.1	0.95

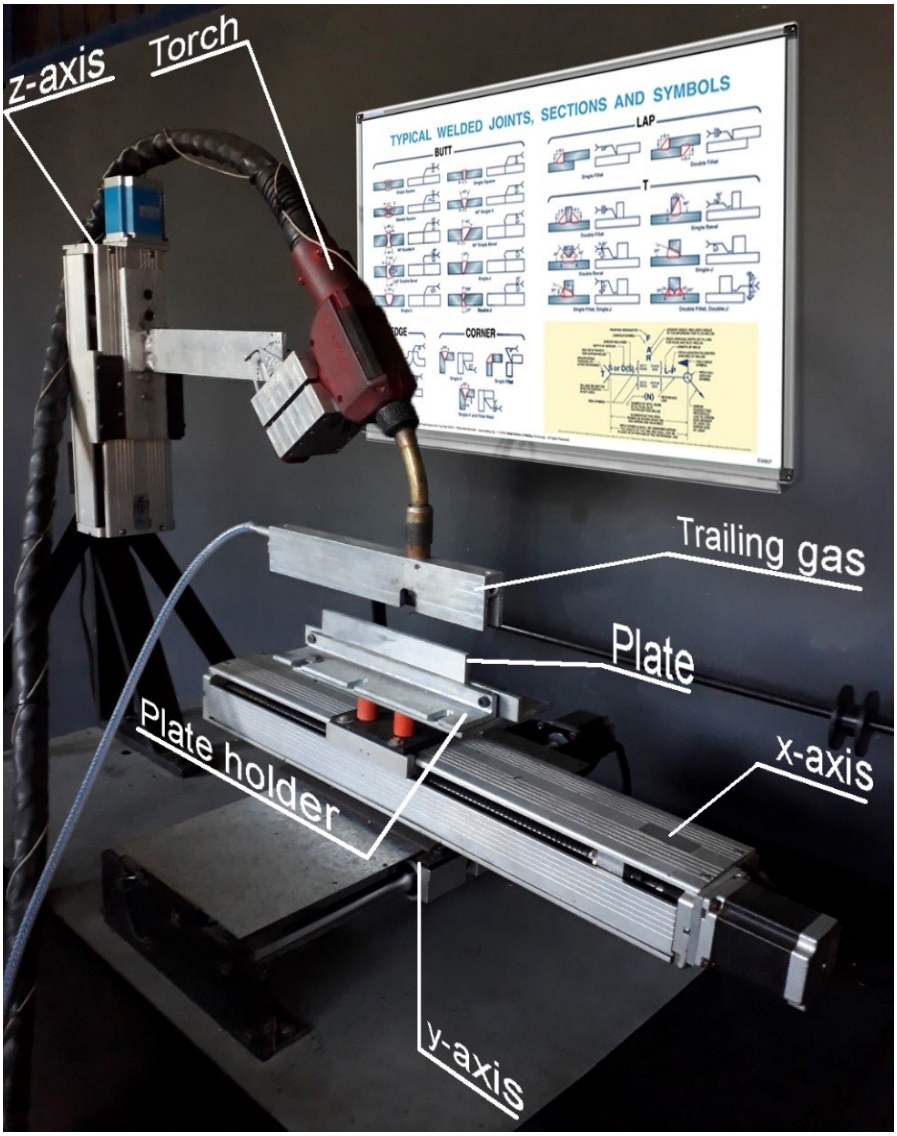

Fig. 2.22 – Experimental rig

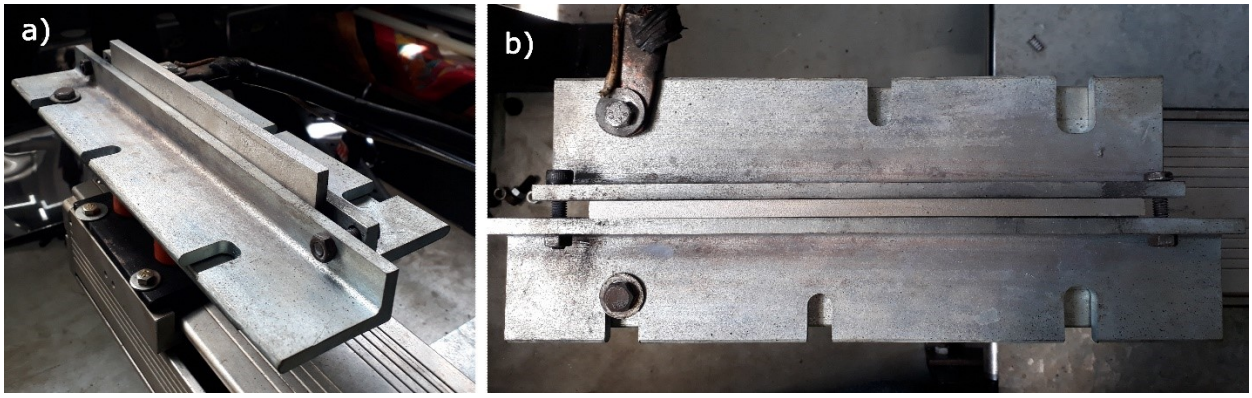

Fig. 2.23 – Test plate and plate holder: a) perspective view b) top view

The common set parameters for the all three experiments were:

- Welding wire = AWS /SFA 5.10 ER5356 (Al-Mg5) (nominal chemical composition is shown in Table 2.3)

- Welding current (I) = 81 A;
- Wire feed speed (WFS) = 4,9 m/min
- Contact tip-work distance (CTWD) =15 mm;
- Shielding gas: Ar 4.5;
- Shielding gas flow (GFR) =15 l/min;
- Equivalent Travel speed (TS_{eq}) = 420 mm/min.

Table 2.3 – Nominal chemical composition of the AWS /SFA 5.10 ER5356 (Al-Mg5) wire

	%									
	Al	**Mg**	**Ti**	**Mn**	**Cr**	**Cu**	**Si**	**Zn**	**Fe**	**Be**
Min	base	4.5	0.06	0.05	0.05	-	-	-	-	-
max		5.5	0.2	0.2	0.2	0.1	0.25	0.1	0.4	0.0008

Fig. 2.24 – Fronius CMT power source

Note: Equivalent travel speed is the speed needed to deposit one given layer length. For unidirectional and bidirectional experiments, equivalent travel speed is the same as travel speed (TS_{eq} = TS). For switchback, an equivalent travel speed must be calculated, as follows:

As seen in Fig. 2.25, Switchback has distinguishable set parameters, such as oscillation frequency (f), oscillation amplitude (Amp), forward stroke length (F), backward stroke length (B), forward stroke speed (S_F) and backward stroke speed (S_B). To keep the same TS, each deposit should be kept the same deposition time (t) to accomplish the same layer length (L_L).

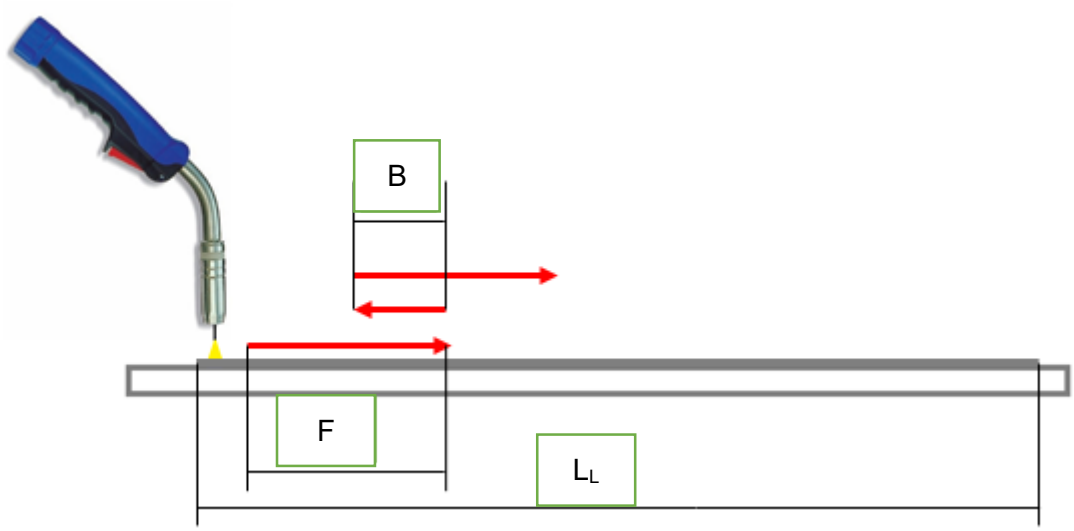

Fig. 2.25 – Switchback distance parameters

The travel speed (TS) is defined as:

$$TS = \frac{L_L}{t} \tag{2.1}$$

where L_L is the length of the layer and t is the deposition time.

During stringer bead torch movement, L_L is equal to the total path of the torch, but during switchback the torch pass (L_{sb}) is longer than L_L. L_{sb} is given by Eq. 2.2.

$$L_{sb=} mF + nB \tag{2.2}$$

where F is the forward stroke length, B is the backward stroke length, *m* is the number of times that the torch moves forward in one full layer deposition length (L_L), *n* is the number of times that the backward happens (*n* = *m* -1). Thus, Equation 2.2 can be re-written as in Equation 2.3.

$$L_{sb=} m\,(F + B) - B \tag{2.3}$$

The equivalent travel speed (TS_{eq}) can also be calculated by using Eq. 2.4.

$$TS_{eq} = \frac{L_{sb}}{t} \tag{2.4}$$

The oscillation frequency (F_{osc}) is given by using Eq. 2.5.

$$F_{osc} = \frac{m}{t} \tag{2.5}$$

At last, as mentioned before, for comparison purpose, the Equivalent Travel speed (TS_{eq}) of a switchback mode must be the same as the travel speed (TS) of the uni and bi-directional modes. And so should be the deposition times (t), which can be calculated for a given desirable travel speed (TS) and length of the layers (L_L) by using equation 2.1. The advantage of using

forward and backward stroke lengths as in Eq. 2.2 rather than using forward and backward stroke speeds is to avoid errors due to acceleration and decelerations during the direction reversions.

F and B are values that should be selected experimentally or based on the practical experience to reach sound deposition layers. For a determined deposition time (t), the switchback torch pass (L_{sb}) can be determined by using Equation 2.3. Therefore, *m*, and, consequently, *n*, can be calculated by Eq. 2.2.

In the present work, it was defined L_L = 190mm, F = 6 mm, B = 3mm. As the torch speed for forward and backward strokes can be different, accordingly, there will exist the forward stroke speed (S_F) and backward stroke speed (S_B). However, in the present work, both speeds were set as the same, i.e., $S_F = S_B$. Using the above reasoning, *t* was determined as 28.6 s, *m* = 66 and *n* = 65. The set switchback parameters used in the present work are shown on Table 2.4.

Table 2.4 – set switchback parameters

Forward stroke length (mm)	F	6
Backward stroke length (mm)	B	3
Equivalent travel speed (mm/min)	TS_{eq}	420
Set travel speed (mm/min)	$S_F = S_B$	1230
Oscillation frequency (Hz)	F_{osc}	2,2

Monitoring of welding parameters is a means of analyzing the stability of the welding process. Thus, during the metal deposition data acquisition of the following welding parameters was carried:

- Arc voltage;
- Welding current;
- Wire feed speed.

These data acquisitions were carried with the aid of a National Instruments NI-6009 data acquisition board. WFS was monitored through an encoder based sensor. Data computation was carried out with a home designed software using a NI LabVIEW 2016 platform.

2.3.3. Determination of the Quality and Economical parameters

For texture visualization of the columnar growth patterns of each wall (a quality parameter), longitudinal sections of the walls were taken at specific places (Fig. 2.26). The samples were milled to remove half of the thickness, then grinded with sandpapers from 400 to 1200 mesh, polished with aluminium oxide of 5 um and etched with a 20% HF acid solution in water for 15 seconds. Optical microscopy with polarized light was used to expose the microstructures. Macrographic photos were taken from longitudinal and cross sections of the

walls. Micrograph and geometry analysis was carried out by aid of a Nikon D5000 camera installed in the optical microscope (Fig. 2.27).

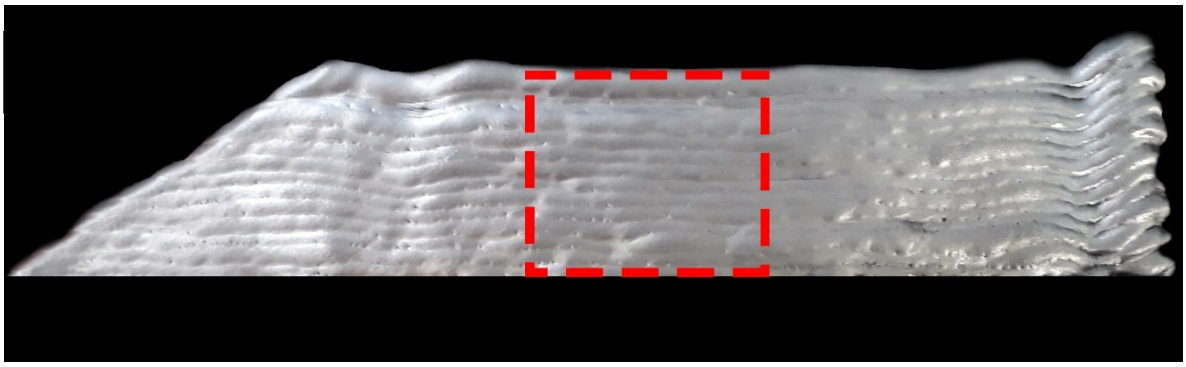

Fig. 2.26 – Longitudinal sampling for micrography analysis taken from each wall

Fig. 2.27 – Olympus BX51M optical microscope

Average grain size was measured according to the ASTM E112-12 standard. According to this standard, the planimetric procedure was chosen. In this procedure, a circle or rectangle (rectangle was used to simplify the calculations) of a known area (1,2 x 1,2 mm or 1,44 mm^2) was superimposed the micrographies. Area of the rectangle must be large enough to embrace at least 50 grains. Then, the number of grains that are completely within the area (N_{inside}) and number of grains intersected by the circumference of the area ($N_{intersected}$) are counted. After that, the number of the grains per area can be calculated by the following equation:

$$N` = N_{inside} + \frac{N_{intersected}}{2} \quad (2.6)$$

The number of grains per mm^2 (N) is reached by Eq. 2.7

$$N = \frac{N`}{A} \tag{2.7}$$

where A is real area of the used rectangle.

Next step is to calculate the Grain size number (G). It can be done by the Eq. 2.8:

$$G = 2 * \frac{\log N}{\log 2} + 1 \tag{2.8}$$

The Grain size number allow to estimate the grain size by the proper tables (ASTM E112-13).

Another approach is to calculate the average grain diameter. For that, it is needed to mark two vertical lines on the specified area (total length of the lines would be doubled length of the side of the used rectangle, i.e., in our case it would be 2,4 mm) and count grain intersections with these two lines. Eq. 2.9 (D_g) gives the average grain diameter

$$D_g = \frac{L}{N_i} \tag{2.9}$$

where L is total length of the lines and N_i is the number of intersected grains.

All operations related to the grain size measuring were repeated over three different areas of each wall sample.

For porosity measurements, another set of walls were built up (unidirectional mode, bidirectional mode and switchback mode). Samples of the same height and length were cut from the middle part of the walls. A sample of the substrate material with same dimension was taken. A gravimetry method was used to evaluate the presence of pores in samples removed from the walls. Gravimetry is based on the Archimedes principle, i.e., on the analysis of the forces acting on the samples outside and inside water. The final result does not show the number of pores and their dimensions, but the percentage of voids in relation to a reference (a sample considered pores free). This method had been successfully applied to measure pores by DA SILVA and SCOTTI (2006). In their work pores in aluminium welds were measured using this approach and compared with X-Ray determinations.

According to the procedure, the sample is weighed in a precision scale in air and "floating" inside a container with water. When in water, there is the presence of the upthrusting force (E) and the weight force (W_c). Upthrusting force, also called buoyant force, is the force that the liquid exerts on an object that is in a liquid. The upthrusting force when a body is floating in water is given by Eq. 2.10.

$$E = g * \rho_f * V_f \tag{2.10}$$

where g = 9,78 m/s^2 (local gravity acceleration), ρ_f = 1 g/cm^3 (water density) and. V_f, in cm^3, refers to the volume of water displaced by the body immersion in the fluid, i.e., the body volume itself. Considering the definition of ρ_f, the upthrusting can be related to the fluid mass (m_f) as expressed by Eq. 2.12. Fluid mass (m_f) is easier to be more accurately measured than fluid volume (V_f).

$$\rho_f = \frac{m_f}{V_f} \tag{2.11}$$

$$E = g * m_f \quad (2.12)$$

It is important to say that in air, due to the environment low density, the upthrusting force is negligible. Therefore, the weight of a body (W_c) can be precisely measured in a scale.

From the gravimetry measurement point of view, when a body of mass m_c and weight W_c is submerged in water, there will be an apparent decreasing of its weight related to the difference in the upthrusting forces, as meant by Eq. 2.13.

$$E = W_c - W_{H_2O} \quad (2.13)$$

where W_{H2O} is the weight of the sample in water and m_{H2O} its mass in water.

Consequently, body density (ρ_c) can be estimated by correlating its weight W_c and its apparent weight W_{H2O}, as in Eq. 14.

$$m_f * g = m_c * g - m_{H_2O} * g \quad (2.14)$$

The volume of the body can be calculated by Eq. 2.15.

$$V_c = \frac{m_c}{\rho_c} \quad (2.15)$$

Replacing m_f (Eq. 2.9) and m_c into Eq. 2.14 and eliminating the common g in all terms, then the body density can be calculated by Eq. 2.16.

$$\rho_c = \frac{m_c}{m_c - m_{H_2O}} \quad (2.16)$$

Finally, a reference density value is required to obtain the porosity of the body. As soon as it would be difficult to take the wire as a reference, it was decided to use the substrate material as a reference (assuming to have no pores). Measured density of the substrate commercial aluminium alloy is known (ρ_{Al} = 2,728). Thus, the percentage of the pores volume can be calculated using the equation 2.17.

$$V_p = (\rho_{Al} - \rho_c) * \frac{100}{\rho_{Al}} \quad (2.17)$$

Concerning now the determination of the economical parameters, the geometry of the wall was carried out through wall cross sections taken at similar positions of the samples for longitudinal sectioning (Fig. 2.28). The most important geometric parameters were the average height per layer, full area of the layers, maximum effective area of the layers and average width of the wall. It is important to notice that during the wall build-ups, a degree of nonconformity was apparent, i.e., walls showed distortion in relation to the Z axis. It was assumed in this work that this happening was not a problem of deposition mode, but probably an equipment related problem. It was assumed as well that this distortion is prone to be avoided by implementation of a control system that would correct torch position during the welding. However, to eliminate the influence of this distortion on the results, it was necessary to adopt a compensation criterion, as follows:

Measurement of the geometrical characteristics (using the open source program ImageJ) was made in four steps. First one was to discharge the two first and two last layers (Fig. 2.29(a)). The second step was to define the center points of the deposited layers, as suggested in Fig. 2.29(b). The third step was to simulate a rectification (straightening) of the wall images, trying to

follow a center line passing through each deposited layer center point, as suggested in Fig. 2.30, rather than assuming an average wall centerline. Therefore, the wall heights were determined based on the rectified lines.

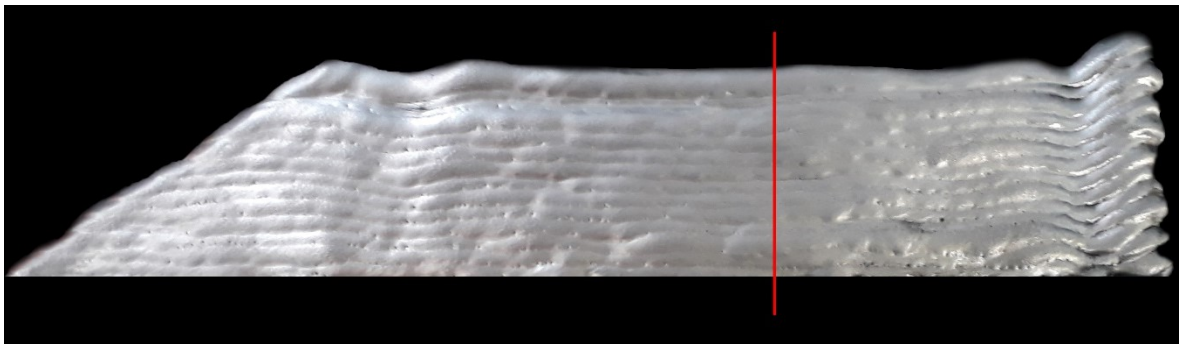

Fig. 2.28 - Place from where cross sections for macrography were taken from each wall

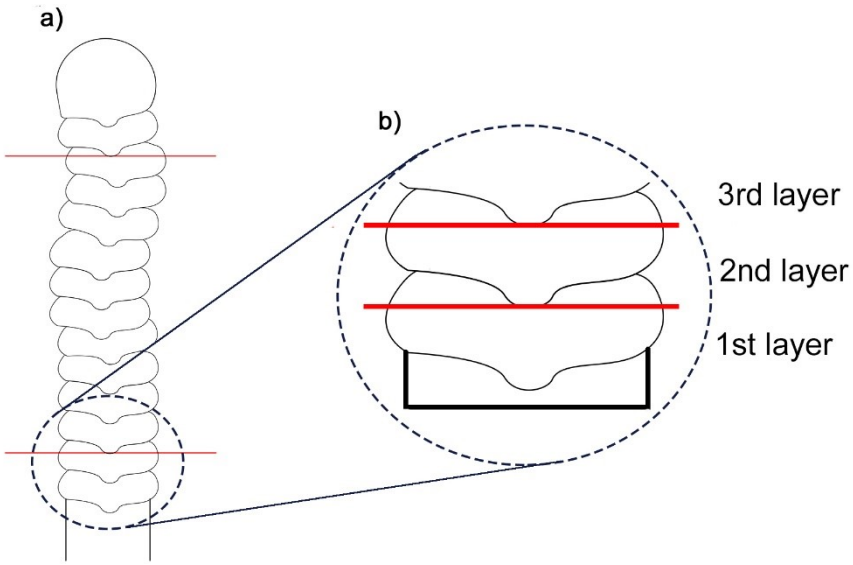

Fig. 2.29 – a) Discharging of first and last two layers; b) Subjective criterion to determine the center points (red line facing the lowest part of each deposition) and heights of the deposited layers (distance between each red line facing the lowest part of each deposition)

The forth step was to measure the full and effective areas of the deposited layers. Maximum effective area is defined here as the largest area of the wall that can be used after machining, and usually are determined by inscribed rectangles within the full areas. As analog as the principle applied to rectify the wall heights, the inscribed rectangles (better saying polygons) should also be oriented by the trajectory of the wall formation. Fig. 2.31 illustrates the measurement of both full area and effective area.

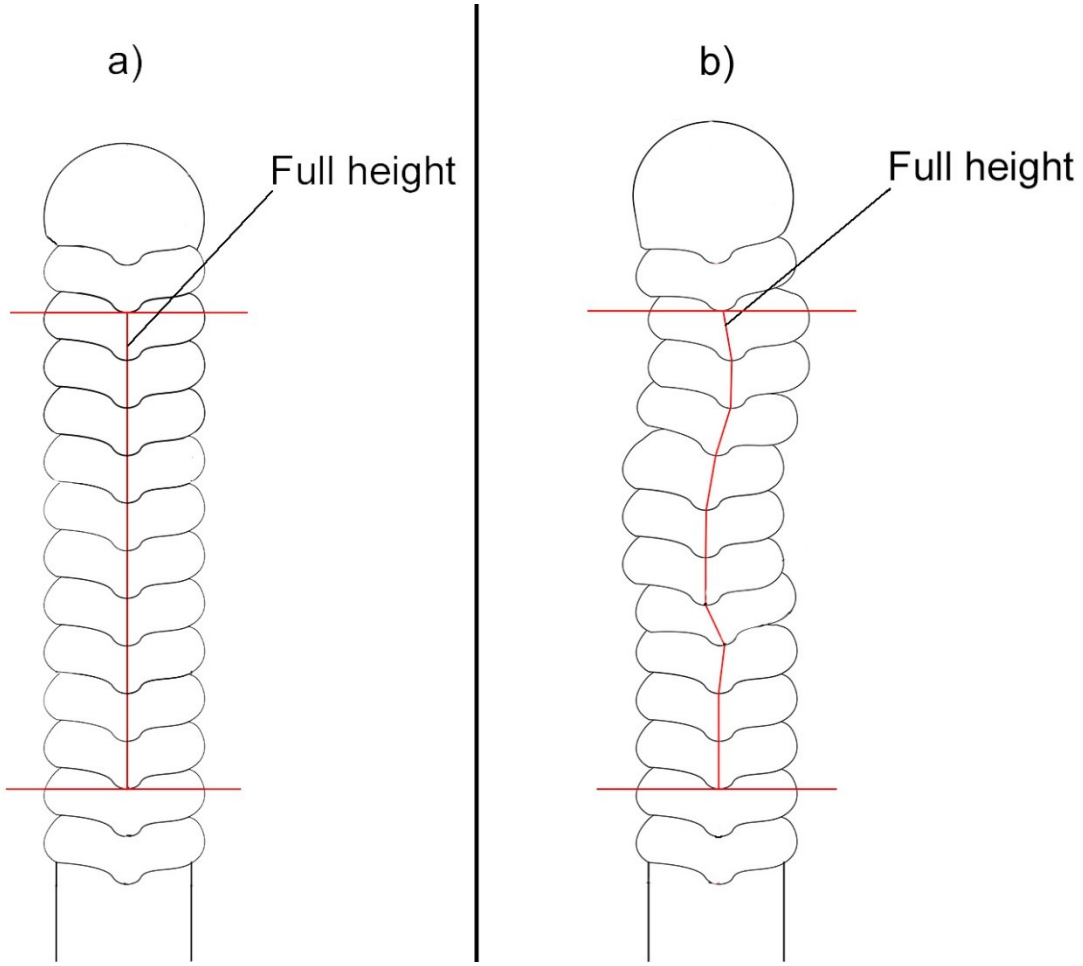

Fig. 2.30 – Subjective criterion to determine the wall height by rectifying (straightening out) the Z-axis distortions: (a) straight wall; (b) distorted wall

Height per layer, average effective width and buy-to-apply factor are calculated after the measurements from the four steps. Height per layer is the ratio between the measured layer height and the number of included layers. From the maximum effective area, the effective width can be estimated through dividing it by layer height. And, finally, buy-to-apply factor is here defined as the ration between full area and maximum effective area of each wall. This factor quantifies the percentage of metal that should be removed from the near net shape to obtain maximum useful thickness: the closer to unit is that ratio, the less machining is needed to reach the net shape.

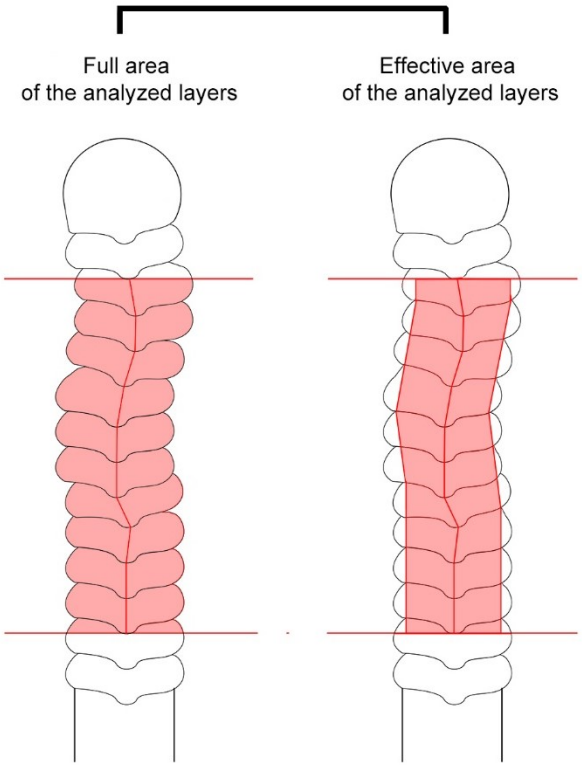

Fig. 2.31 – Full and effective area measurement schematic

2.4. Results and Discussion

2.4.1. Monitoring of the deposition parameter

Fig.2.32, Fig. 2.33 and Fig. 2.34 shows the average welding current, wire feed speed and voltage values, respectively for each layer of each wall. As seen, monitored current corresponds to the set parameters. The average monitored current was about 85 A, the average wire feed speed was about 5 m/min and average voltage was about 12,5 V. However, the parameter of most interest in the scope of this work is welding current, because it governs the heat input, consequently grain growth and bead formation.

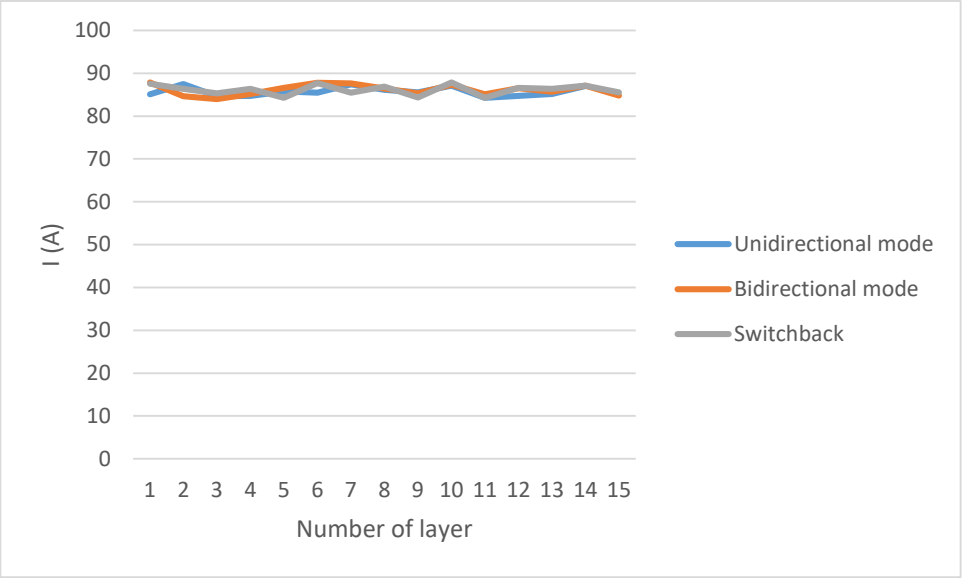

Fig. 2.32 – Comparison of average current for each welding technique with respect to each layer

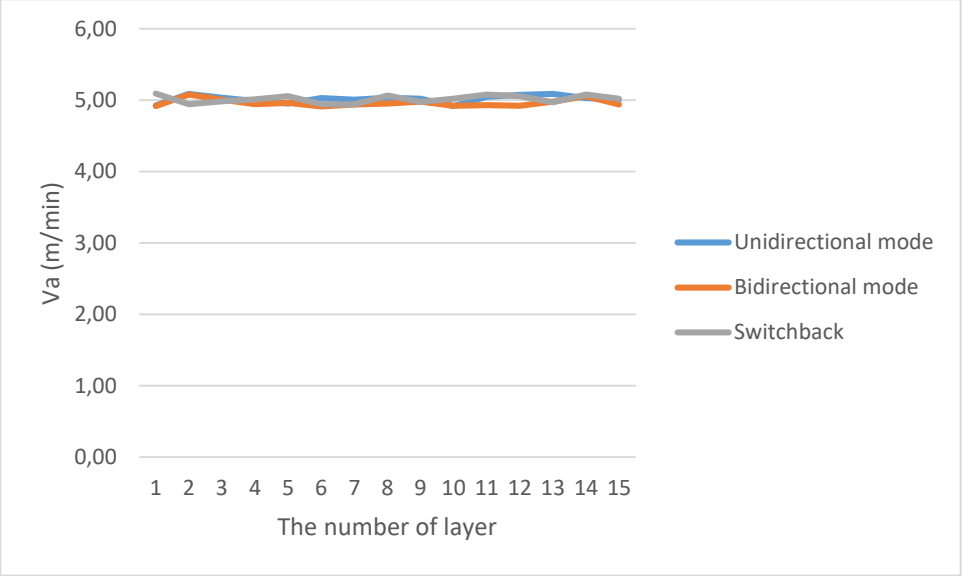

Fig. 2.33 – Comparison of wire feed speed average value for each welding technique

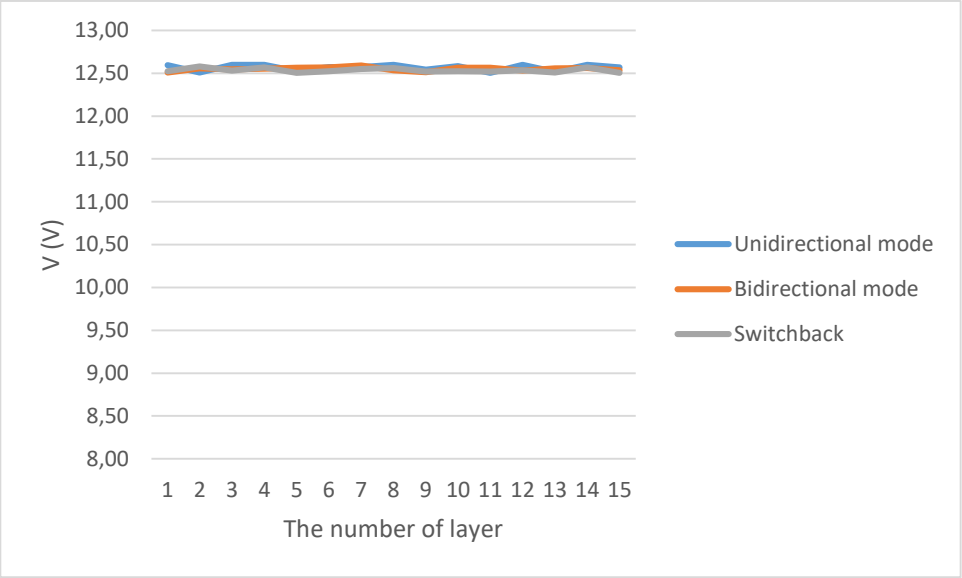

Fig. 2.34 – Comparison of average voltage for each welding technique with respect to each layer

2.4.2. Visual analysis

Fig. 2.35 present the general aspects of the 3 walls. As one can see, there is significant difference amongst the walls. The wall built-up by unidirectional welding (Fig. 2.35(a)) has a hump at the layer deposition start point and a descendent ramp at the end. In relation to WAAM of aluminium, this humping is due to the high cooling rate when each layer deposition starts (cold wall material). As long as the heat distribution along the wall reaches the steady state, the humping disappears. Due to analog effect, yet inverse, at the end of the layers, one can see the opposite situation (descendent ramp rather than humping). To avoid these effects, operational parameters corrections can be applied in manufacturing of actual parts.

The wall printed using switchback technique (Fig. 2.35(c)) presented the same behavior as the unidirectional deposition in relation to the presence of humping at the beginning and descent ramp at the end. Despite this, much better regularity and smoothness of the surface is perceived. In the wall made using bidirectional depositions (Fig. 2.35(b)), humping was not observed, once the humps are remelted at the end of each layer.

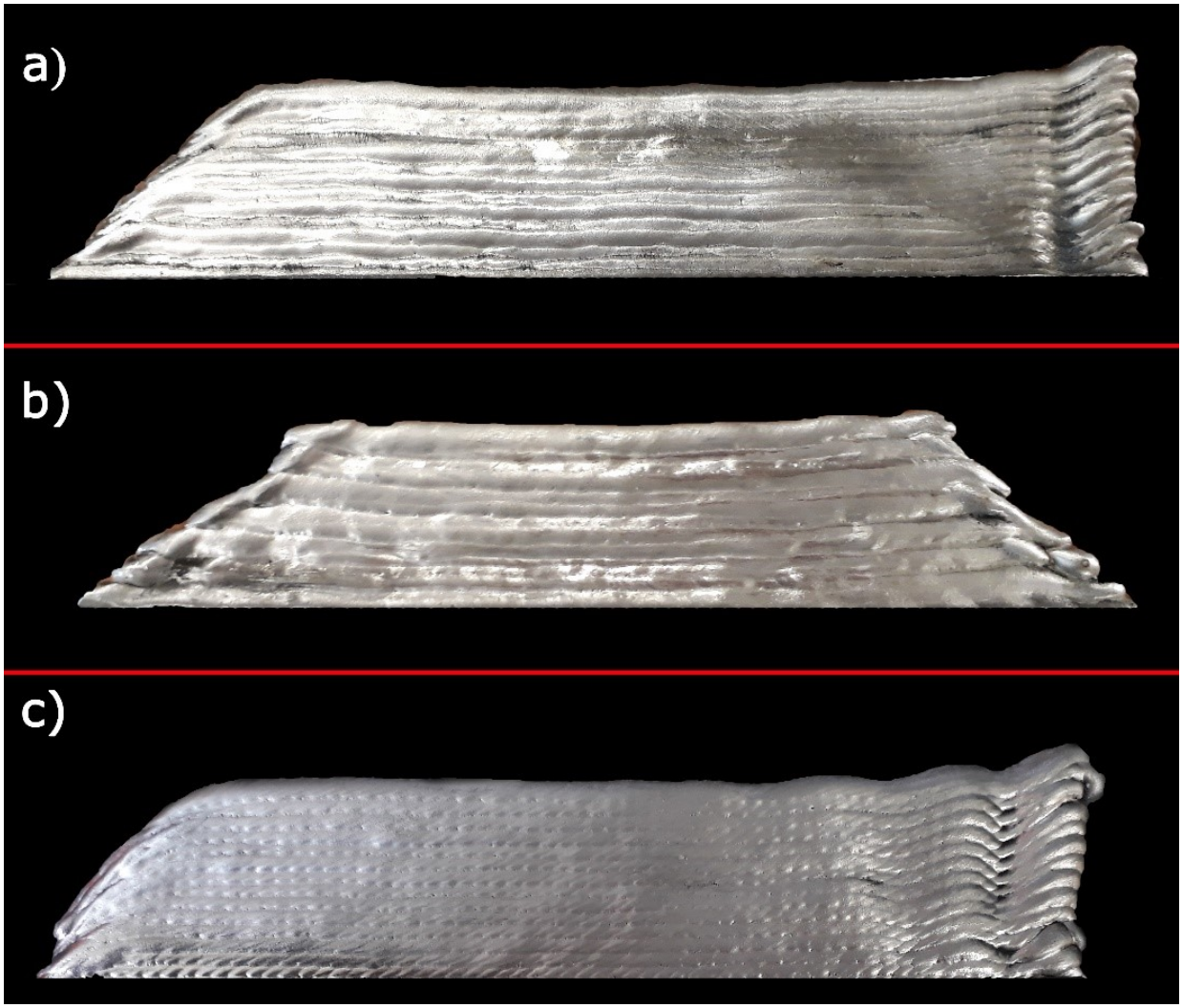

Fig. 2.35 – Walls built up using different techniques: a) unidirectional welding; b) bidirectional welding; c) switchback mode (for (a) and (b) modes, the welding direction was from right to left)

2.4.3. Microstructural analysis

Considering that the main scope of this work is related to columnar epitaxial grain growth and microstructural refinement, Fig. 2.37(a) and (b) initially makes clear that the unidirectional and bidirectional dispositions, as expected, presented typical solidification patterns, respectively with continuous columnar growth and zig-zag like columnar growth. These phenomena have already been reported by several researchers, amongst them PARIMI et al. (2014), as illustrated in Fig. 2.36. Figure 2.37(c), deposited with switchback mode, suggest no trends concerning direction of the epitaxial columnar grain growth. As mentioned before, from this characteristic of the switchback mode of deposition one can expected much more isotropic properties of the wall.

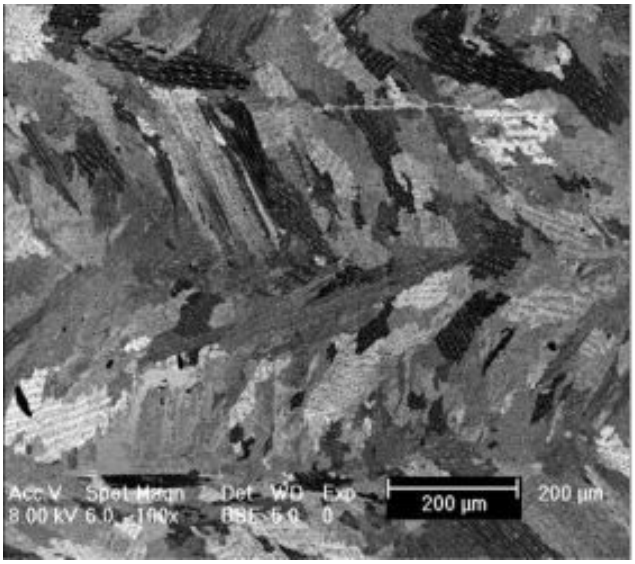

Fig. 2.36 – Zig-Zag grain growth during bidirectional laser deposition of IN718 (from PARIMI et al., 2014)

Fig. 2.38 present an amplification of the microstructures presented in Fig. 2.37. Visually, one cannot see remarkable differences in grain sizes. However, the quantification of the grain sizes applied on the same longitudinal sections shows, as summarized in Table 2.5, smaller grains when bidirectional and switchback modes were applied.

Note: measuring was carried on 6 different sections of micrograph for each specimen, in Table 2.5 are presented the average values.

The reason for grain refinement with bidirectional deposition mode may be based on the breakage of the growth direction at each deposited layer surface, which happens following the direction of the maximum temperature gradient. Switchback, on the other hand, plays the same role, yet in a much shorter decomposition length. This latter fact may justify the same level of grain refinement of both bidirectional and switchback modes.

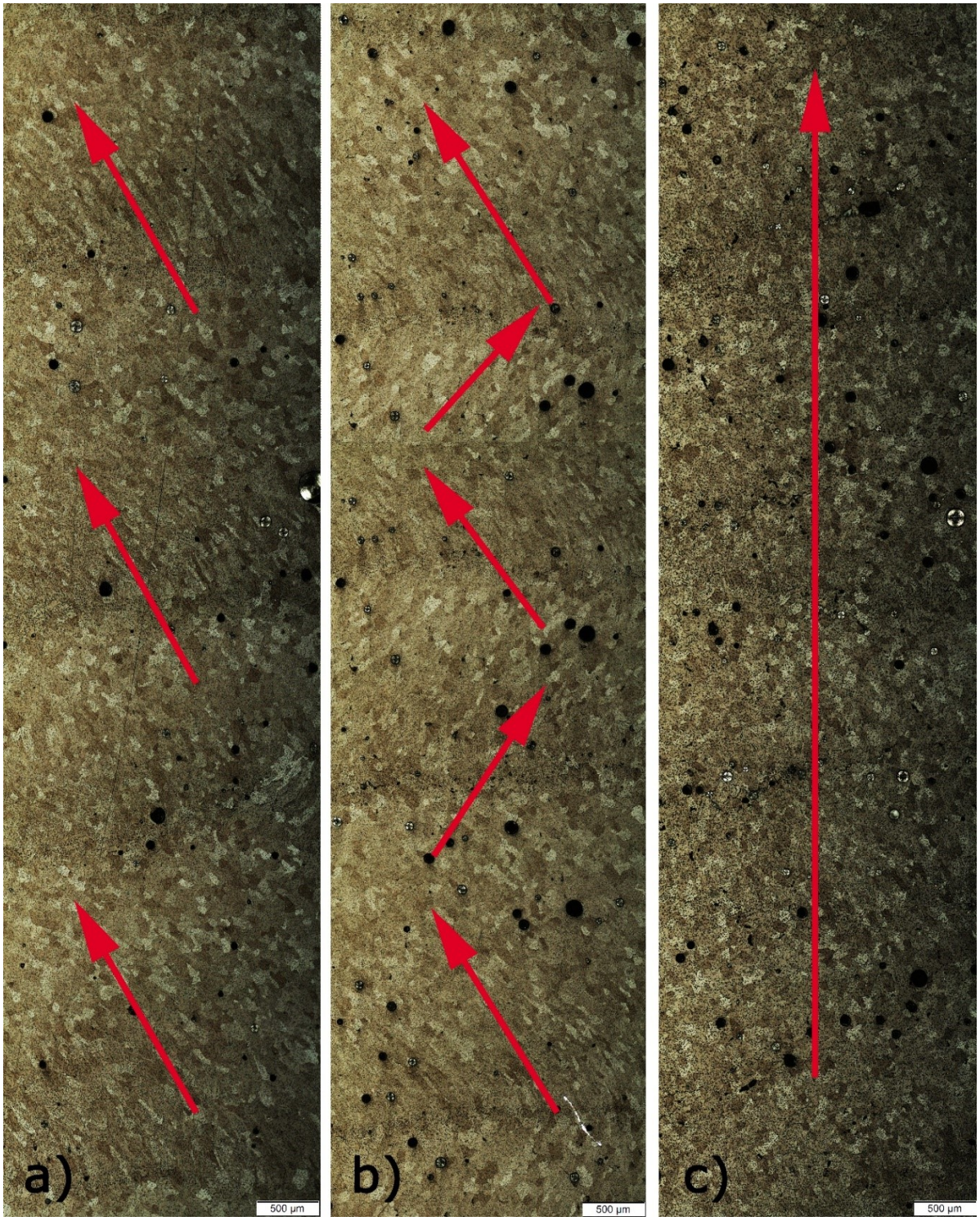

Fig. 2.37 – Longitudinal macrostructures of the walls, emphasizing the pattern of columnar grain growth: a) unidirectional mode; b) bidirectional mode; c) switchback mode (amplification of a cross section from the 4th to the 8th layers of each wall)

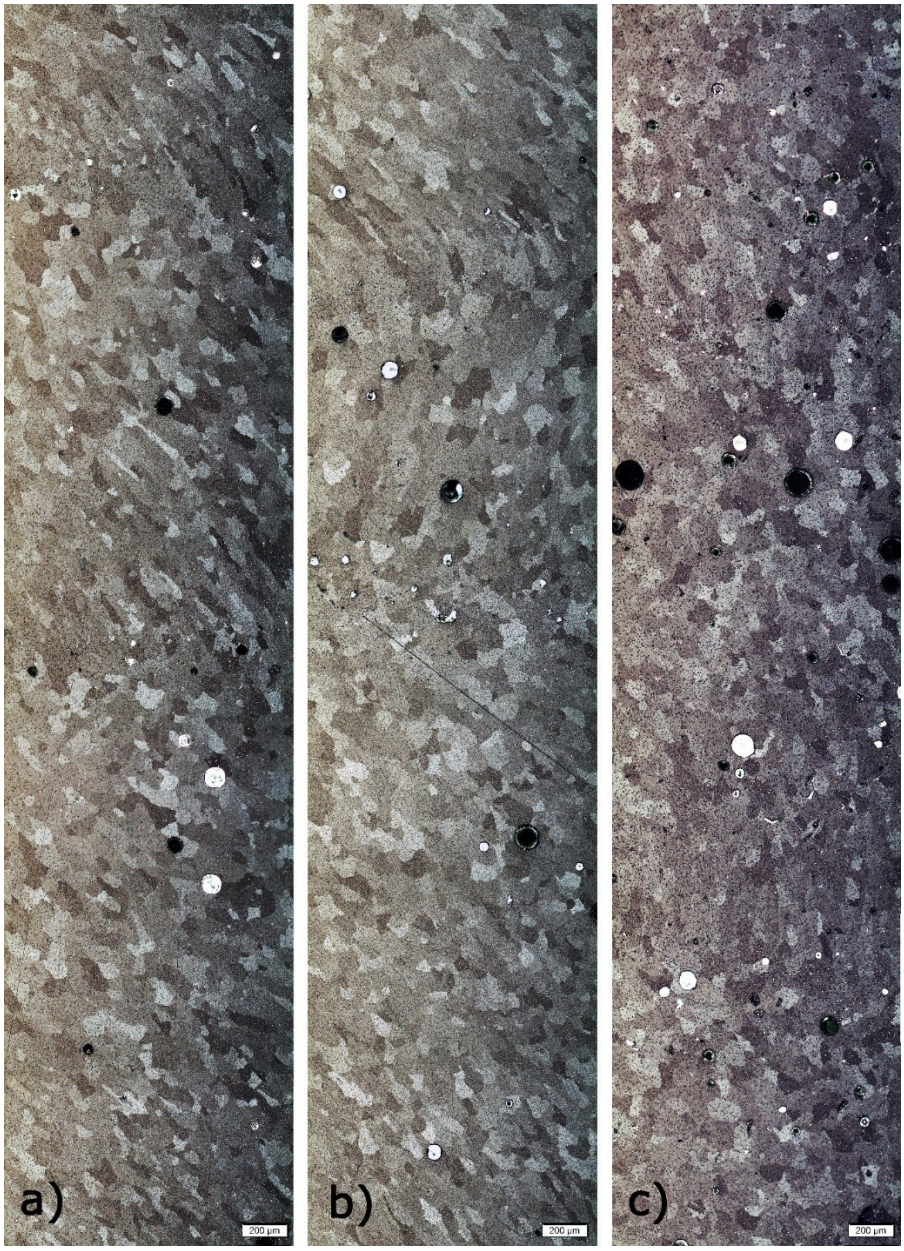

Fig. 2.38 – Longitudinal microstructures of the walls, emphasizing the grains sizes: a) unidirectional mode; b) bidirectional mode; c) switchback mode (amplification of a cross section from the 5th to the 7th layers of each wall)

Despite all advantages so far obtained by the switchback technique applied to WAAM of an aluminium alloy, and interesting microstructure related phenomenon was observed when this deposition mode is applied. As seen in Fig. 2.39, black dots are present and spread on the microstructures. TANSKI et al. (2017), when studying the microstructure and mechanical properties of two binary AlMg3 and AlMg5 alloys deformed using equal channel angular pressing (the method in which the workpiece is successively extruded through several channels of the same cross-section, intersecting at an angle.) on alloy, observed these black dots too. They suggested, using also transmission electron microscopy, that these back dots are β-Al3Mg2 phase built into an α-Al matrix. However, one can also see that on the micrography of the samples

taken from the wall printed using of the switchback deposition mode that the dots are bigger than on the other two samples. Based on Fig. 2.40, one can suggest that dots tended to gather in clusters on the grain borders with the switchback mode, likely due to more frequent heating cycles.

Table 2.5 – Grain sizes of the wall microstructures (according to ASTM E112-12 standard)

Sample	Average Number of grains per square millimeter, units/mm^2	ASTM Grain number	Average grain diameter, mm	Standard deviation of the grain diameter
Unidirectional mode	84.3	7.4	0.064	0.002
Bidirectional mode	92.8	7.5	0.058	0.001
Switchback mode	101.0	7.7	0.054	0.001

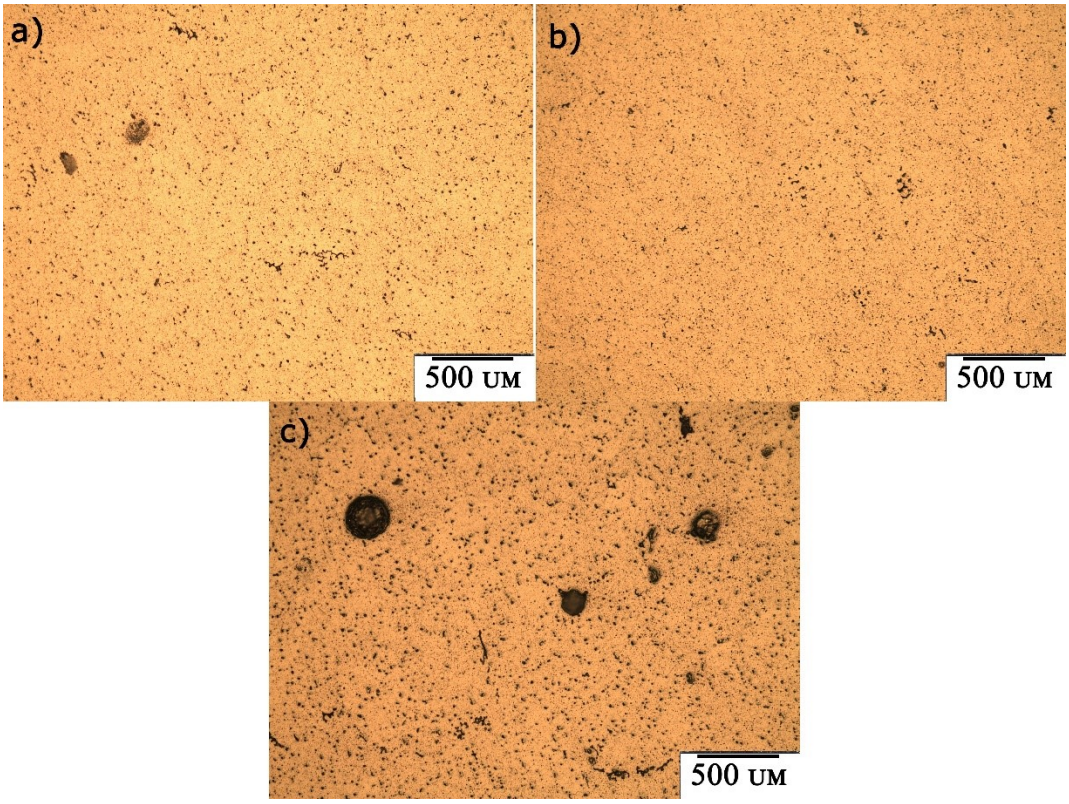

Fig. 2.39 – Microstructure of the walls, using bright field: a) unidirectional mode; b) bidirectional mode; c) switchback mode

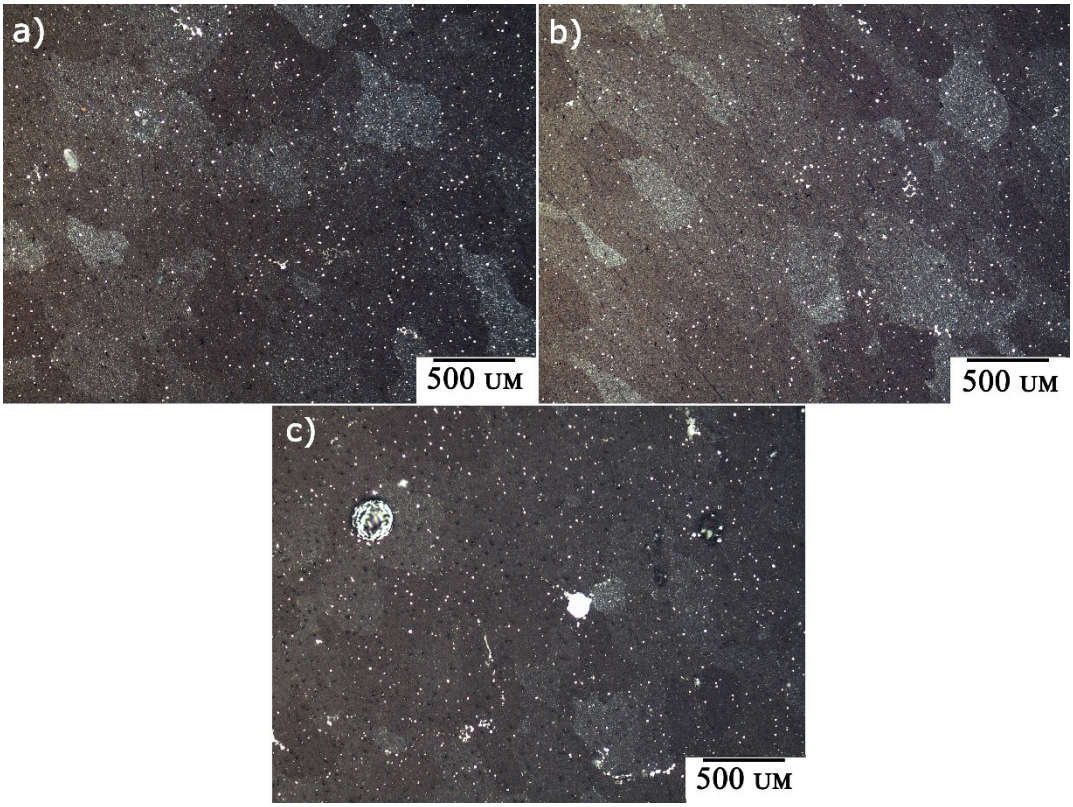

Fig. 2.40 – Microstructure of the walls, under polarized light: a) unidirectional mode; b) bidirectional mode; c) switchback mode

2.4.4. Geometry analysis

It is important to point out that the wall printed using bidirectional mode showed a profile more irregular than the others, as illustrated in Fig. 2.41. This happened probably due to thermal differences during interlayers. As explained, during the experiments the walls were cooled down before starting a subsequent deposition layer until they were possible to be grasped with bare hand. This criterion was probably not good enough, because this qualitative measuring was made at the center of the wall length. With bidirectional mode of deposition, the subsequent layer started at the end of the previous layer. Thus, the starting point happened over a hotter material, tending the deposited pool to sag to the laterals. When using unidirectional or switchback modes, there is no such problem. To support this explanation, GENG et al. (2017) had already shown that even a difference in the interpass temperature of 30 °C from the room temperature can provide significant impact on the bead formation.

However, as explained in the methodology, the geometry measurement was based on a simulated rectification. Assuming this approach, Table 2.6 presents the summary of the measured geometric values, according to the procedure described in section 2.3.3. As one can see in this table, with switchback mode of deposition the wall is the thinnest and tallest, for a same current, wire feed speed and travel speed as of the others (consequently the same deposition rate per unit of wall length). Correspondingly, the average height per layer of the deposition made in the

switchback mode was the biggest. This slender profile of the wall deposited with switchback mode is a positive characteristic, since it broadens the application of the WAAM by reaching a thinner wall. One could argue, to some extent, that the differences in the wall width between the layer deposition with switchback and the other modes were very small (0.2 to 0.3 mm). However, these figures represent walls from 3 to 5 % thinner. The differences in the buy-to-apply factor between the un/bidirectional modes and the switchback mode seem to be insignificant, yet reaching 1 % of machining (time and cost) savings. However, this confirm the low deviation of flatness when using WAAM with aluminum alloys.

Table 2.6 – Geometry parameters of the walls

Sample	Rectified Height (mm) of 10 layers	Average Height per Layer (mm)	Full Area (mm^2)	Maximum Effective Area (mm^2)	Buy-to-apply factor	Average Effective Wall Width (mm)
Unidirectional mode	23.6	2.4	146.4	143.4	1,02	6.1
Bidirectional mode	24.0	2.4	147.8	144.3	1,02	6.0
Switchback mode	25.2	2.5	150.1	147.6	1,01	5.8

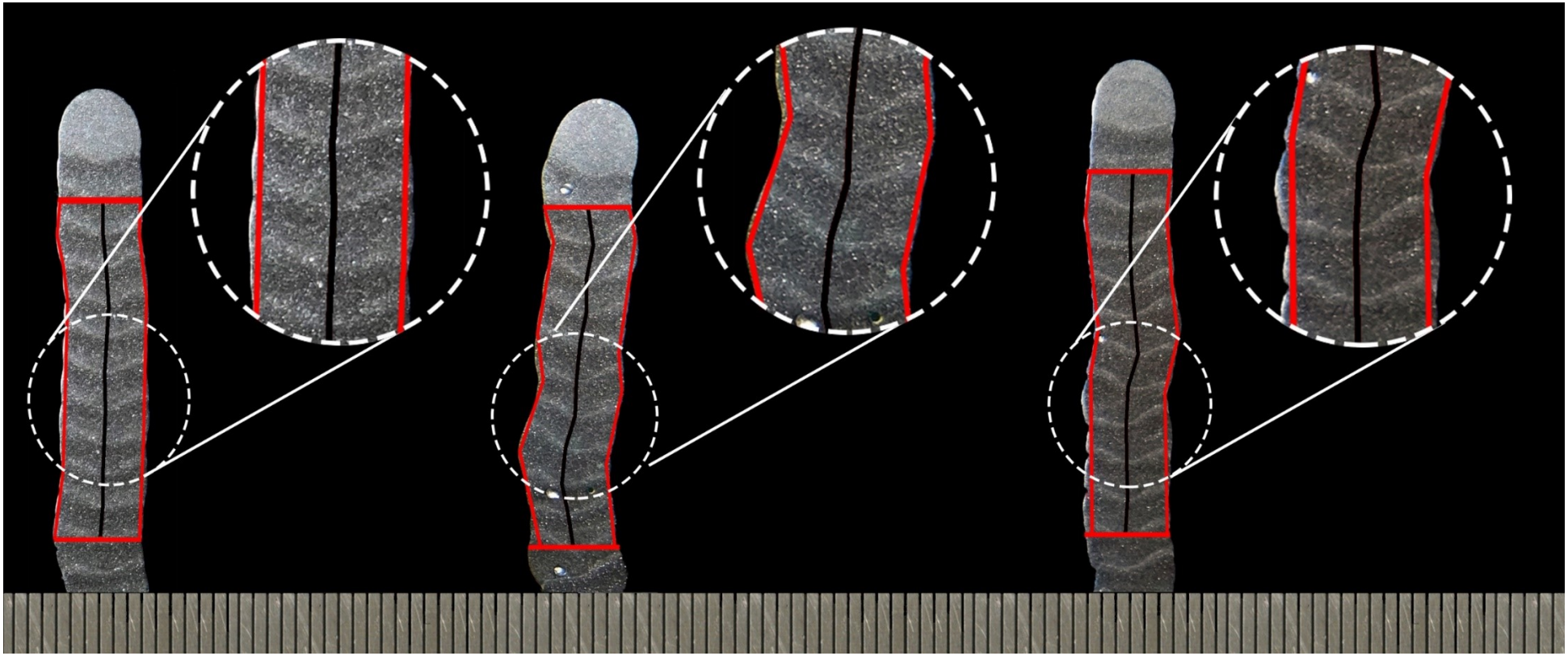

Fig. 2.41 – Wall cross sections for the geometry analysis : a) unidirectional mode; b) bidirectional mode; c) switchback mode

2.4.5. Porosity measurement

Table 2.7 presents the results of pore measurements by gravimetry. One can see less porosity in the wall using switchback mode of deposition (from 3 to 19 % less). The switchback movement may have stirred the pool in such a way to facilitate escaping of trapped gases. On the other hand, to find out the principles that led the wall built with bidirectional mode to higher porosity is subject for future studies. It is important to mention that, according to results obtained by DA SILVA and SCOTTI (2006) with double pulse GMA welding of the aluminium, porosity can reach 6 % depending on the welding parameters used. Consequently, one can consider that pores generated in AWAM of aluminium alloys is low and the use of switchback mode lessens porosity.

Table 1.7 – Porosity of the walls

Samples	Body mass in air (m_c) [g]	Body mass in water (m_{H2O}) [g]	ΔBody mass [g]	Body Density, (ρ_c) [g/cm3]	Relative volume of voids (V_v) [%]
Measured Reference	74,48	47,18	27,30	2,73	-
Unidirectional mode	62,73	39,01	23,72	2,64	3,06
Bidirectional mode	62,95	39,00	23,95	2,63	3,66
Switchback mode	66,72	41,25	25,20	2,65	2,95

2.5. Conclusion

In this study, the potential of the switchback technique applied to WAAM of an aluminium alloy for mitigating of the epitaxial columnar grain growth through layers and grain refinement was assessed. It was showed that the switchback deposition mode can prevent continuous homoepitaxial grain growth, by breaking the solidification pattern, and, in addition, to refine the grain sizes. This finding suggest that with this performance, switchback deposition mode can be a means of solving the problem of anisotropy of the mechanical properties that is observed in parts produced by WAAM. The results also showed that switchback mode decreases porosity in printed parts, improves surface quality of the walls, and allow, for a same deposition rate per unit of wall length, the production of thinner walls.

2.6. Future work

In this study was observed strange effects of the wall geometry distortion and increasing of the porosity while depositing each layer in opposite direction. Finding out the principles that leads to these happenings can be a valuable work that would allow to increase the attractivity of the WAAM.

CHAPTER III

PROOF OF CONCEPT OF THE INOCULATION USAGE TO MITIGATE CONTINOUS COLLUMNAR EPITAXIAL GRAIN GROWTH

3.1. Background (Bibliographic review)

One of the approaches to refine grain size in solidification is called inoculation. Along the past years, inoculation with different substances has been widely and successfully used in casting to avoid epitaxial grain growth in aluminium alloys (Fig. 3.1), There is also reference to the use of inoculation in welding (Fig. 3.2). Inoculation of molten cast may be defined as an introduction of nuclei into the melt (temperature below or inside the freezing range) in order to influence the solidification process or structural formation in the casting in a specific way. Nuclei are fine particles (≤ 4 μm in size) which serve as crystallization centers for solidification or particles formation. The main characteristics of inoculation are its abilities to homogenize the solidification pattern in the whole component and to refine grain size. Consequently, mechanical properties are improved.

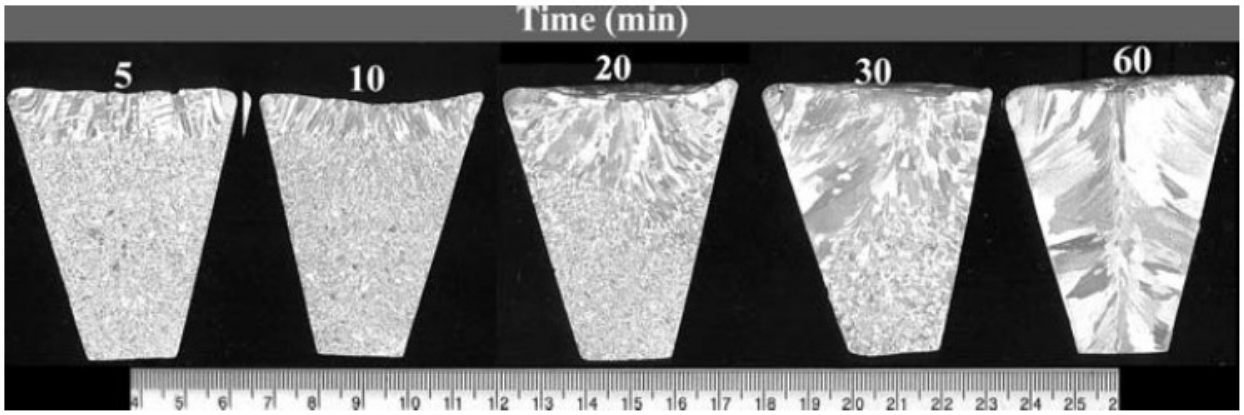

Fig. 3.1 –Macrographs of commercial aluminium casts with grains refined by Al-1.2Ti-0.5B, 50 ppm Ti addition changing the holding time after addition of inoculants from 5 to 60 s (After RAMACHANDRAN, 2008)

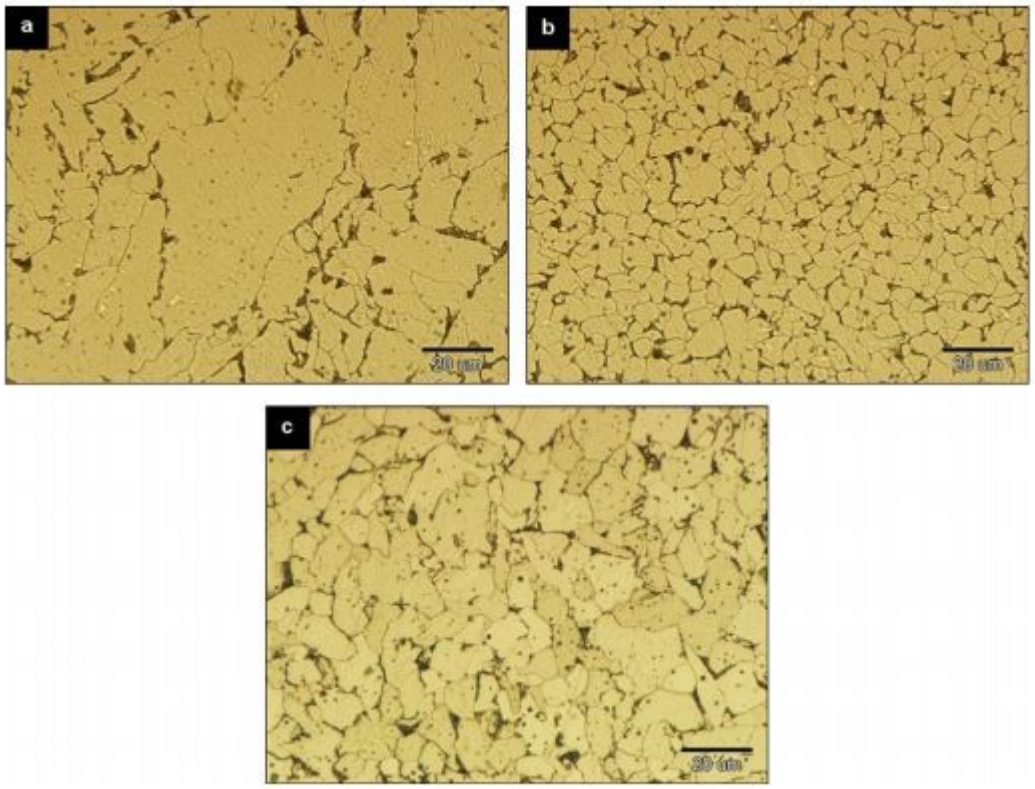

Fig. 3.2 – Weld beads microstructural formation in the melted zone of GTA welded low carbon steels with (a) low, (b) medium, and (c) high TiO2 content nanoparticles. After FATTAHI et al. (2011)

Inoculation in casting is used for grain refinement mostly due to its low cost, reproducible results and facility in application. Research on grain refinement of cast metals has been conducted for over sixty years (ZHILIN 2017). If a molten metal contains a sufficient number of inoculants, heterogeneous nucleation of new grains ahead of the advancing solid/liquid interface is greatly promoted. The density of inoculants may alter the columnar-to-equiaxed transition (CET), as indicated by equation 4.1 (Hunt 1984), where G is a temperature gradient, N_0 represents nucleon density (1/m3), ΔT_c represents undercooling of columnar growth (K), and ΔT_n represents nucleation undercooling (K).

$$G < 0.617 {N_0}^{1/3} \left(1 - \frac{{\Delta T_n}^3}{{\Delta T_c}^3}\right) \Delta T_c \qquad (4.1)$$

According to YAN (2017), equation 4.1 addresses the criterion for equiaxed growth. It can be further devised that as more inoculants are injected into the melt, more nucleation sites are provided.

As welding and casting are metallurgically similar, it can be assumed that inoculation could work in welding as well, there are, however, some differences related to the potentiality of inoculation between welding and casting. Firstly, a molten metal in casting usually has big volume, while welding pool has small volume. In addition, solidification of the molten metal happens with

different solidification modes if in casting or welding. In casting, firstly cooling rate on the interface molten metal-mold is initially high. Moreover, the mold surface cannot provide nucleation (due to the fact that the mold is cold when it is filled by the molten metal, the grains on the surface of the mold does not act as nuclei). These two circumstances make easier for equiaxed grains to form. However, as the mold is heated by the molten metal inside, the heat transfer turns to be slow after the first grains of nucleation. A slow cooling rate nucleation favor columnar and dendritic grain growth. In welding, in turn, the interface solid-liquid is at the same temperature, and the grains of the metal turn large (Coarse HAZ) and act as nuclei. Even though the cooling rate can be fast, columnar growth is possible

Even with these differences, there are some publications that confirm the possibility of using inoculation in welding. For instance, in 1989 YUNJIA et al. (1989) have added titanium and zirconium grain refiners in the weld metal by inserting master alloy strips into a machined slot on the surface of the plate of Al 1100, and have melted the alloy by three passes of gas tungsten arc welding. The experiment was repeated 5 times for zirconium inoculant (0 wt%, 0.05 wt%, 0.09 wt%, 0.18 wt%, 0.23 wt%), and 5 times for titanium inoculant (0 wt%, 0.07 wt%, 0.13 wt%, 0.19 wt%, 0.26 wt%). Microstructure of the welds and solidification conditions were analyzed as exemplifies with the effect zirconium inoculant presented in Fig. 3.3. The authors showed that additions of zirconium up to 0.23 wt-% and of titanium up to 0.26 wt-% have significantly refined the grain size of 1100 aluminum gas tungsten arc weld metal. It was an important result, because it meant that even though welding is characterized by a high temperature gradient and fast crystallization, inoculation can be successfully implemented in welding due to the purpose of the grain refinement.

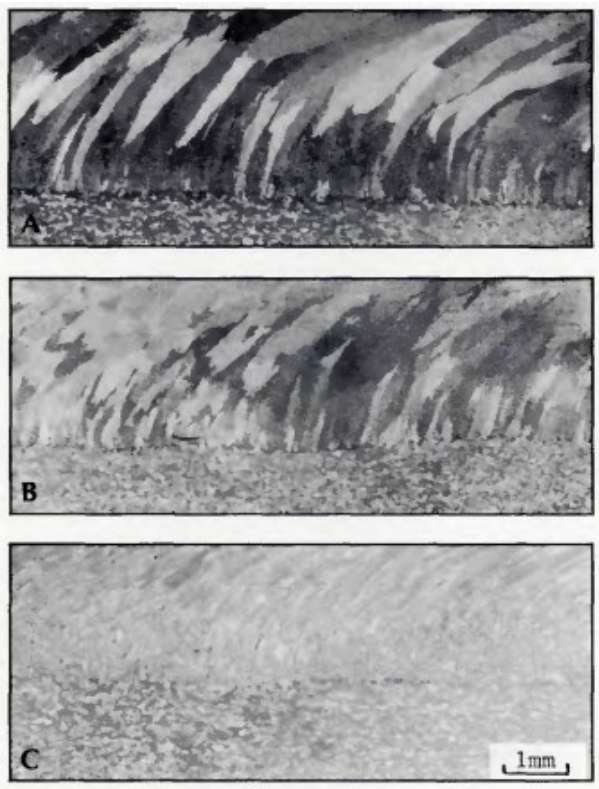

Fig. 3.3 –Macrostructures from longitudinal sections as a function of increasing zirconium addition to 1100 aluminum weld metal: (a) Zr = 0 wt-%; (b) Zr = 0.05 wt-%; (c) Zr = 0.23 wt-% (After: YUNJIA, 1989)

Similar experiment was performed in 2015 by FATTAHI et al. (2015). They used TiC/Al composite filler material with different content of TiC nanoparticles during GTA welding of the Al 6061 plates. The authors observed the same effect of significant grain refinement due to the increasing of the TiC nanoparticles amount in the weld. Results of the inoculation are shown on Fig. 3.4.

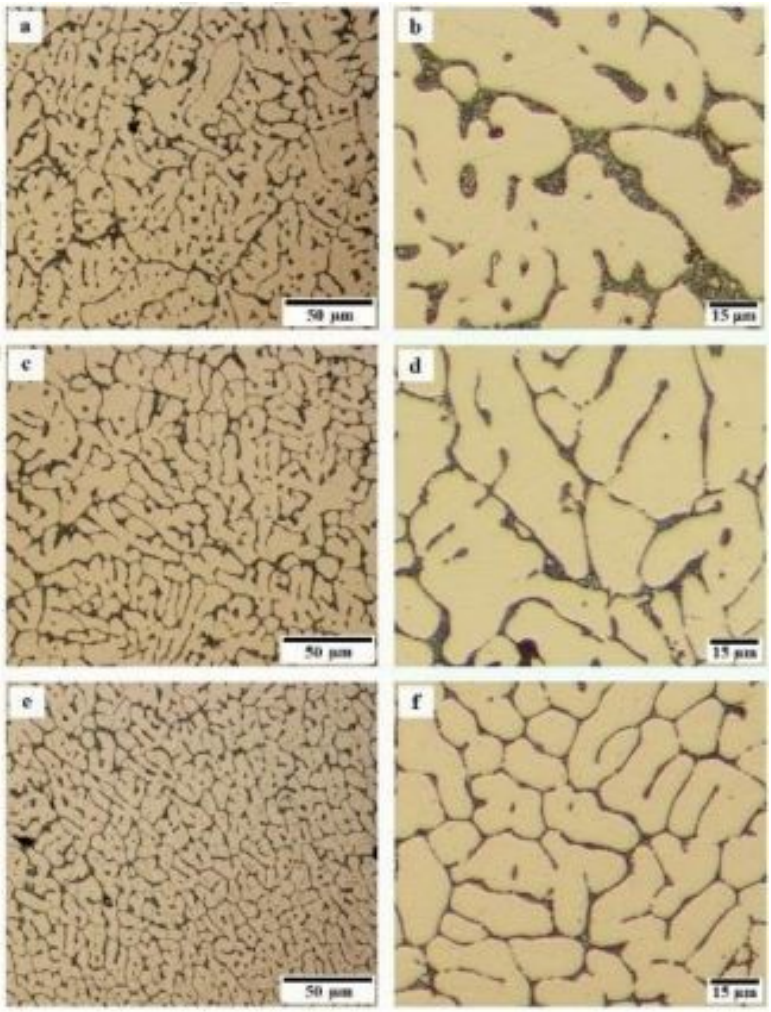

Fig. 3.4 – Optical micrographs in different magnifications showing the microstructural changes in melted zone of the Al 6061 GTA welds containing: (a) and (b) 0; (c) and (d) 2.5 and (e) and (f) 5 wt.% TiC nanoparticles (after FATTAHI et al., 2015)

Last year, simultaneously with the developing of the present work, a work of MEREDDY et al. (2017) was published. They studied microstructure of the WAAM printed Ti6Al4V inoculated with silicon nanoparticles. In their study, each layer of the WAAM printed wall was brushed with solution of the Si nanoparticles in alcohol gel. Three walls with different wt% of Si nanoparticles in the solution were printed. After brushing, the alcohol evaporated and only a thin layer of nanoparticles was left on the layer surface. Microstructures obtained with different amounts of the Si nanoparticles are presented on Fig. 3.5.

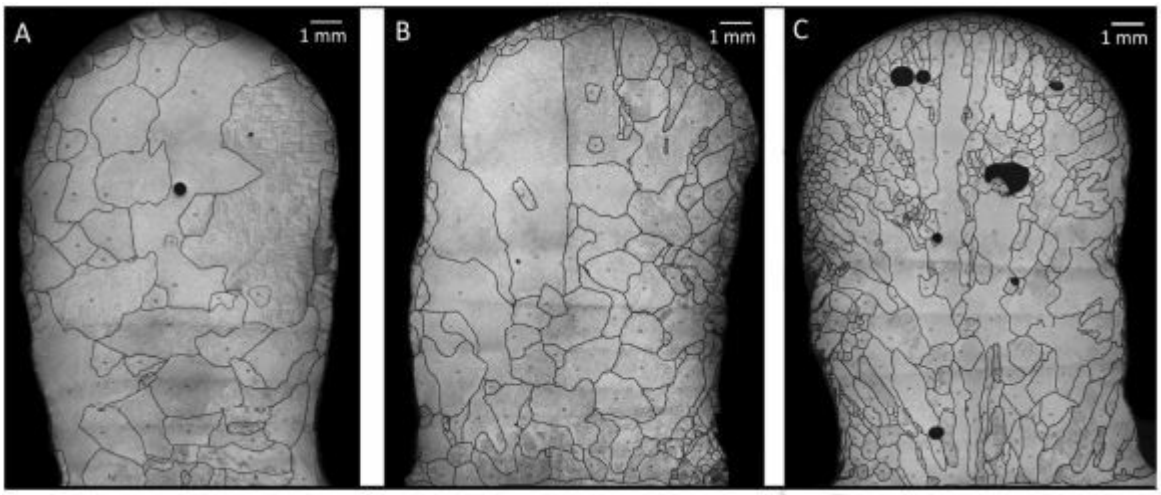

Fig. 3.5 – Structure of additive manufactured Ti6Al4V with addition of a) 0.04% Si; b) 0.19% Si and c) 0.75% Si (after MEREDDY et al., 2017)

However, despite the promising results, inoculation approach is far from being widely applied in welding manufacturing, because of several setbacks, such as:

- There is no established technology that allow to add nanoparticles to the welding pool;
- It is hard to estimate the portion of nanoparticles that should be added, since welding pool varies of size and cooling rate according to the parameters;
- It is hard to reach even distribution of nanoparticles over the weld pool.

3.2. Objective

The specific objective of this work described in this chapter was to explore the concept of using nano-inoculation in welding. If this concept can be proved to be functional, this approach could be applied to solve the problem of columnar epitaxial grain growth during WAAM of aluminium alloys in a simpler way.

3.3. Methodology

3.3.1. Proof of concept: performance of experiments with inoculants during welding

Considering the intrinsic difficulties for using WAAM in such exploratory stage, it was decided to make more simple and controllable experiments to prove the feasibility of inoculation in small volume of metal, with very high temperature and fast cooling rates, as in welding or layer deposition pools.

Note of the author: Although the target application of the results from the work described in this chapter is WAAM (deposition of material, layer by layer, and not material joining) of aluminium alloys, the proof of concept will be developed using welding and stainless steel as base

metal. The reason for that is the fact that inoculation in WAAM would be connected to some difficulties, such as:

- *WAAM is a complicated process, with many not fully known and uncontrollable variables. The addition of inoculants would enlarge the number of the variables, fact that would complicate the interpretation of the results;*
- *Some additional equipment should be designed and manufactured to apply inoculants into the weld.*

In these experiments, the chosen welding process was the more technologically controllable TIG, aiming to decrease the number of the variables. No metal filler was used, also to keep the number of variables as low as possible. Direct current electrode negative (DCEN) mode was set, using a 2% thoriated Tungsten electrode with 3.2-mm-diameter, include angle of 60°, shielded with pure argon (99,999%) at a flow rate of 12 L/min. The weldments were carried in flat position, without inclination of the torch, using an electronic power source (MTE Digitec 600). Torch linear movement was reached by using a programmable two axes table, illustrated on Fig. 3.6. A common set of welding parameters were played:

- Welding current (I_w) = 250 A;
- Welding travel speed (v_w) = 24 cm/min;
- Electrode tip to plate distance = 10 mm.

Note of the author: as soon as the purpose of the experiment was not to joint two plates, but to see effect of the nanoinoculants, Electrode tip to plate distance used was higher than conventional values (2 to 3 mm) to melt bigger area and form higher volume of molten metal for inoculant to act in.

Fig. 3.6 – X-Y coordinate table used to provide movement of the torch

AISI 304 austenitic stainless steel was chosen as parental metal, due to the fact that this stainless-steel class does not have secondary phase transformation, alike aluminium, and low thermal conductivity. Consequently, coarse grains are expected in the Fusion Zone of this material when welded, making more sensitive the experiment when inoculation is assessed. Nominal chemical composition of the parent metal is presented in Table 3.1. The test plates were composed by two bars of the parent metal (120/200 mm x 38 mm x 5 mm) laterally placed as an I butt weld joint (no gap). The bars were pressed together before welding to avoid deformations during welding, as illustrated in Fig. 3.7.

Fig. 3.7 – Assembling of the bars to form the test plates before welding

Table 3.1 – Chemical composition of the 304 stainless steel (Atlas Steels, 2013)

	%							
	C	**Mn**	**Si**	**P**	**S**	**Cr**	**Ni**	**N**
Min	-	-	-	-	-	17.5	8	-
max	0.07	2	0.75	0.45	0.03	19.5	10.5	0.1

SiO_2 nanoparticles of 50 nm diameter were chosen for inoculation. A nanoparticle solution was prepared, having acetone as solvent, with a concentration of 3 g of nanoparticles per 3 ml of acetone. The nanoparticle solution was applied with brush on one of the bar side faces. After acetone evaporation, the nanoparticles formed a fine white layer on the edge surface of the metal that compose the groove (Fig.3.8).

Note of the author: A first method that one would consider applying the nanoparticles would be like A-TIG (on the surface of the plates). As widely known, A-TIG was invented to increase the penetration depth of TIG process and to increase its productivity. One of the hypothesis of how A-TIG works is based on the Marangoni effect (Lu et al. 2003). According to this hypothesis, activating flux is changing the surface tension of the welded metal that causes its convection, in such a way that overheated metal goes down and melt the base metal. However, this an A-TIG like application would not reach necessarily the full volume of the molten metal (fusion zone), acting more on the surface. This was the reason to devise the application in the surfaces of a groove to form the I-butt joint.

There were two position related methods for nanoparticles application. The first one is illustrated in Fig. 3.9, in which the nanoparticles covered all the surface of the side faces. The second method was to leave a section free of nanoparticles at the middle part of the test plate centerline of the butt joint, as illustrated in Fig. 3.10. The approach was to have three sequential sections, i.e., one with nanoparticles, another without nanoparticles and a third one again with nanoparticles. The reason for this is top observe the repeatability of the nanoparticle effect in a same welding.

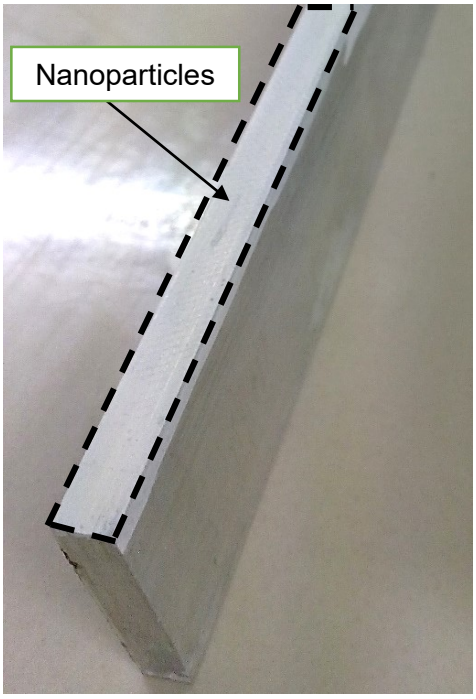

Fig. 3.8– Nanoparticles on the 5-mm-edge surface of the base metal

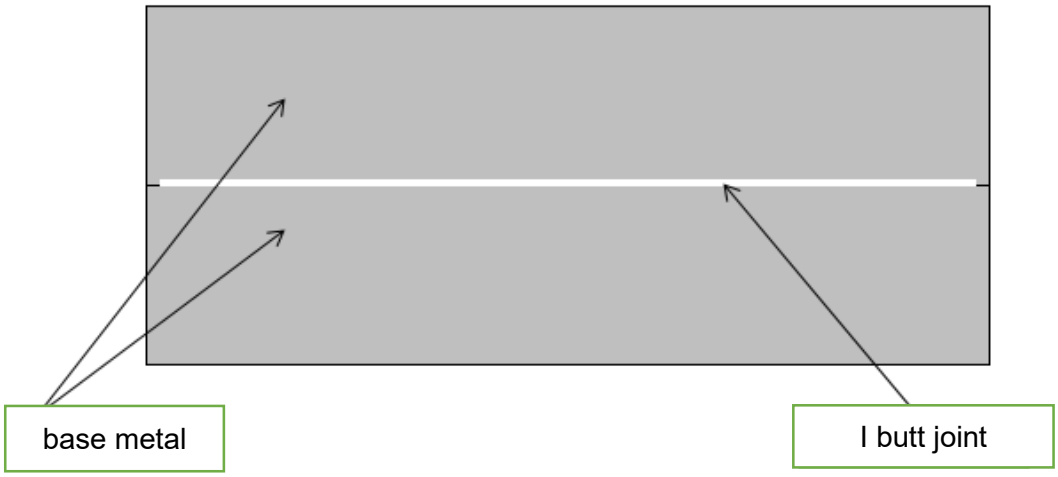

Fig. 3.9 – Full joint length nanoparticles application

Three experiments were run, as follows:

- Welding on test plate (120-mm-long) without nanoparticles;
- Welding on test plate (120-mm-long) with nanoparticles at the full joint length;
- Welding on test plate (220-mm-long) with nanoparticles at the stretched joint length (with nanoparticles-without nanoparticles-with nanoparticles).

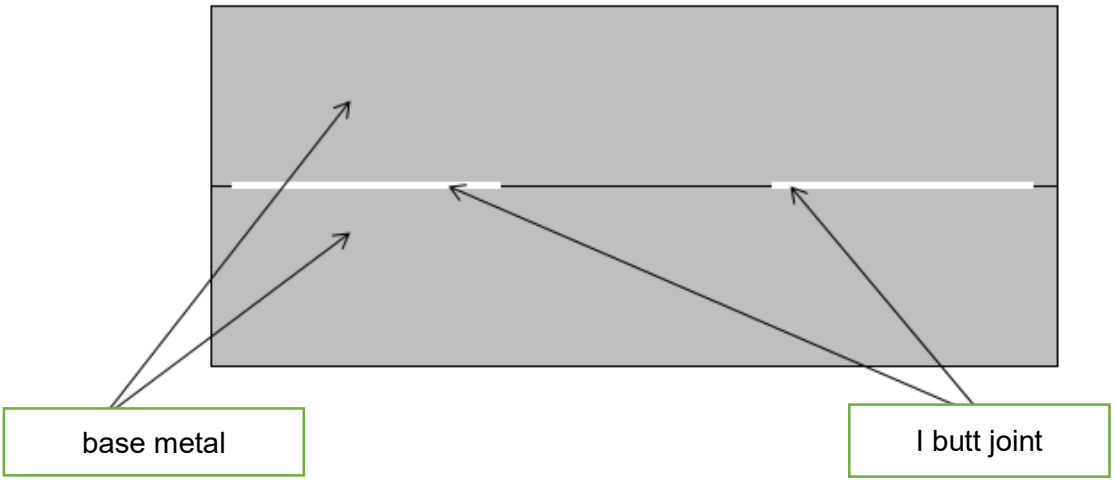

Fig. 3.10 – Intersectional joint nanoparticles application

3.3.2. Analysis of the welds

After welding, cross section samples were cut off at specific places. For the first two experiments, the samples were taken at the middle of the weld length. For the third experiment, three samples were taken at the middle part of each section. The cross sections were grinded with sandpaper of 400, 600 and 1200 mesh, then polished with chrome oxide (10 um) and aluminium oxide (5 um) solutions. The macro and microstructures were revealed after etching by aqua regia for 5 sec. Macrographs were taken by using a camera Nikon D5000. The microstructures were obtained in an optical microscope Leica DM 750M, with camera Leica MC170.

The cross sections were analyzed in relation to the bead profile and the formed microstructures (grain type and size). Delta ferrite content was also quantified. According to WEGRZYN (1992) increasing of delta ferrite in austenitic stainless-steel welds have some disadvantages, such as:

- Decreasing of the corrosion resistance;
- Solidification cracks formation, due to the difference between the thermal expansion coefficients of the ferrite and austenite.

On the other hand, delta ferrite substantially raises the yield point of CrNi austenitic welds, and particularly the welds of very low carbon and nitrogen content (about 0.02% C and 0.05% N).

Thus, if the content of the delta ferrite in the produced weld changes due to the presence of nanoparticles, this would be an evidence of the nanoparticle action.

Magnetic delta ferrite measurement was carried by an ferritoscope (FISCHER MP30), with 10 measurements on each of the polished cross section surfaces. The equipment was calibrated with appropriate standards, with detection limit of 0.5 % ferrite. This procedure was described by

Forgas Jr et al. (2016). The ferritoscope is a method that measures the volume of the ferromagnetic phase. The measurement method is based on magnetic induction in which a magnetic field is generated by a coil that interacts with the magnetic phase of the sample. The changes in the magnetic field induce a voltage proportional to the ferromagnetic phase content in a second coil. This voltage is then evaluated.

3.4. Results and Discussion

The bead profiles are pictured in Fig. 3.11. As one can see, the addition of the nanoparticles caused changes in the bead shape. The bead of the section made without addition of nanoparticles present a TIG ‘finger like” shaped bead (Fig 3.11(a), (b)). The sections made with addition of nanoparticles (Fig 3.11(c), (d) and (e)) show a more rounded form. The change in the bead shape is an evidence of the effect of the nanoparticles. However, increase of penetration was not noted, which suggest that nanoparticles in this case did not worked as happens in A-TIG processes. One could suggest that the heat flow inside of the liquid metal is not from top to the bottom, but rather disordered and presented mostly on horizontal plane. This fact might be caused by an even distribution of the nanoparticles along all depth of the weld and, as a result, the inexistence of difference between surface tension on the surface of the weld and at the bottom.

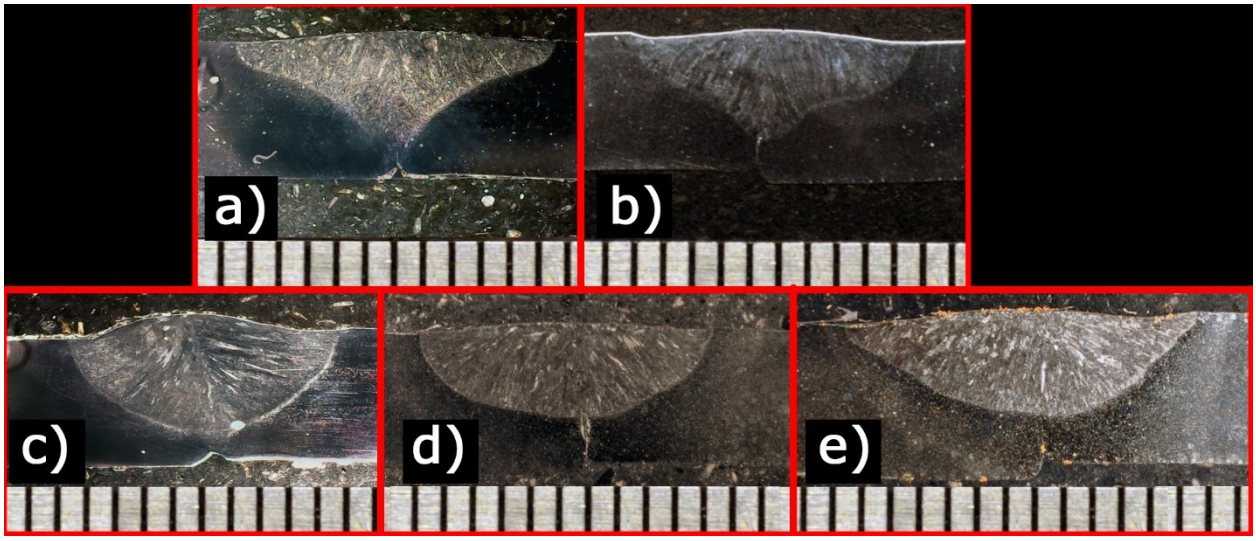

Fig. 3.11 – Macrography of the samples. a) 1-st experiment, without nanoparticles; b) 3-rd experiment, zone 2, without nanoparticles; c) 2-nd experiment, with nanoparticles; d) 3-rd experiment, zone 1, with nanoparticles; e)3-rd experiment, zone 3, with nanoparticles

Fig. 3.12 presents the typical microstructures of the 3-cross sections from test-plate 3. One can see classic structure of the austenitic stainless-steel welds, as described by INOUE and KOSEKI (2007), consisting of vermicular delta ferrite (dark phase) and austenite (light phase).

However, one can also see small difference in the shape and distribution of vermicular delta ferrite when nanoparticle was used (Fig. 3.12(b), (c) and (e)) and not used (Fig. 3.12(a) and (d)).

Yet considering that this microstructural difference was small, it was decided to measure the grain sizes. As weld microstructure is dendritic, ASTM E122-13 standard for measuring grain sizes cannot be used. Thus, it was decided to use the line intersections technique for dendritic grain size estimation. The bigger the interception number in a given line length, the finer the dendritic grain size. The length of the line was of 200 um, purposely perpendicular to the direction of the dendrites growth.

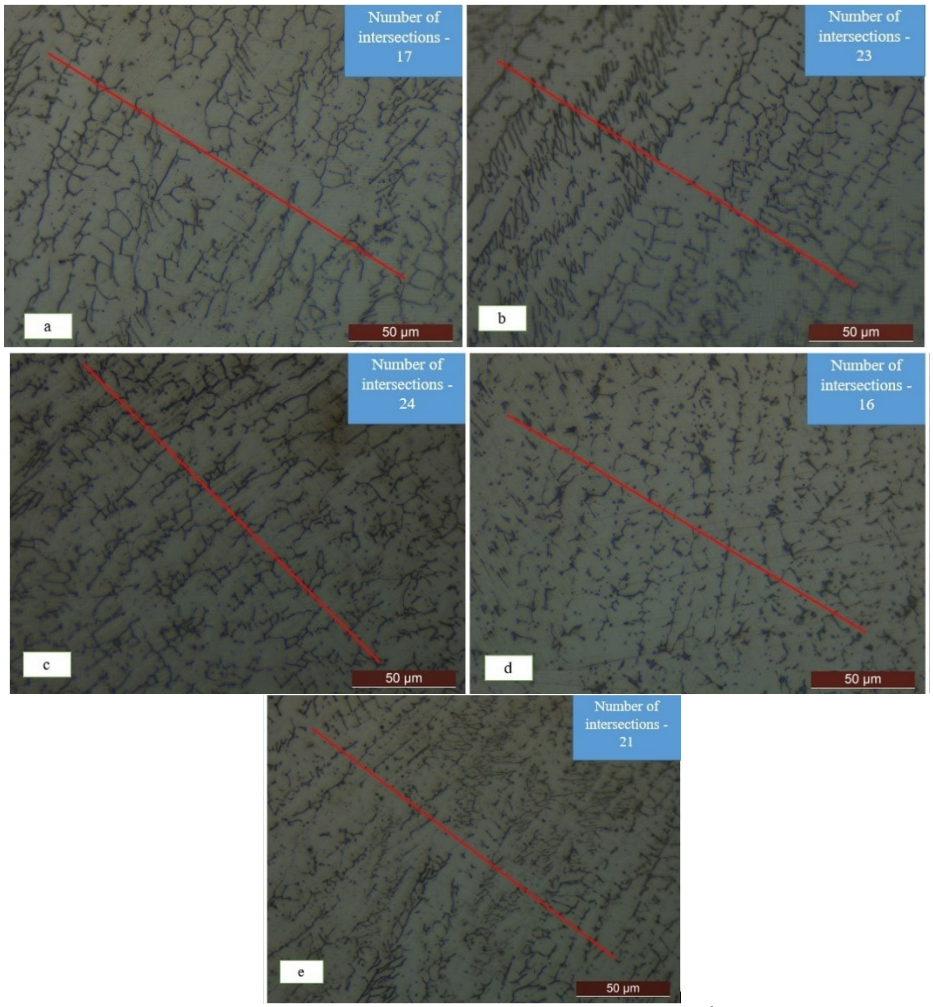

Fig. 3.12 – Microstructure of the cross sections sampled from: a) 1st test plate (no nanoparticles); b) 2nd test plate (with nanoparticles); c) 3rd test plate, stretch section 1 (with nanoparticles); d) 3rd test plate, stretch section 2 (no nanoparticles); e) 3rd test plate, stretch section 3 (with nanoparticles)

The compiled results of size estimation are presented at Table 3.2. From this table, the addition of the nanoparticles to the weld promoted grain refinement. These figures give ground for believing that the inoculation is possible to be used in welding.

Table 3.2 – Austenite grain size estimation data

	1st test plate (no nanoparticles)	3rd test plate, stretch 2 (not nanoparticles)	2nd test plate (with nanoparticles)	3rd test plate, stretch section 1 (with nanoparticles)	3rd test plate, stretch section 3 (with nanoparticles)
Number of intersections per 200 μm	17	16	23	24	21

Results of delta ferrite contents are presented in Table 3.3. The content of delta ferrite was also measured in the base metal for reference, showing a much smaller amount of delta ferrite, as expected. One can see that the presence of the nanoparticles in the liquid metal also affected the content of delta ferrite in the welds. These results give again ground for believing that the inoculation is possible to be used in welding.

Table 3.3 – Delta ferrite percentage in different samples

Sample	Percentage of the ferrite, %										
	1st measure	2nd measure	3rd measure	4th measure	5th measure	6th measure	7th measure	8th measure	9th measure	10th measure	Average
No nanoparticles (section 2)	6.9	6.7	6.8	6.7	7.2	6.6	6.6	6.7	6.6	6.8	6.8
With nanoparticles (section 1)	8.2	7.3	7.7	7.4	8.0	8.1	8.0	7.8	8.0	8.2	7.9
With nanoparticles (section 3)	6.3	7.6	7.3	7.1	7.5	6.4	7.5	7.8	7.5	7.6	7.3
Base metal	1.7	1.7	1.4	1.5	1.7	1.3	1.6	1.6	1.8	1.6	1.6

3.5. Conclusion

To proof of concept of the possibility of using inoculation for weld grain refinement, through addition SiO_2 nanoparticles) was planned and executed by comparing the results of three welds: one without nanoparticles, one with nanoparticles and one with an intercalated section (with nanoparticles-without nanoparticles-with nanoparticles). Macro- and microanalysis of the weld metal structures were analyzed in relation to bead profile and microstructure (micro constituent type and grain size). Delta ferrite content in the welds was also quantified.

The addition of the SiO_2 nano-inoculants showed to change the bead profiles and the microstructure and to reduce austenite grain size and to increase the content of delta ferrite.

Consequently, inoculation can be usefully used in welding as much as it has been used in casting. The reach of this performance can be attractive to additive manufacturing, mitigating the typical problem of columnar continuous epitaxial grain growth.

3.6. Future work

In this exploratory work, the potential of using inoculation in weld was verified with austenitic stainless-steel, SiO_2 nanoparticles as inoculate and TIG as welding process. Considering that the main objective of work is grain refinement of aluminum deposition layers during WAAM process, as further work is suggested to assess this principle by finding appropriate nanoparticle to aluminium, to apply with GMAW WAAM and to design a method for introduction of the nanoparticle in during the layer depositions.

CHAPTER IV

DETERMINATION OF THE LAYER MELTED VOLUME EFFECT ON THE GEOMETRIC QUALITY OF THE DEPOSITS CARRIED OUT WITH WAAM OF ALUMINIUM ALLOYS

4.1. Bibliographic review

For a wider implementation of WAAM process, it is important to know the operational envelop of the technique. Usually, the operational envelope in welding is defined by a graphical plane in which the X-axis represent the range of travel speed (TS) and in the Y-axis is represented the range of other variables, such as arc length, current, etc. In this X-Y plane, there will exist a polygonal central area in which the combination of TS and the other parameter provides sound welds. Outside this area, the parameter combinations lead to imperfections, such as root burn-through, excessive reinforcement, etc. In WAAM, the degree of freedom to set an arc length is small. Therefore, travel speed and current (a function of the wire feed speed) would be the most significate coordinates to compose an operational map. When it comes to travel speed for a given wire feed speed, the useful range can be used to define the wall width that can be achieved during the printing process. The wider is the range of possible travel speeds, the wider is the range of the possible widths. Unfortunately, travel speed cannot be increased infinitely. At a critical value of the travel speed, the deposit layer does not form properly. It happens due to a humping phenomenon that takes place on high travel speeds.

Humping is the phenomenon related to formation of humps and vales in a weld bead at regular intervals during welding (Fig. 4.1). There is no consensus about the nature of the humping phenomenon, yet different models have been proposed and plubished to describe the mechanism of humping formation. These models were described in details by SODERSTROM and MENDEZ (2006). To summarize their work, there would exist 5 main models that describe humping formation:

- Marangoni model;
- Compound vortex model;
- Hydraulic jump model;
- Capillary instability humping model;
- Arc induced humping model.

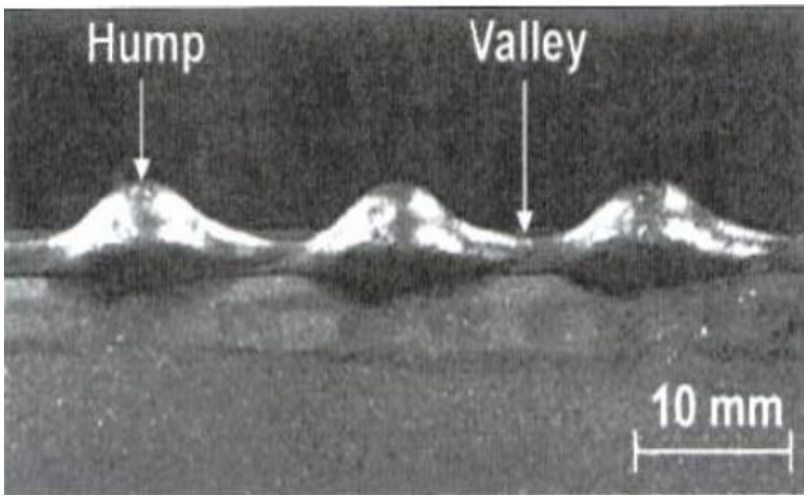

Fig. 4.2 – Humping phenomenon. After ADEBAYO et al. 2012

SODERSTROM and MENDEZ (2006) also mentioned about different morphologies of humping. They pointed out two main morphologies:

- gouging region morphology (GRM);
- beaded cylinder morphology (BCM).

GRM morphology is characterized by open and unfilled dry spots between humps. Besides, the front of the weld pool exhibits a very large depression known as gouging region (Fig 4.2).

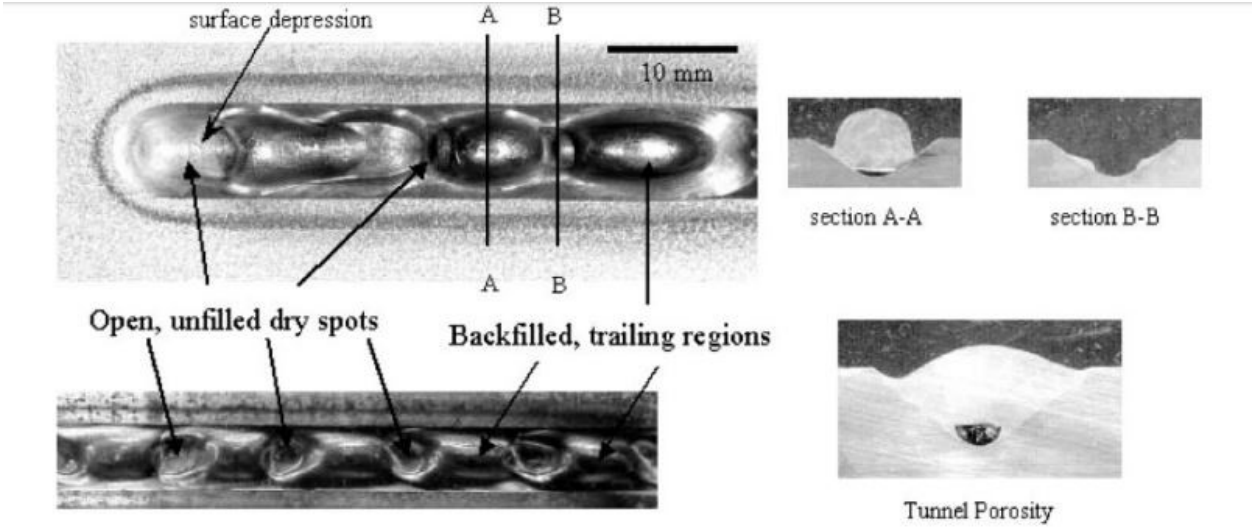

Fig. 4.2 – Characteristics of the gouging region morphology (GRM) humping. After SODERSTROM and MENDEZ (2006)

BCM, in turn, does not show presence of the gouging region, but includes beadlike protuberances that sit above the surface of the workpiece and are connected by a narrow central channel. The weld bead in this case has a continuous undulating aspect (Fig. 4.3).

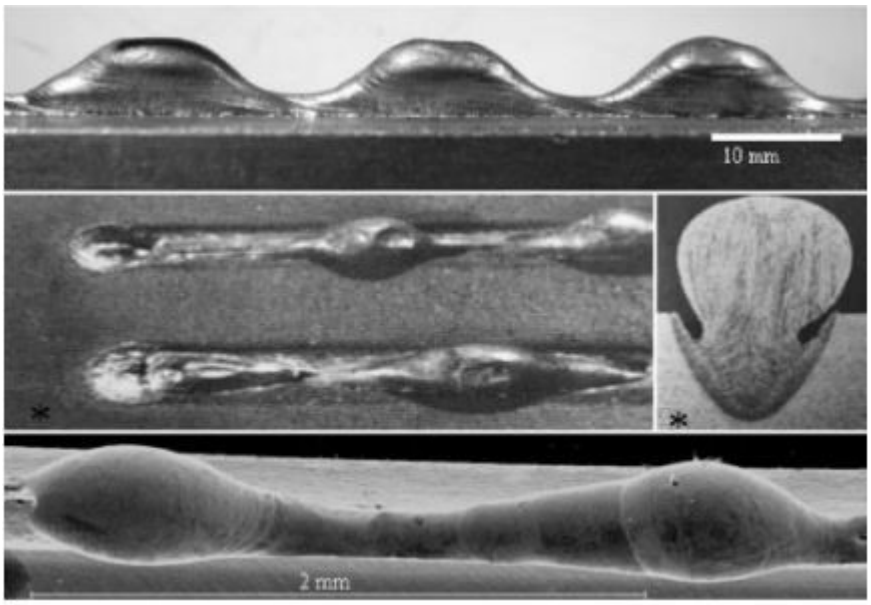

Fig. 4.3 – Characteristics of the beaded cylinder morphology (BCM) humping. After SODERSTROM and MENDEZ (2006)

Unfortunately, there are no enough experimental works to confirm or refute any of these theoretical models. Despite of this, there are consensus (for instance, from Harris, 2009; Wu et al., 2012; Ye et al., 2017) that humping happens mainly at high travel speeds. The sense of the effect of travel speed on humping formation can be seen in Fig.4.4.

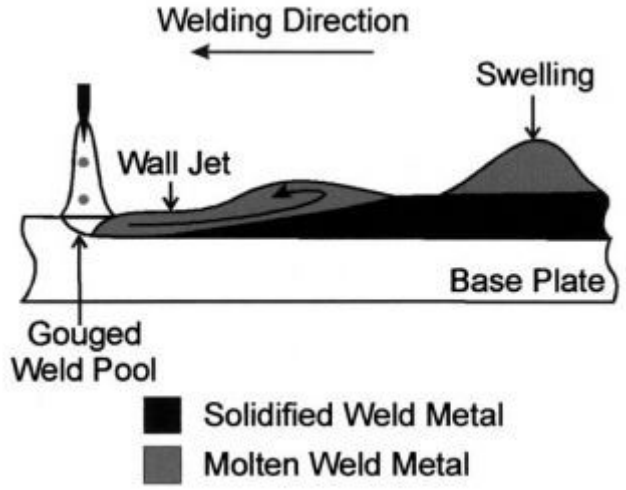

Fig. 4.4– Humping formation. After NGUYEN (2005)

With WAAM, a similar to humping phenomenon can be observed, but not so characteristic as the humping above discussed. In WAAM, it is more common to have undulated layer surface

due to the high travel speed. It is not the scope of this work to study humping, but only to demonstrate the conditions where humping or a humping-like bead formation happens in WAAM of an aluminium alloy.

4.2. Objective

The main objective of the work described in this chapter was to understand the role played by the layer melted volume over the geometric quality of the deposit carried out with WAAM of aluminium alloys.

4.3. Methodology, Results and Discussion

The objective of this work might be reached if an operational envelop, in which the X-axis is represented by travel speed and the Y-Axis by at least one value of deposition rate (mass of material deposit per unit of time), is determined for deposits made by WAAM. To reach the proposed objective, two approaches were proposed:

a) To define the travel speed limits for a same deposition rate;
b) To define the operational, envelop for a different deposition rates yet keeping the same ratio deposition rate/travel speed.

Deposited layers of an aluminium alloy were obtained following the same procedure and experimental rig already described in section 2.3.1 (Experimental Procedure) of Chapter II, including the test plate that plays the role of subtract for the WAAM. The main welding parameters were as follows:

- Welding wire = AWS /SFA 5.10 ER5356 (Al-Mg5)
- Welding current (I) = 81 A;
- Wire feed speed (WFS) = 5.0 m/min
- Contact tip-work distance (CTWD) =15 mm;
- Shielding gas: Ar 4.5;
- Shielding gas flow (GFR) =15 l/min;

4.3.1. Determination of the travel speed upper limit for an aluminium WAAM

a) Experimental Procedure

Subjectively, the lower speed limit was considered the speed that gave a wall with 6 mm of width (the same as the thickness of the plates used in experiment). This lower limit found was with a speed of 425 mm/min. Below this limit, as the depositions were carried on the top surface

of the test plate/previous layer, the molten metal would flow down the plate. On the other hand, the upper speed limit was determined experimentally.

The experiments to determine the upper limit was carried in two stages, to minimize the number of experiments:

- Determination of a range within which the upper speed limit would be lying;
- Refinement of this range for determination of the upper speed limit.

At the first stage, the test plate was divided into 4 segments, each one programmed with staggered deposition of increasing travel speeds (steps of 525 mm/min) and other welding parameters kept the same. The deposition during the first stage was carried upon two previously deposited layers. This was made to provide conditions similar to the conditions that are presented in more stable layers of a printed wall. The deposit conditions that presented undulated wall surface were considered to be outside the envelop. In this way, the travel speed upper limit would stand between the first non-conform deposition and the closest to the border surface free of undulations. This whole procedure is illustrated in Fig. 4.5 and described as follows.

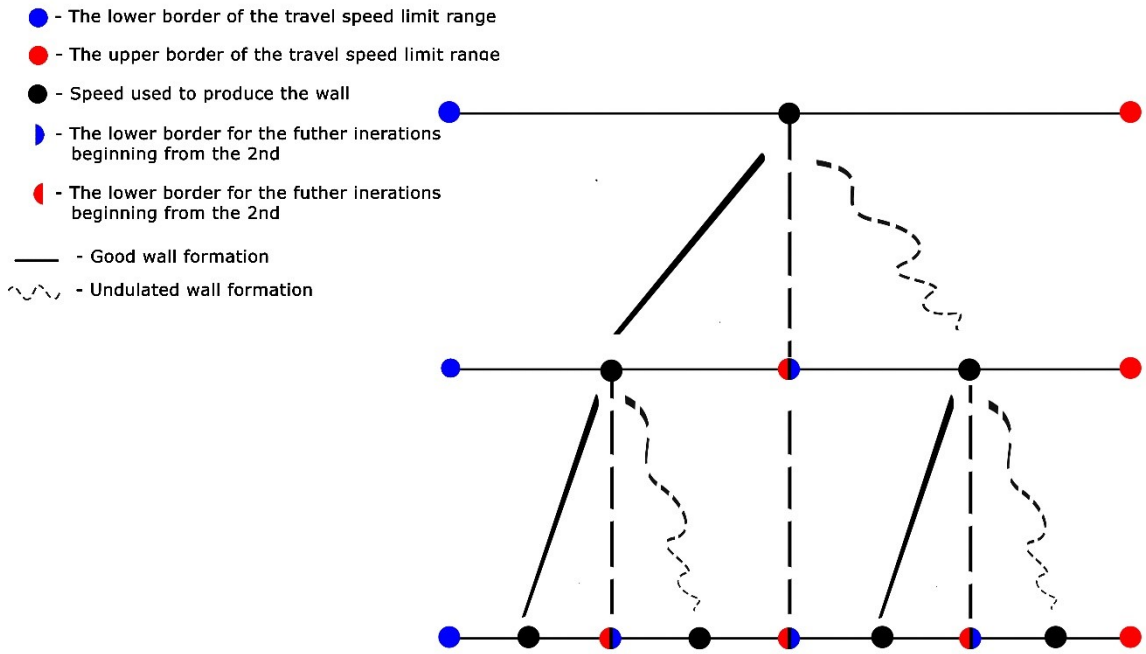

Fig. 4.5 – Graphical demonstration of procedure for the travel speed limit range constriction

It was expected that bead formation would become undulated beyond a certain travel speed (called here as the higher border of the speed limit), after implemented the 4 staggered depositions of increasing travel speeds at a given large steps. To constrict a potential big range of the travel speed limits (if the steps are too large), the next deposition was carried out on a first segment of another test plate with the travel speed set at approximately the middle value of the rough interval (always starting after a second layer already deposited as defined for the first stage). If there is no undulation with this speed, an even closest travel speed to the upper limit would have been found. This experimental reasoning is repeated until the envelop limit had been

superseded and the previous travel speed is assumed as the upper limit of the operational envelop. To confirm if the found travel speed were a stead the upper limit, a wall of 14 layers was printed with this speed and the surface of each layer was examined. Otherwise, another recursive reduction of travel speed would be tried on another segment up to a step of at least 50 mm/min is reached.

Then wall obtained on the lower travel speed limit (that was chosen 420 mm/min for this experiment) and on the higher travel speed limit (determined by abovementioned procedure) were prepared and analyzed in terms of the geometrical parameters using methodology described in section 2.3.3.

b) Results and discussion

During the first stage of this experiment, two deposits were obtained, as shown in Fig. 4.4. As one can see in Fig. 4.6(a), slight undulations can be observed in the segment with travel speed of 2000 mm/min. However, as this feature was not very clear, it was decided to carry out one more layer deposition with increasing travel speed in each segment (Fig. 4.6(b)). From this deposition, one can clearly see that the travel speed upper limit lies between 1475 and 2000 mm/min.

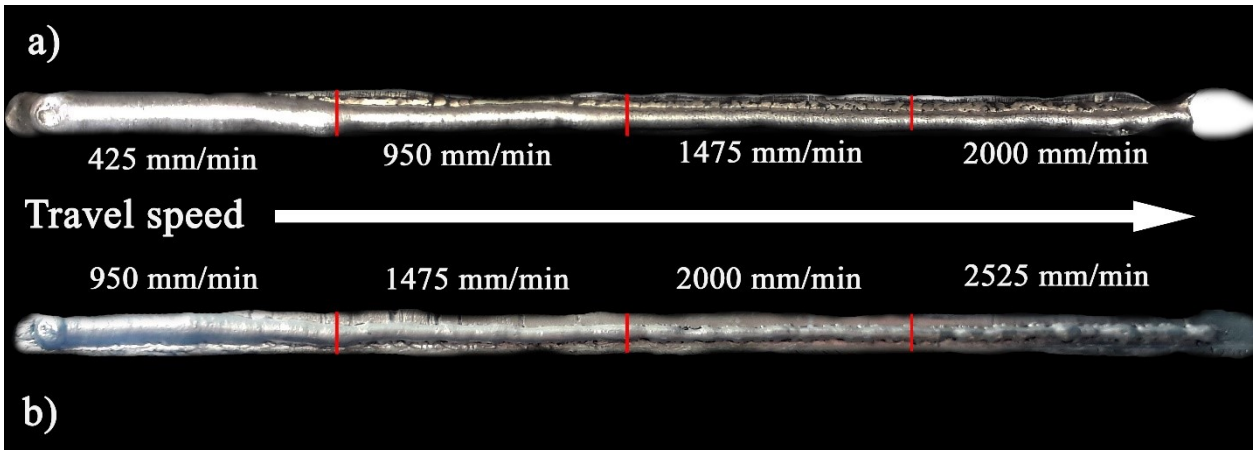

Fig. 4.6 – Results of the first stage of the experiments: a) travel speeds from 425 to 2000 mm/min; b) travel speeds from 950 to 2525 mm/min

To constrict the above range, in a second step of the experiment three walls were deposited, as shown in Fig. 4.7. From this figure, one can see that travel speed upper limit stands between 1750 and 1800 mm/min. Smooth flat layer formation was achieved with travel speed of 1750 mm/min only. By increasing of the travel speed above this limit, undulated surface took place. Thus, it can be assumed that for such used welding configuration and parameters WAAM process can be carried with travel speeds from 420 mm/min to 1750 mm/min, as illustrated in Fig. 4.8.

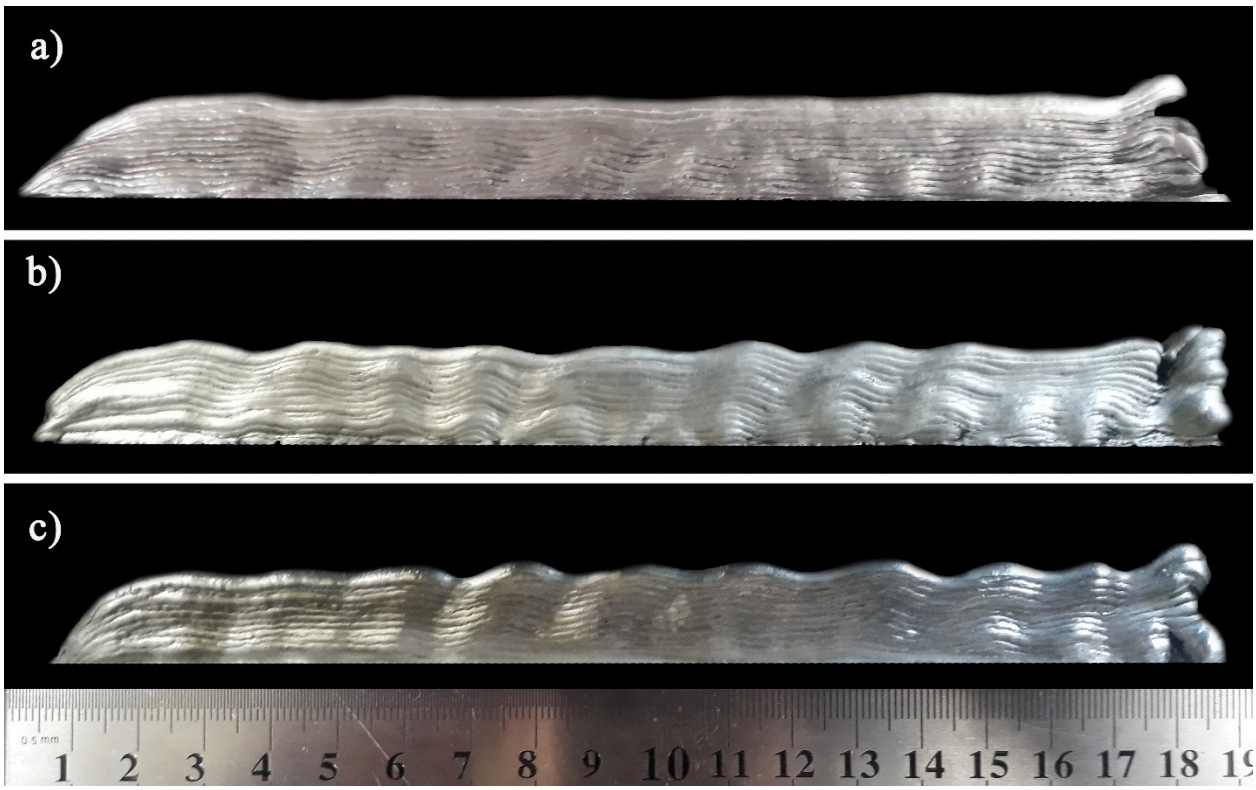

Fig. 4.7 – Walls printed with high deposition speeds: a) 1750 mm/min; b) 1800 mm/min; c) 1850 mm/min

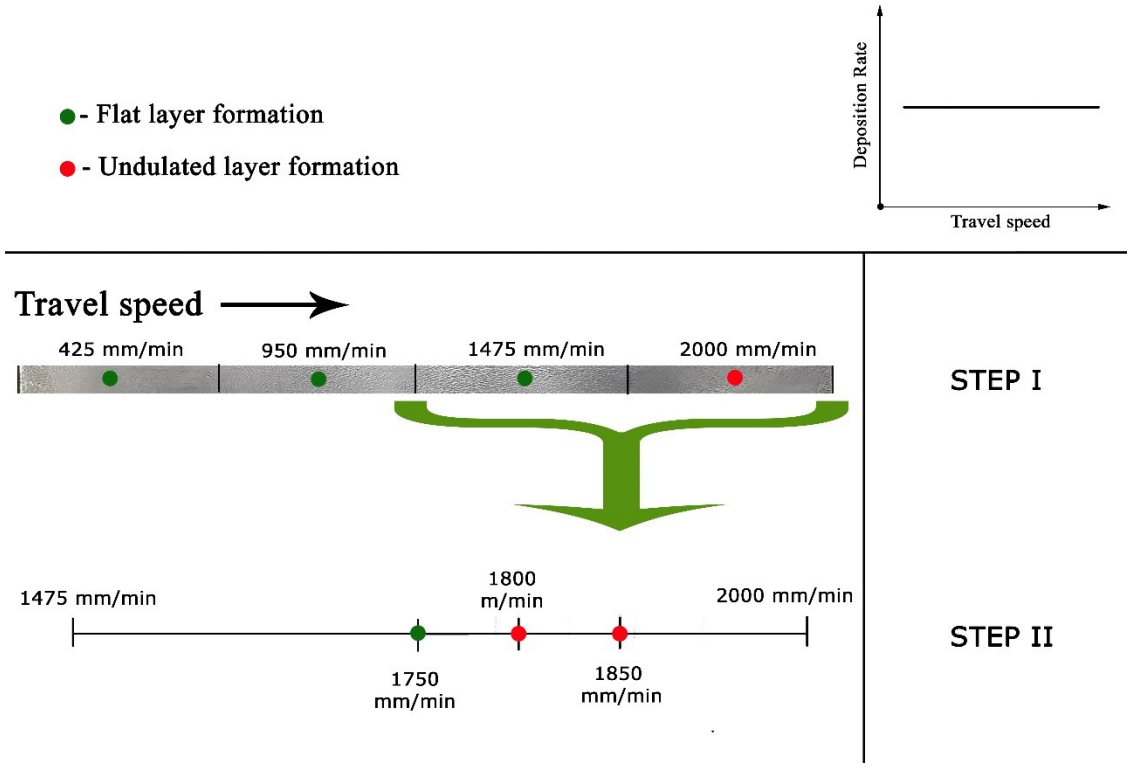

Fig. 4.8 – Graphical summary of the results of the speed limits experimental procedure

A comparison of the wall profiles and the cross-section geometries at the middle way of the layer lengths are shown in Fig. 4.9 (obtained with deposition speeds of 425 mm/min and 1750 mm/min). Amplifications of the cross sections are presented in Fig. 4.10. Geometry parameters of each wall are presented in Table 4.1. On the base of the results, the optimal strategies for each desired part to be produced can be chosen. To see how exactly these results can be used, let one consider that a 100-mm-high and 6-mm-thick wall with length 200 mm is the target. Using simple calculations, it is easy to see that If lower travel speed limit is used, 44 passes (1 pass per layer) would need to be deposited, lasting 20,7 min. If the highest limit speed is used, 84 layers with 168 passes (2 passes per layer) would have to be performed, which would take 19,2 min to be accomplished. Is important to mention that no dead time during stop and start of a pass was considered in this demonstration (a higher number of passes would spend longer dead times), even though the dead time is less expensive than the deposition time (no material and energy consumed). Anyhow, one could argue that the difference in time of these two speeds is marginal. However, in percent the difference is 7,27 %, which can be significant in terms a high scale manufacturing. However, If the needed wall to be printed were wider, for instance, 12-mm-thick, the use of the lower speed limit would allow finishing the printing after 41,4 min, while using the higher travel speed limit, the part would be produced after 28,8 min, which makes the difference in favor of using faster speeds to go to 30,5 % of time saving. The graph presented in Fig. 4.11 shows the time that would be spent to produce walls of a wide range of thickness with lower and higher travel speed limits. One can deduce that using of travel speeds that are closer to the lower limit is unreasonable.

Note: The provided calculations are rough and probably cannot be used in conditions of real manufacturing process, however, they show the trends.

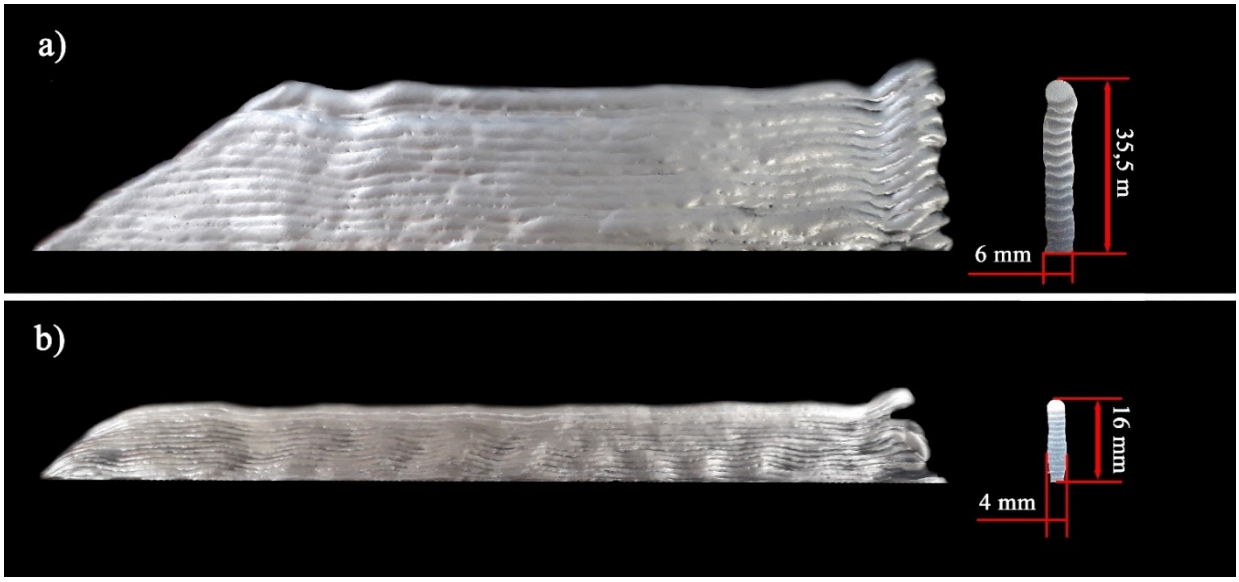

Fig. 4.9 – Comparison of the WAAM printed walls made using limit values of the deposition speed: a) lower speed limit; b) higher speed limit

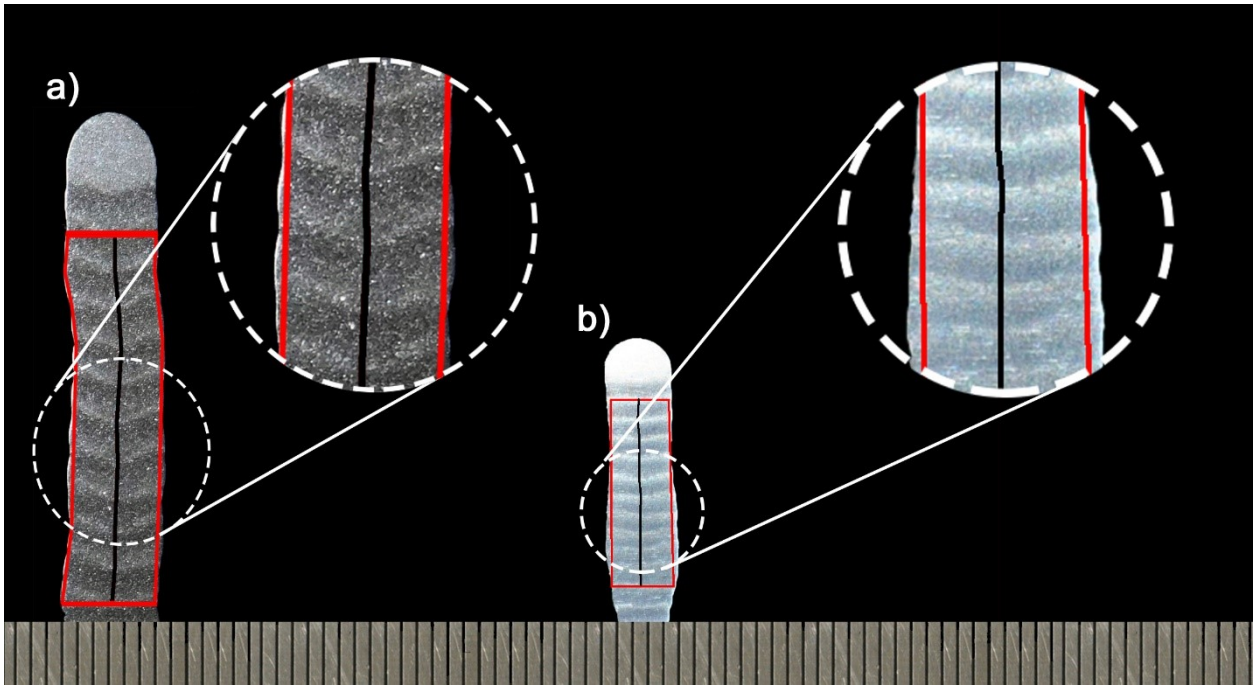

Fig. 4.10 – Geometry analysis of the WAAM printed walls made using limit values of the deposition speed: a) lower speed limit; b) higher speed limit

Table 4.1 – Geometrical parameters of the printed walls

Walls	Rectified height of the 10 layers (mm)	Average Height per layer (mm)	Full area (mm^2)	Effective area (mm^2)	Buy-to-apply factor	Average effective wall width (mm)
Lower travel speed limit	23.6	2.4	146.4	143.4	1,02	6.1
Higher travel speed limit	12.2	1.2	52.8	48.0	1,10	3.9

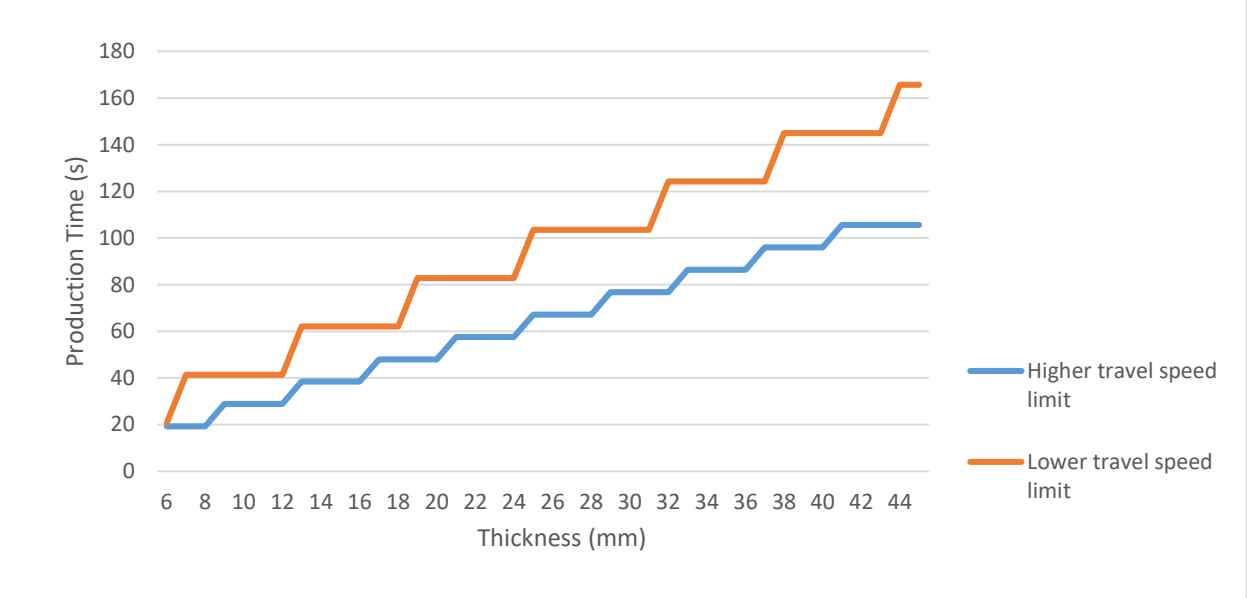

Fig. 4.11 – Time spent for wall production with 100 mm of height, 200 mm of length and with thickness from 6 to 44 mm by WAAM, using the found values of lower and higher travel speed limits

It is important to state that the above results can be complemented by the outcomes of GENG et al. (2016). They showed that humping effect for a given travel speed can be eliminated by increasing of the interpass temperature (Fig. 4.12). Moreover, they have figured out the range of interpass temperatures that can be used with other parameters fixed, and they still showed that different non-conformities appear both below lower limit and above upper limit of the interpass temperature. For GENG et al., when interpass temperature is too low, undulated surface of the deposit is observed, while when too high, the layer width will gradually increase with simultaneous decreasing of the high. This means that the quality of the deposited layers and subsequent walls

increases up to some optimum values and then begins to fall, as graphically represented in Fig. 4.13.

Transporting Geng at al.'s finding to the subject of the present work, it would be reasonable to state that the lower and upper limits of travel speed would increase with interpass temperatures, as suggested in Fig. 4.14. If on one hand, the increase the interpass temperature favors the use of higher travel speeds in production, on the other hand, the increase of the value of lower limit would not benefit the process from the flexibility point of view, Therefore, one can conclude that to make the usable travel speeds range wider, one should use higher preheating temperature for higher travel speeds and no preheating temperature for lower travel speeds.

Fig. 4.12. – Imperfection that are caused by going beyond the borders of the interpass temperature limits: a) above the upper limit (high interpass temperature); b) below lower limit (low interpass temperature)

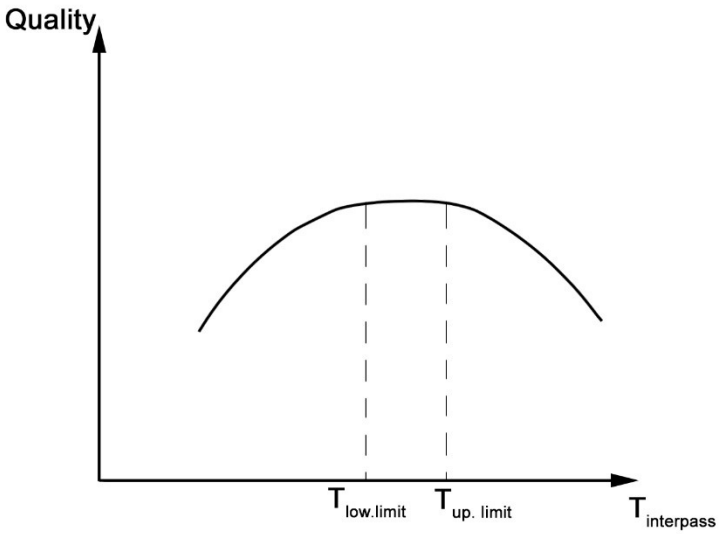

Fig. 4.13 – Illustration of hypothetical changes in the deposited layer quality due to the increase of the interpass temperature

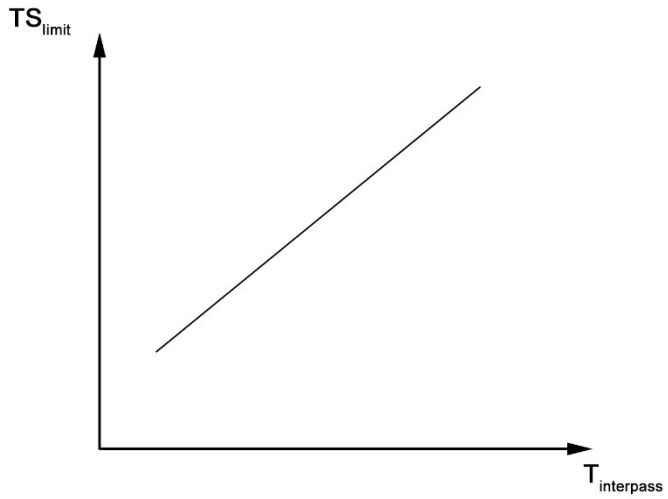

Fig. 4.14 – Illustration of hypothetical changes of the travel speed limits due to the increase of the interpass temperature

4.3.2. Definition of the operational envelope for a different deposition rates keeping the same ratio deposition rate/travel speed

The ground for this approach was the theory that the range of travel speed found in the first part of the work was related to a range of molten deposited pool in each layer. If this volume is too big (below the lower limit), the pool tends to flow out of the precedent deposited layer. If this volume is too small, the conditions for the existence of humps take place (above the upper limit). However, one could assume that for a given combination of wire feed speed and travel speed that would provide a pool volume inside this referred range, the increase of wire feed speed followed by a proportional increase of travel speed (WFS/TS constant) would keep this volume the same.

a) Experimental procedure

During this part of the work, 5 walls with 14 layers were printed. For each new wall, both travel speed and wire feed speed were proportionally increased, i.e., the travel speed augmented yet keeping the same deposition rate per unit of wall length. The same welding process, rig, welding wire and base metal of the previous section was used. The set of parameters that was used for each wall are presented in Table 4.2. Wall no. 1 in Table 4.2 was used as a reference (already demonstrated in the part 1). After the printings, each wall was prepared and analyzed in terms of geometrical parameters, using the procedure described in section 2.3.3. For each wall data acquisition of current, voltage and wire feed speed were carried out.

Table 4.2 – Set parameters used during experiment (CTWD = 15 mm)

wall	I_m (A)	WFS (m/min)	TS (mm/min)	WFS/TS
1	81	4.9	425	11.53
2	89	5.1	440	11.59
3	96	5.3	460	11.52
4	113	5.5	480	11.46
5	118	5.7	500	11.40

Note: Deposition efficiency considered to be 100 %, however, on welding currents 113 and 118 A was observed spattering that should be taken in count in further studies.

b) Results and Discussion

To be able of analyzing the results, the starting point was the calculation of the real values of the WS/TS ratio, the I/TS ratio and the Arc Energy from the monitored values of wire feed speed (WFS), current (I) and voltage (U). The resultant calculations are presented in Table 4.3. As seen in Figure 4.15, as the set WFS is increased, the deviation of the measured value to the set value is wider. This is not a problem of calibration, but a result of the welding self-control of the welding machine used in this work, to adapt to new conditions (for instance, if a new current is set, the control can make changes in WFS and voltage to adapt the parametrization to keep stable arc length and the desired current).

Table 4.3 – Monitored and calculated parameters (the wall 3 shows outlier characteristics)

	Monitored			Calculated		
Wall	I_m (A)	U (V)	WFS (m/min)	WFS/TS	Energy (J/mm)	I/TS (As/mm)
1	83.46	12.84	4.91	11.55	151.28	0.19
2	90.22	13.07	5.09	11.57	160.79	0.20
3	96.42	13.38	5.32	11.57	168.27	0.21
4	114.07	13.80	5.58	11.63	196.77	0.24
5	119.4	14.52	5.81	11.62	208.04	0.24

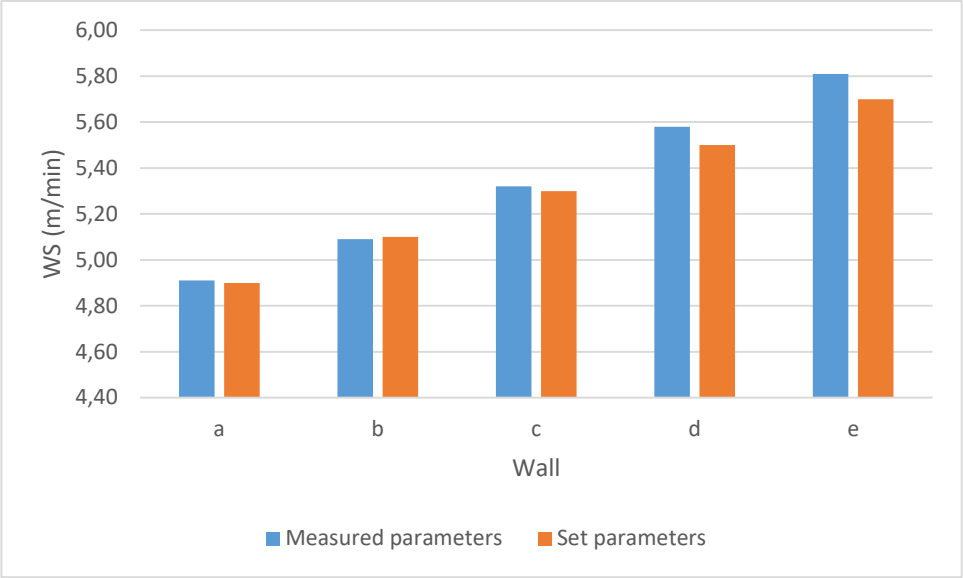

Fig. 4.15 – Comparation of set and measured wire feed speed, a) TS – 425 mm/min, WS – 4.9 m/min; b) TS – 440 mm/min, WS – 5.1 m/min; c) TS – 460 mm/min, WS – 5.3 m/min; d) TS – 480 mm/min, WS – 5.5 m/min; e) TS – 500 mm/min, WS – 5.7 m/min

The appearances of the 5 walls are shown in Fig. 4.18, while the comparison of the cross-sections and geometry analysis are presented in Fig. 4.17. Geometrical parameters of the walls are shown in Table 4.3.

As one can see, the third wall (TS 460 mm/min; WS 5.3 m/min) presents undulated formation and comes out of the trends in terms of geometrical parameters (an outlier). As long as the author cannot see any reason for such result, the author consider that it could be an experimental error (such as to have higher interpass temperatures than the other). Therefore, this wall was excluded from the analysis. However, the author believes that these results should be presented as evidence in case of someone wishes to repeat the present experiment with the same or other material.

Excluding the 3rd wall, all the deposition conditions were free from superficial undulations, as illustrated in the graphical scheme of Fig.4.16.

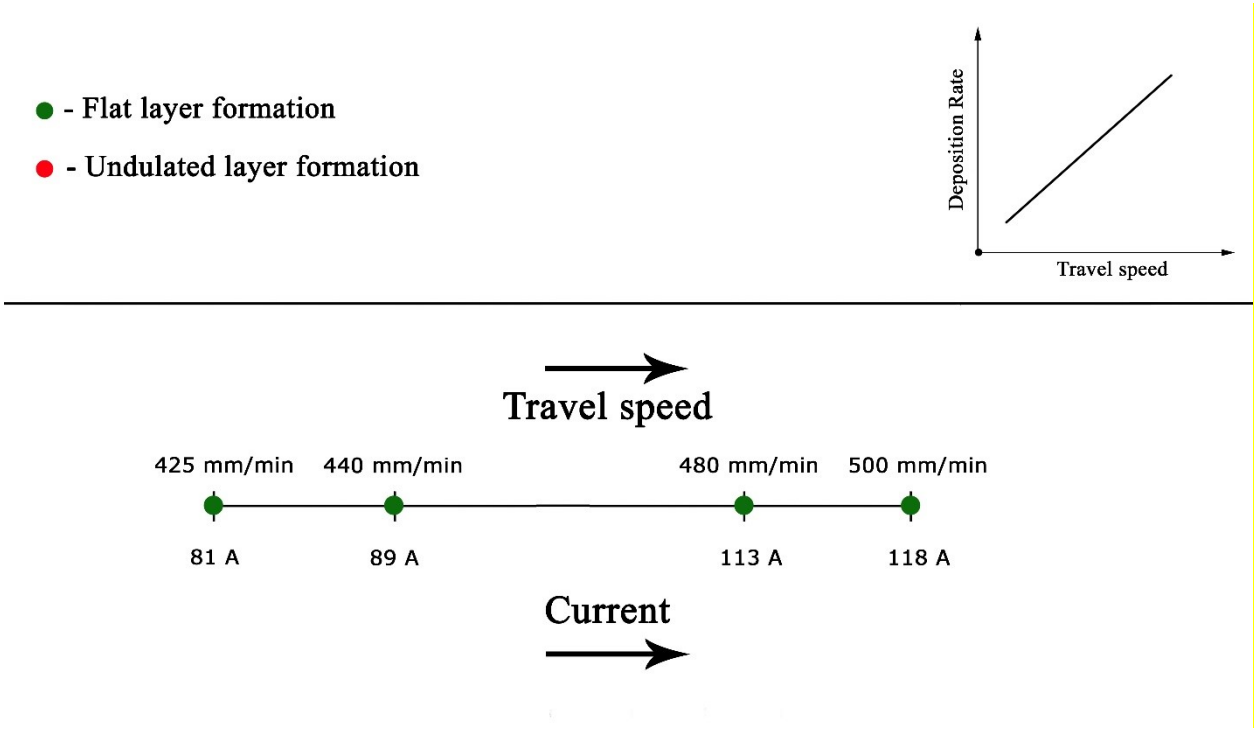

Fig. 4.16 – Graphical summary of the results of the speed limits experimental procedure

As expected, the full cross-section areas of the 2 first and 4th and 5th walls were, in pairs, almost the same, considering that the ratio WFS/TS was kept the same (≈ 11.56 and 11.62, respectively). However, the last two walls have full cross-sections a little higher than the others, reflecting the difference between the set and the measured values of WFS (Table 4.3). The increase of the ratio WFS/TS (Table 4.3) was not intentional, yet it justifies the results.

Regardless this difference between WFS/TS ratio, as one can be seen from Table 4.4, there are trends for the increasing production rates, as follows:

a) Height decreases;
b) Width increases;
c) BTA factor keeps the same

The trends of reducing the wall height and increasing the wall width as production rate (WFS for a same WFS/TS) is increased can be explained by a combination of influencing factors:

a) Arc energy and the ratio I/TS also increased (Table 4.3), making heat to accumulate more on the previous layer and increasing the deposition pool;
b) Increasing of the arc pressure with the increasing current, pushing down the molten pool while liquid (making it wider and shorter).

This shortening and thickening of the deposited layers as production rate is increased is just a characteristic, not necessarily adverse, as long as the wall finish and the geometric

tolerances are not affect, as seen to have not happen based on the statically equal BTA factor (Table 4.4) and the wall appearances in Figure 4.18. However, this characteristic suggests that the potential increase of production is counterbalanced by an increase in the minimal wall thickness.

To assess now the economic efficiency of production rates changes, one can consider the same reasoning as of from the previous section. As seen in Fig. 4.19, one can say that the production time for a same target wall thickness is lesser for smaller values of WFS and TS. In addition, the reduction of production time amongst the combinations of WFS and TS turns more significant as the target thickness is wider.

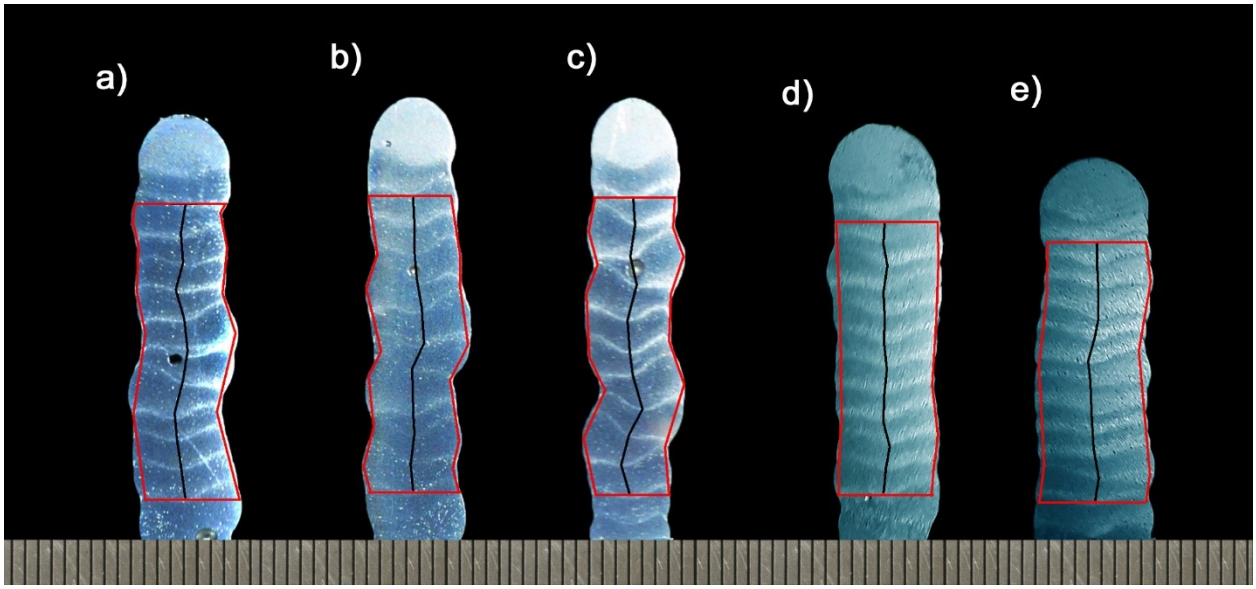

Fig. 4.17 – Cross section geometry comparison: a) TS – 425 mm/min, WS – 4.9 m/min; b) TS – 440 mm/min, WS – 5.1 m/min; c) TS – 460 mm/min, WS – 5.3 m/min; d) TS – 480 mm/min, WS – 5.5 m/min; e) TS – 500 mm/min, WS – 5.7 m/min

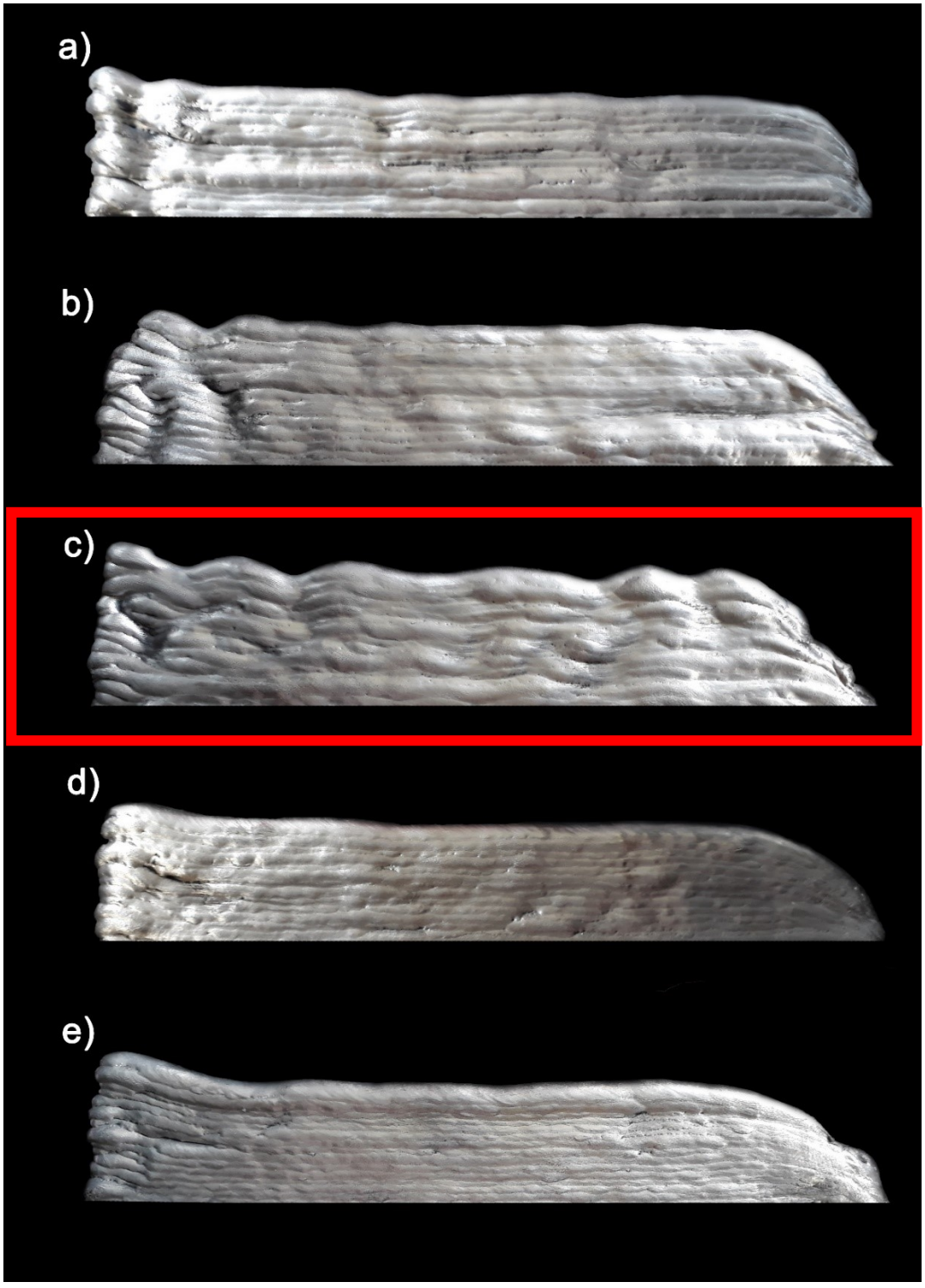

Fig. 4.18 – Appearance of the walls obtained during experiment: a) TS – 425 mm/min, WS – 4.9 m/min; b) TS – 440 mm/min, WS – 5.1 m/min; c) TS – 460 mm/min, WS – 5.3 m/min; d) TS – 480 mm/min, WS – 5.5 m/min; e) TS – 500 mm/min, WS – 5.7 m/min (marked wall was considered outlier)

Table 4.4 – Geometrical parameters of the printed walls (third all was considered outlier)

Wall	Rectified height of 10 layers (mm)	Average Height per layer (mm)	Full area (mm^2)	Effective area (mm^2)	Buy-to-apply (BTA)factor	Average effective wall width (mm)
TS – 425 mm/min, WS – 4.9 m/min	23.4	2.3	148.4	141.3	1,04	6.0
TS – 440 mm/min, WS – 5.1 m/min	23.3	2.3	152.9	144.6	1,05	6.2
TS – 460 mm/min, WS – 5.3 m/min	25.5	2.6	150.5	142.6	1,05	5.9
TS – 480 mm/min, WS – 5.5 m/min	21.3	2.1	159.0	148.6	1.07	7.0
TS – 500 mm/min, WS – 5.7 m/min	20.8	2.1	160.1	151.6	1.05	7.3

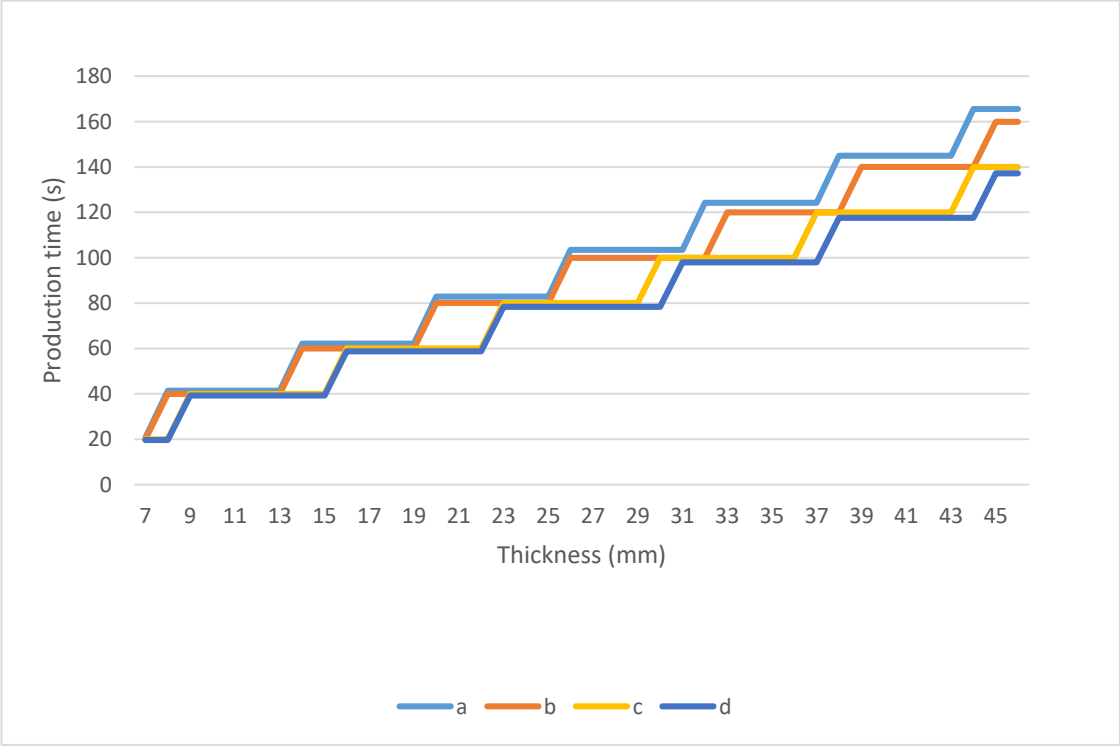

Fig. 4.19 – Time spent for production of the wall of 100 mm height, 200 mm length and with thickness from 6 to 44 mm by WAAM using different production rates: a) TS – 425 mm/min, WS – 4.9 m/min; b) TS – 440 mm/min, WS – 5.1 m/min; c) TS – 480 mm/min, WS – 5.5 m/min; d) TS – 500 mm/min, WS – 5.7 m/min

4.4 Conclusion

- There is a range of travel speed for WAAM of the aluminium when other parameters are kept fixed (quality aspect);
- Above the upper limit of the range, superficial undulations take place in the wall building-ups (quality aspect);
- The deposition speed for a fixed set of parameters can be used for reaching the desired wall thickness per pass per layer (the faster the speed, the thinner the minimum wall width), also a quality aspect;
- However, if the target are thicker walls (more than one pass per layer), the time spent to produce walls reduces by using deposition speeds close to the lower limit of the speed range;
- If production rate increase (economical aspect) is meant through an increase of wire feed speed (consequently, current), yet keeping the same WFS/TS to maintain the deposition condition within the useful range (quality aspect), there are a shortening and thickening of the deposited layers as production rate is increased, yet wall finish and the geometric tolerances are not affect (quality aspect);
- Consequently, the potential increase of production is counterbalanced by an increase in the minimal wall thickness (quality aspect);
- If production time (economical aspect) increase is meant through an increase of wire feed speed (consequently, current), yet keeping the same WFS/TS to maintain the deposition condition within the useful range, the production time for a same target wall thickness is lesser for smaller values of WFS and TS;
- The reduction of production time amongst the combinations of WFS and TS turns more significant as the target thickness is wider.

4.5 Future work

To eliminate all imprecisions of the work presented in this chapter, the experiments should be repeated to find out if undulated formation of the wall obtained with TS 460 mm/min and WS 5.3 m/min was an experimental error or an operational envelope break point.

CHAPTER V

CONCLUSIONS

5.1. About the mitigation of the epitaxial columnar grain growth

In first two parts of the work was design to assess two possible approaches to mitigate epitaxial growth of large columnar grains during WAAM process of aluminium. The first approach was through the application of a special welding technique called “Switchback”, whereas the second one was by means of inoculation. Both approaches showed ability to refine grain size, fact that, as known from the literature, can lead to the improving of the mechanical properties of the printed parts by minimizing anisotropy of the mechanical properties that is usually observed in parts produced by WAAM.

The mains conclusions on these objectives were:

- Switchback deposition mode applied in WAAM of aluminium alloy can prevent continuous homoepitaxial grain growth, by breaking the solidification pattern, and, in addition, to refine the grain sizes;
- In addition, switchback mode decreases porosity in printed parts, improves surface quality of the walls, and allow, for a same deposition rate per unit of wall length, the production of thinner walls;
- Inoculation applied in autogenous stainless TIG welding (through addition SiO2 nanoparticles) showed to change the bead profiles and the microstructure and to reduce austenite grain size and to increase the content of delta ferrite;
- Consequently, inoculation can be usefully used in welding/additive manufacturing as much as it has been used in casting.

5.2. About the determination of the operational envelope of the process

In the third part of the work, operational envelope of the WAAM of aluminium was considered in terms of the travel speed and production rate. The main objective of this work part was to understand the role played by the layer melted volume over the geometric quality and economical

aspects of the deposit carried out with WAAM of aluminium alloys. To reach the proposed objective, two approaches were used for the definition of the travel speed limits for a same deposition rate and for the definition of the operational envelop for a different deposition rates yet keeping the same ratio deposition rate/travel speed. The main conclusions were:

- There is a range of travel speed for WAAM of the aluminium when other parameters are kept fixed (quality aspect);
- Above the upper limit of the range, superficial undulations take place in the wall building-ups (quality aspect);
- The deposition speed for a fixed set of parameters can be used for reaching the desired wall thickness per pass per layer (the faster the speed, the thinner the minimum wall width), also a quality aspect;
- However, if the target are thicker walls (more than one pass per layer), the time spent to produce walls reduces by using deposition speeds close to the lower limit of the speed range;
- If production rate increase (economical aspect) is meant through an increase of wire feed speed (consequently, current), yet keeping the same WFS/TS to maintain the deposition condition within the useful range (quality aspect), there are a shortening and thickening of the deposited layers as production rate is increased, yet wall finish and the geometric tolerances are not affect (quality aspect);
- Consequently, the potential increase of production is counterbalanced by an increase in the minimal wall thickness (quality aspect);
- If production time (economical aspect) increase is meant through an increase of wire feed speed (consequently, current), yet keeping the same WFS/TS to maintain the deposition condition within the useful range, the production time for a same target wall thickness is lesser for smaller values of WFS and TS;
- The reduction of production time amongst the combinations of WFS and TS turns more significant as the target thickness is wider.

REFERENCES

ALMEIDA, H. A. L.; MOTA, C. A. M.; SCOTTI, A. Effects of the reversion course length and torch leading angle on the bead solidification structure in GMAW welding with Switch Back. **Soldagem & Inspeção**. v.17, p.123-137,2012.
https://doi.org/10.1590/S0104-92242012000200006

ALMEIDA, P. S.; WILLIAMS, S. Innovative process model of Ti–6Al–4V additive layer manufacturing using cold metal transfer (CMT). **Proceedings of the 21st annual international solid freeform fabrication symposium**. p. 25–36, 2010.

ALTENKIRCH, J.; STEUWER, A.; WITHERS, P.; WILLIAMS, S.; POAD, M.; WEN, S.W. Residual stress engineering in friction stir welds by roller tensioning. **Science and Technology of Welding and Joining**. v. 14, p. 185–192, 2009.
https://doi.org/10.1179/136217108X388624

ASTM E112-13, Standard Test Methods for Determining Average Grain Size. **ASTM International**, 28p, 2013.

BARKER, R. US **Patent** US1533300A. Method of making decorative articles, 1920.

BEKKER, A. C. M.; VERLINDEN, J. C.; GALIMBERTI, G. CHALLENGES IN ASSESSING THE SUSTAINABILITY OF WIRE + ARC ADDITIVE MANUFACTURING FOR LARGE STRUCTURES. **2016 Annual International Solid Freeform Fabrication Symposium.** 2016.

BICKERT, C. Paul Héroult - The Man Behind the Invention. **The Minerals, Metals and Materials Society**. 2013.
https://doi.org/10.1002/9781118788011.ch7

COLEGROVE, P. A.; COULES, H. E.; FAIRMAN, J.; MARTINA, F.; KASHOOB, T.; MAMASH, H.; COZZOLINO, L. D.; Microstructure and residual stress improvement in wire and arc additively manufactured parts through high-pressure rolling. **Journal of Materials Processing Tech**. v. 213, p. 1782–1791, 2013.
https://doi.org/10.1016/j.jmatprotec.2013.04.012

COLEGROVE, P. A.; MCANDREW, A. R.; DING, J.; MARTINA, F.; KURZYNSKI, P.; WILLIAMS, S. System Architectures for Large Scale Wire + Arc Additive Manufacture. **10th International Conference on Trends in Welding Research.** 2016.

CUIURI D. **Control of short circuit gas metal arc welding process using instantaneous current regulation.** 2000, Ph.D. thesis - University of Wollongong.

DA SILVA, C. L.M.; SCOTTI, A. The influence of double pulse on porosity formation in aluminum GMAW. **Journal of Materials Processing Technology**. v. 171, p. 366-372, 2006. https://doi.org/10.1016/j.jmatprotec.2005.07.008

DEBROY, T.; WEI, H. L.; ZUBACK, J. S.; MUKHERJEE, T.; ELMER, J. W.; MILEWSKI, J. O.; ZHANG, W. Additive manufacturing of metallic components – Process, structure and properties. **Materials Science and Engineering**. v. 92, p. 112-224, 2018. https://doi.org/10.1016/j.pmatsci.2017.10.001

DICKENS, P. M.; PRIDHAM, M. S.; COBB, R. C.; GIBSON, I.; DIXON, G. Rapid prototyping using 3-D welding. **Proceedings of the 3rd symposium solid freedom fabrication.** p. 280–290.1992.

DINDA, G. P.; DASGUPTA, A. K.; MAZUMDER, J. Texture control during laser deposition of nickel-based superalloy. **Scripta Mater**. v. 67, 2012. https://doi.org/10.1016/j.scriptamat.2012.06.014

DING, D.; PAN, Z.; CUIURI, D.; LI, H. Wire-Feed Additive Manufacturing of Metal Components: Technologies, Developments and Future Interests. **Int J Adv Manuf Technol**. v. 81, p. 465–481, 2015. https://doi.org/10.1007/s00170-015-7077-3

DING, J.; COLEGROVE, P. A.; MEHNEN, J; GANGULY, S.; ALMEIDA, S. P. M.; WANG, F.; WILLIAMS, S. Thermo-mechanical analysis of Wire and Arc Additive Layer Manufacturing process on large multi-layer parts. **Computational Materials Science**. v. 50, p. 3315–3322, 2011. https://doi.org/10.1016/j.commatsci.2011.06.023

DONOGHUE, J.; ANTONYSAMY, A. A.; MARTINA, F.; COLEGROVE, P.A.; WILLIAMS, S.; PRANGNELL, P.B. The effectiveness of combining rolling deformation with Wire–Arc Additive Manufacture on β-grain refinement and texture modification in Ti–6Al–4V. **Materials Characterization**. v. 114, p 103–114, 2016. https://doi.org/10.1016/j.matchar.2016.02.001

FATTAHI, M.; MAHAMMADI, M.; SAJJADI, N.; HONARMAND, M.; FATTAHI, Y.; AKHAVAN, S. Effect of TiC Nanoparticles on the Microstructure and Mechanical Properties of Gas Tungsten Arc Welded Aluminum Joints. **Journal of materials processing technology**. v. 217, p. 21-29, 2015. https://doi.org/10.1016/j.jmatprotec.2014.10.023

FATTAHI, M.; NABHANI, N.; VAEZI, M.R.; RAHIMI, E. Improvement of impact toughness of AWS E6010 weld metal by adding TiO2 nanoparticles to the electrode coating. **Materials Science and Engineering**. v. 528, p. 8031-8039, 2011.

FERRARESI, V. A.; FIGUEIREDO, K. M.; ONG, T. Hiap. Metal transfer in the aluminum gas metal arc welding. **J. Braz. Soc. Mech. Sci. & Eng**. v. 25, p. 229-234, 2003. https://doi.org/10.1590/S1678-58782003000300003

GANAHA, T.; PEARCE, B. P.; KERR, H. W. Grain structure in aluminum alloy GTA welds. **Metallurgical Transactions**. v. 11, p. 1351–1359, 1980.

https://doi.org/10.1007/BF02653489

GARLAND, J. G.; DAVIES, G.J. Solidification Structures and Properties of Fusion Welds. **Int. Mater. Rev**. v. 1, p. 83–108, 1975.
http://dx.doi.org/10.1179/imr.1975.20.1.83

GENG, H.; LI, J.; XIONG, J.; LIN, X. Optimisation of interpass temperature and heat input for wire and arc additive manufacturing 5A06 aluminium alloy. **Sci. Technol. Weld. Join**. v. 22, p. 472–483, 2017.
https://doi.org/10.1080/13621718.2016.1259031

GU, D. Laser Additive Manufacturing (AM): Classification, Processing Philosophy, and Metallurgical Mechanisms. **Laser Additive Manufacturing of High-Performance Materials**. p 15-7, 2015.
https://doi.org/10.1007/978-3-662-46089-4_2

HALL, E. O. The Deformation and Ageing of Mild Steel: III Discussion of Results. **Proceedings of the Physical Society.** v. 64, p. 747, 1951.

HARRIS, H. D. HIGH-SPEED GMAW AND LASER GMAW HYBRID WELDING OF STEEL SHEET. 2009. Ph.D. thesis - University of Cranfield.

HOYE, N. **Characterisation of Ti-6Al-4V deposits produced by arc-wire based additive manufacture**. 2015. Ph.D. thesis - University of Wollongong.

ISO 17296-2. Additive manufacturing - General Principles Part 2: Overview of process categories and feedstock. **British Standards Institution**, 25p, 2015.

ISO/ASTM 52900. Additive manufacturing - General principles – Terminology. **ISO/TC 261**, 19p, 2015.

KANEKO, Y.; YAMANE, S.; OSHIMA, K. Numerical simulation of MIG weld pool in switchback welding. **Welding in the World**. 2009.
http://dx.doi.org/10.1007/BF03263476.

KURKIN, S.; ANUFRIEV, V. Preventing distortion of welded thin walled members of AMg6 and 1201 aluminum alloys by rolling the weld with a roller behind the welding arc, **Welding Production.** v. 31, p. 32–34, 1984.

KUSSMAUL, K.; SCHOCH, F. W.; LUCKOW, H. High quality large components ‘shape welded’ by a SAW process. **Weld J.** v. 62, p. 17-24, 1983.

LIN, D. C.; WANG, G. X.; SRIVATSAN, T. S. A mechanism for the formation of equiaxed grains in welds of aluminum-lithium alloy 2090. **Materials Science and Engineering**. v. 351, p. 304-309, 2003.
https://doi.org/10.1016/S0921-5093(02)00858-4

MA, Y.; CUIURI, D.; HOYE, N.; LI, H.; PAN, Z. The effect of location on the microstructure and mechanical properties of titanium aluminides produced by additive layer manufacturing using in-

situ alloying and gas tungsten arc welding. **Material Science and Engineering**. v. 631, p. 230–240, 2015.
https://doi.org/10.1016/j.msea.2015.02.051

MANION, B.; HEINZMAN, J. Plasma arc welding brings better control. **Tooling & Production.** 1999.

MARTINA, F, WILLIAMS, S. Wire+arc Additive Manufacturing vs. Traditional Machining from Solid: A Cost Comparison. **Welding Engineering and Laser Processing Centre, Cranfield University.** 2015.

MARTINA, F. High pressure rolling of Ti-6Al-4V WAAM structures. **Cranfield University**. 2014

MARTINA, F.; COLEGROVE, P.A.; WILLIAMS, S.W.; MEYER, J. Microstructure of Interpass Rolled Wire + Arc Additive Manufacturing Ti-6Al-4V Components. **Metallurgical and Materials Transactions**. v. 46, p. 6103–6118, 2015.
https://doi.org/10.1007/s11661-015-3172-1

MCANDREW, A. R.; ROSALES, M.A.; COLEGROVE, P. A.; HÖNNIGE, J. R.; HO, A.; FAYOLLE, R.; EYITAYO, K.; STAN, I.; SUKRONGPANG, P.; CROCHEMORE, A.; PINTER, Z.; Interpass rolling of Ti-6Al-4V wire + arc additively manufactured features for microstructural refinement. **Additive Manufacturing**. v. 21, p. 340-349, 2018.
https://doi.org/10.1016/j.addma.2018.03.006

MEREDDY, S.; BERMINGHAM, M.J.; STJOHN, D.H.; DARGUSCH, M.S. Grain refinement of wire arc additively manufactured titanium by the addition of silicon. **Journal of Alloys and Compounds**. v. 695, p. 2097-2103, 2017.
https://doi.org/10.1016/j.jallcom.2016.11.049

MESSLER, R. W. Joining of Materials and Structures. **Butterworth-Heinemann.** 2004.

MOURITZ, A. P. Introduction to aerospace materials. **Woodhead Publishing**. 2012.
https://doi.org/10.2514/4.869198

NGUYEN, T. C.; WECKMAN, D. C.; JOHNSON, D. A.; KERR, H. W. The humping phenomenon during high-speed gas metal arc welding. **Science and Technology of Welding and Joining**. v. 10, p. 447 – 459, 2005.
https://doi.org/10.1179/174329305X44134

NORRISH, J. Advanced welding processes. **Institute of Physics Publishing.** 1992.

O'BRIEN, R. L. Welding handbook: Welding processes. **American Welding Society**. v. 2, 1991.

PAN, Z.; DING, D.; WU, B.; CUIURI, D.; LI, H.; NORRISH, J. Arc Welding Processes for Additive Manufacturing: A Review. Transactions on Intelligent Welding Manufacturing. **Springer**, p. 3-24, 2018.
https://doi.org/10.1007/978-981-10-5355-9_1

PARIMI, L. L.; RAVI G. A.; CLARK, D.; ATTALLAH, M. M. Microstructural and texture development in direct laser fabricated IN718. **Materials Characterization**. v. 89, p. 102-111, 2014.
https://doi.org/10.1016/j.matchar.2013.12.012

RAMACHANDRAN, T. R.; SHARMA, P. K.; BALASUBRAMANIAN, K. Grain Refinement of Light Alloys. **68th WFC – World Foundry Congress**. p. 189-193, 2008.

RIBEIRO, A. F.; NORRISH, J. Rapid prototyping process using metal directly. **7th Annual Solid Freeform Fabrication Symposium**. p. 249–256, 1996.

RIBEIRO, F.; NORRISH, J. Metal based rapid prototyping for more complex shapes. **Biennial international conference on "Computer Technology in Welding".** p. 1–11, 1996.

SAMES, W. J.; LIST, F. A.; PANNALA, S.; DEHOFF, R. R.; BABU, S. S. The metallurgy and processing science of metal additive manufacturing, **International Materials Reviews**. v. 61, p. 315-360, 2016.
https://doi.org/10.1080/09506608.2015.1116649

SCOTTI, A.; PONOMAREV, V.; LUCAS, W. A scientific application oriented classification for metal transfer modes in GMA welding. **Journal of Materials Processing Technology.** v. 212, p. 1406-1413, 2012.

SHEN, C.; PAN, Z.; CUIURI, D.; ROBERTS, J.; LI, H. Fabrication of Fe-FeAl functionally graded material using the wire-arc additive manufacturing process. **Metall Mater Trans**. v. 47, p. 763–772, 2016.
https://doi.org/10.1007/s11663-015-0509-5

SODERSTROM, E.; MENDEZ, P. Humping mechanisms present in high speed welding. **Science and Technology of Welding and Joining**. v. 11, pp. 572-579, 2006.
https://doi.org/10.1179/174329306X120787

SPENCER, J. D.; DICKENS, P. M.; WYKES, C. M. Rapid prototyping of metal parts by three-dimensional welding. **Proceedings of the Institution of Mechanical Engineers**. v. 212, p. 175–182, 1998.
https://doi.org/10.1243/0954405981515590

STAVROPOULOS, P.; FOTEINOPOULOS, P. Modelling of additive manufacturing processes: a review and classification. **Manufacturing Rev**. v. 5, 2018.
https://doi.org/10.1051/mfreview/2017014

TANSKI, T.; SNOPINSKI, P.; HILSER, O. Microstructure and mechanical properties of two binary Al-Mg alloys deformed using equal channel angular pressing. **Materialwissenschaft und Werkstofftechnik**. v. 48, p. 439-446, 2017.
https://doi.org/10.1002/mawe.201700020

UJIIE, A. US Patent US3558846A. Method of and apparatus for constructing substantially circular cross section vessel by welding, 1971.

VAEZI, M.; CHIANRABUTRA, S.; MELLOR, B.; YANG, S. Multiple material additive manufacturing – Part 1: a review. **Virtual and Physical Prototyping**. v. 8, p. 19-50, 2013. https://doi.org/10.1080/17452759.2013.778175

VAYRE, B.; VIGNAT, F.; VILLENEUVE, F. Metallic additive manufacturing: State-of-the-art review and prospects. **Mechanics & Industry**. v.13, p. 89-96, 2012. https://doi.org/10.1051/meca/2012003

WANG, F.; WILLIAMS, S.; COLEGROVE, P.; ANTONYSAMY, A. A. Microstructure and mechanical properties of wire and arc additive manufactured Ti-6Al-4V. **Metallurgical and Materials Transactions**. v. 44, p. 968-977, 2013. https://doi.org/10.1007/s11661-012-1444-6

WANG, F.; WILLIAMS, S.; RUSH, M. Morphology investigation on direct current pulsed gas tungsten arc welded additive layer manufactured Ti6Al4V alloy. **The International Journal of Advanced Manufacturing Technology**. v. 57, p. 597–603, 2011. https://doi.org/10.1007/s00170-011-3299-1

WANG, J.; HUANG, Y.; XIAO, J.; FENG, J.; TIAN, C. Y.; WANG, J. Metal Transfer with Force Analysis in Consumable and Nonconsumable Indirect Arc Welding Process. **Welding Journal.** v. 93, p. 431-438, 2014

WEI, H. L.; MUKHERJEE, T.; DEBROY, T. Grain Growth Modeling for Additive Manufacturing of Nickel Based Superalloys. **Proceedings of the 6th International Conference on Recrystallization and Grain Growth (ReX&GG 2016)**. p. 265-269, 2016. https://doi.org/10.1007/978-3-319-48770-0_39

WEI, H.L.; ELMER, W.; DEBROY, T. Origin of grain orientation during solidification of an aluminum alloy. **Acta Materialia**. v 115, p. 123-131, 2016. https://doi.org/10.1016/j.actamat.2016.05.057

WILLIAMS, S. W.; MARTINA, F.; ADDISON, A. C.; DING, J.; PARDAL, G.; COLEGROVE, P. A. Wire + Arc additive manufacturing. **Mater Science and Technology**. v. 32, p. 641-647, 2016. https://doi.org/10.1179/1743284715Y.0000000073

WU, C. S.; HU, Z. H.; ZHONG L. M. Prevention of humping bead associated with high welding speed by double-electrode gas metal arc welding. **International Journal of Advanced Manufacturing Technology**. v. 63, p. 573 – 581, 2012. https://doi.org/10.1007/s00170-012-3944-3

YAN, F.; XIONG, W.; FAIERSON, E.J. Grain Structure Control of Additively Manufactured Metallic Materials. **Materials**. v. 10, p. 1260-1270, 2017. https://doi.org/10.3390/ma10111260

YE, D.; WU, D.; HUA, X; XU, C.; WU, Y. Using the multi-wire GMAW processes for controlling the formation of humping. **Weld World**. v. 61, p. 649–658, 2017. https://doi.org/10.1007/s40194-017-0458-5

YUNJIA, H.; FROST, R. H.; OLSON, D. L.; EDWARDS, G.R. Grain refinement of aluminum weld metal. **Welding Journal.** v. 68, p.280–289, 1989.

ZHILIN, L. Review of Grain Refinement of Cast Metals Through Inoculation: Theories and Developments. **Metallurgical and Materials Transactions**. v. 48, p. 4755-4776, 2017. https://doi.org/10.1007/s11661-017-4275-7

ZHU, Y.; TIAN, X.; LI, J.; WANG, H. The anisotropy of laser melting deposition additive manufacturing Ti–6.5Al–3.5Mo–1.5Zr–0.3Si titanium alloy. Materials & Design. v. 67, pp. 538-542, 2015. https://doi.org/10.1016/j.matdes.2014.11.001